EPIMUSCULAR MYOFASCIAL FORCE TRANSMISSION: INSIGHTS ON BTX-A INTERVENTION AND MUSCLE SPINDLE SENSORY FEEDBACK

by

Evrim Ozan Yılmaz

B.S., in Mechanical Engineering, Istanbul University, 2017

Submitted to the Institute of Biomedical Engineering
in partial fulfillment of the requirements
for the degree of
Doctor
of
Philosophy

Boğaziçi University
2024

EPIMUSCULAR MYOFASCIAL FORCE TRANSMISSION: INSIGHTS ON BTX-A INTERVENTION AND MUSCLE SPINDLE SENSORY FEEDBACK

APPROVED BY:

Prof. Dr. Can A. Yücesoy .....
(Thesis Advisor)

Prof. Dr. Arzu Çelik .....

Prof. Dr. Yunus Ziya Arslan .....

Assoc. Prof. Dr. Bernhard Englitz .....

Assoc. Prof. Dr. Daniela Schulz .....

DATE OF APPROVAL:

ACKNOWLEDGMENTS

I would like to express my deepest gratitude to Prof. Dr. Can A. Yücesoy for his unwavering encouragement and guidance throughout this journey. His vision and motivation have been invaluable in shaping both my academic and personal growth. I am grateful for his confidence in my potential to become a truly independent researcher.

I am sincerely grateful to Assoc. Prof. Dr. Bernhard Englitz for welcoming me into his lab and for his encouragement when I was overly critical of my work. His passion for science has been inspiring, and his warm welcome made my time in the Netherlands both cheerful and reassuring.

I appreciate my lab mates in the Biomechanics Laboratory, as well in the Computational Neuroscience Laboratory, for their support during the long experiment days and their friendship outside the lab. Their company made the challenging times bearable.

I thank Prof. Dr. Yunus Ziya Arslan and Prof. Dr. Arzu Çelik for serving on my dissertation committee. I am grateful for the time they dedicated. It was an honor to share my work with you and to receive your valuable feedback and expertise, which has enriched my perspective.

I appreciate Assoc. Prof. Dr. Zeynep Deniz Akdeniz Doğan and Dr. M. Taygun Oluklu for their contributions to the rat experiments, willingness to teach me microsurgery techniques, and our chats during the experiments.

I want to thank to Debbie Tilburg-Ouwens for her guidance on histological preparations and to Dr. Jelle Postma for his support and insights on imaging them. Their expertise and practical assistance were crucial to my research.

My deepest appreciation goes to my friends for their immense contribution to my personal life. Their support, belief in me, and the joy they brought into my life have helped me relax and recharge. They have played a significant role in shaping my character and personality, and I am deeply grateful for their presence and encouragement throughout this journey.

I would like to acknowledge the laboratory animals used in my research. Their contribution was essential to the advancement of scientific knowledge, and I recognize the importance of their role in this work. I was committed to ensuring that their use was conducted with the utmost care and respect.

I extend my sincere thanks to my *silicon friends*, the AI tools and technologies, for being the tireless companions who helped me through my doctoral journey.

I owe a profound debt of gratitude to my parents, my loving mother Melahat Yılmaz and humorous father Dursun Yılmaz, for their constant interest in my academic journey over the years. Conversations with them after long days of work were always rewarding and kept me grounded. Thank you for raising me into the person I am proud to be today.

I dedicate this thesis to my little sister, Simge Gökçem Yılmaz, the most valuable and irreplaceable part of my life. Besides being my intern for a while, her emotional support throughout this thesis has been unmatched, and I am profoundly grateful for her presence in my life.

Parts of this thesis work were supported by the iNavigate grant H2020-MSCA-RISE-2019-873178 (to Evrim Ozan Yılmaz), the NeurotechEU grant EPP-EUR-UNIV-2020-101004080 (to Evrim Ozan Yılmaz), and The Scientific and Technological Research Council of Turkey (TÜBİTAK) through the 2214A scholarship program 2022/2-1059B142201459 (to Evrim Ozan Yılmaz) and grant 116S393 (to Can A. Yücesoy).

ACADEMIC ETHICS AND INTEGRITY STATEMENT

I, Evrim Ozan Yılmaz, hereby certify that I am aware of the Academic Ethics and Integrity Policy issued by the Council of Higher Education (YÖK) and I fully acknowledge all the consequences due to its violation by plagiarism or any other way.

Name :

Signature:

Date:

ABSTRACT

EPIMUSCULAR MYOFASCIAL FORCE TRANSMISSION: INSIGHTS ON BTX-A INTERVENTION AND MUSCLE SPINDLE SENSORY FEEDBACK

Mechanical equilibrium between skeletal muscles is maintained via connective tissues that surround the musculoskeletal system as a continuum. Muscle contraction generates forces that spread within the muscle compartment through connective tissues, facilitating epimuscular myofascial force transmission (EMFT). This thesis explored mechanical and sensory implications of EMFT using *in vivo* animal experiments. First, the long-term effects of botulinum toxin type-A (BTX-A), a common spasticity management drug, on individual and intermuscular muscle mechanics was studied in rats. Although BTX-A-induced paralysis was sustained, findings contradicted clinical aims at the individual muscle level (e.g., 12% increase in passive forces in the injected muscle and narrowed range of force exertion in the non-targeted bi-articular muscle by 15% distally and 32% proximally). Importantly, unlike in acute observations, diminished EMFT was not observed. Given its clinical relevance in spastic muscle mechanics, BTX-A's efficacy seems tied to its impact on EMFT. These studies highlighted complex and uncontrolled BTX-A effects on intermuscular mechanics, suggesting limitations in long-term outcomes for managing spasticity. Then, the influence of EMFT on muscle spindle (MS) sensory feedback was tested in mice. Synergistic muscle stimulation resulted in significant increase in MS afferent firing (53% on average) due to intermuscular mechanical interactions. Variability in MS responses indicated that MSs sense local length changes across the muscle that arise from muscle fiber-extracellular matrix interactions. Findings provided insights for optimizing spasticity management strategies and EMFT's role in sensorimotor integration.

Keywords: Epimuscular Myofascial Force Transmission, Muscle Force-Length Characteristics, Botulinum Toxin Type-A, Muscle Spindle, Spasticity Management, Sensorimotor Integration.

ÖZET

Epimüsküler Miyobağdokusal Kuvvet İletimi: BTX-A Müdahalesi ve Kas İğciği Duyusal Geri Bildirimi Üzerine İçgörüler

İskelet kasları arasındaki mekanik denge, kas-iskelet sistemini bütünüyle saran bağ dokularıyla sağlanır. Kas kasılması, bağ dokuları yoluyla kas kompartmanına yayılan kuvvetler üretir ve epimüsküler miyobağdokusal kuvvet iletimine (EMKİ) olanak sağlar. Bu tez, EMKİ'nin mekanik ve duyusal etkilerini *in vivo* hayvan deneyleriyle araştırmıştır. İlk olarak, spastisite yönetiminde yaygın olarak kullanılan olan botulinum toksin tip A'nın (BTX-A), tekil kas ve kaslar arası mekanikler üzerindeki uzun vadeli etkileri sıçanlarda incelenmiştir. BTX-A ile indüklenen paralizi devam etmesine rağmen, elde edilen bulgular bireysel kas düzeyinde klinik amaçlarla çelişmektedir (örn., enjekte edilen kasın pasif kuvvetlerinde %12'lik artış ve hedeflenmeyen iki eklemli kasın kuvvet etkime aralığında distal uçta %15, proksimal uçta %32'lik daralma). Önemli olarak, akut gözlemlerin aksine, EMKİ'de azalma görülmedi. Spastik kas mekaniğinde klinik olarak önemli olan bu durumda, BTX-A'nın etkinliğinin EMKİ üzerindeki etkileriyle ilişkili olduğunu belirtmektedir. Bu çalışmalar, BTX-A'nın kas etkileşimleri üzerindeki karmaşık ve kontrolsüz etkilerini vurgulayarak, spastisite yönetiminin uzun vadeli sonuçlarındaki kısıtlara işaret etmektedir. Daha sonra, EMKİ'nin kas iğciği (Kİ) duyusal geri bildirimi üzerindeki etkisi farelerde test edildi. Sinerjist kas stimülasyonu, kaslar arası etkileşimler nedeniyle Kİ afferent ateşlenmesinde anlamlı bir artışa (ort. %53) yol açtı. Kİ yanıtlarındaki değişkenlik, Kİ'lerin kas fiberleri-ekstraselüler matris etkileşimlerinden kaynaklanan kas boyunca lokal uzunluk değişikliklerini algıladığını göstermektedir. Bulgular, spastisite yönetim stratejilerinin optimize edilmesiyle ve EMKİ'nin duyusal-motor entegrasyonundaki rolüyle ilgili içgörüler sağlamaktadır.

Anahtar Sözcükler: Epimüsküler Miyobağdokusal Kuvvet İletimi, Kas Kuvvet-Uzunluk Karakteristiği, Botulinum Toksin Tip-A, Kas İğciği, Spastisite Yönetimi, Duyusal-Motor Entegrasyon.

TABLE OF CONTENTS

ACKNOWLEDGMENTS iii
ACADEMIC ETHICS AND INTEGRITY STATEMENT v
ABSTRACT vi
ÖZET vii
LIST OF FIGURES xii
LIST OF SYMBOLS xiii
LIST OF ABBREVIATIONS xiv
1. INTRODUCTION 1
1.1 Related literature 1
1.1.1 Skeletal Muscle Anatomy and Physiology 1
1.1.2 Epimuscular Myofascial Force Transmission (EMFT) 3
1.1.3 Mechanical Implications of EMFT 5
1.1.3.1 EMFT in the Use of BTX-A in Spasticity Management 6
1.1.4 Sensory Implications of EMFT 8
1.1.4.1 EMFT in Muscle Spindle Function 9
1.2 Thesis Outline 11
1.2.1 Aims 11
1.2.2 Overview 12
1.3 List of Publications Resulting from the Thesis 14
1.3.1 Journal Articles 14
1.3.2 Conference Proceedings 14
2. BTX-A AFFECTS INDIVIDUAL MUSCLE MECHANICS BUT SUSTAINS EMFT IN THE LONG-TERM 15
2.1 Introduction 15
2.2 Materials and Methods 17
2.2.1 Subjects 17
2.2.2 Surgical Procedures 18
2.2.3 Experimental Setup 19
2.2.4 Experimental Conditions and Procedure 19

2.2.5 Biochemical Analysis 20
2.2.6 Data Processing 22
2.2.7 Statistical Analyses 23
2.3 Results 25
2.3.1 Effects of BTX-A on Muscular Mechanics 25
2.3.1.1 TA Force-Length Characteristics 25
2.3.1.2 EDL Forces 26
2.3.1.3 EHL Forces 28
2.3.2 Changes in Intramuscular Connective Tissue Content Due to BTX-A 28
2.4 Discussion 29
2.4.1 Altered Mechanics of Muscles Exposed to BTX-A 30
2.4.2 Mechanical Interactions Between Partially Paralyzed Muscles . 30
2.4.2.1 Effects on individual muscles 30
2.4.2.2 Changes in collagenous and muscular tissue 31
2.4.3 Limitations and Implications of the Study 32
2.5 Conclusion 34
3. LONG-TERM BTX-A EFFECTS ON NON-TARGETED BI-ARTICULAR MUSCLE MECHANICS AND EMFT 35
3.1 Introduction 35
3.2 Materials and Methods 36
3.2.1 Injection Protocol 36
3.2.2 Surgical Procedure 37
3.2.3 Experimental Procedure 38
3.2.4 Data processing 40
3.2.5 Statistics 41
3.3 Results 42
3.3.1 Effects of BTX-A on Restrained Muscles 42
3.3.2 Effects of BTX-A on Mechanics of the Bi-articular Muscle . . . 42
3.3.2.1 Distal Lengthening 42
3.3.2.2 Proximal Lengthening 44
3.3.3 Effects of BTX-A on EMFT 44

3.4 Discussion 46
4. MUSCLE SPINDLES PROJECTING TO MOUSE Me5 SENSE SYNERGISTIC MUSCLE ACTIVITY
THROUGH EMFT 50
4.1 Introduction 50
4.2 Materials and Methods 52
4.2.1 Animals 52
4.2.2 Surgical procedures 52
4.2.2.1 Headpost implantation 52
4.2.2.2 Recording session 53
4.2.3 Electrophysiological recordings 53
4.2.4 Experimental design 54
4.2.4.1 Mechanical stimulation trials 54
4.2.4.2 Electrical stimulation trials 55
4.2.5 Histology 56
4.2.6 Neural Data Analysis 57
4.2.7 Statistical analyses 58
4.2.7.1 Single-cell analysis 59
4.2.7.2 Population analysis 59
4.3 Results 60
4.3.1 MS afferent and origin identification 61
4.3.1.1 Jaw opening condition 61
4.3.1.2 Muscle surface pressure condition 61
4.3.2 The effects of synergistic muscle stimulation 62
4.3.2.1 Masseter MSs 63
4.3.2.2 Temporalis MSs 64
4.4 Discussion 65
4.4.1 Limitations 68
4.4.2 Conclusion 70
5. INTEGRATED DISCUSSION 71
5.1 EMFT in Spasticity Management Using BTX-A 71
5.2 EMFT's Contribution to Sensorimotor Integration 74

5.3 Final Remarks and Future Directions 75
APPENDIX A. ILLUSTRATION OF LONGER SARCOMERE EFFECT . . 76
APPENDIX B. BTX-A INJECTION PROCEDURES IN ANIMAL EXPERIMENTS VS. CLINICAL PRACTICE 77
REFERENCES 78

LIST OF FIGURES

Figure 1.1	Skeletal muscle structure: the three connective tissue layers.	2
Figure 1.2	Skeletal muscle length-force relationship.	3
Figure 1.3	Mechanically integrated neuromusculoskeletal system.	9
Figure 2.1	The animal experimental set-up.	21
Figure 2.2	Representative force-time traces recorded at muscle tendons.	24
Figure 2.3	TA muscle forces as a function of TA muscle-tendon length.	26
Figure 2.4	EDL muscle forces as a function of TA muscle-tendon length.	27
Figure 2.5	EHL muscle forces as a function of TA muscle-tendon length.	28
Figure 2.6	Collagen concentration in the TA, EDL, and EHL muscles.	29
Figure 3.1	Schematic view of the experimental setup.	39
Figure 3.2	Length-force characteristics of EDL muscle obtained after distal lengthening.	43
Figure 3.3	Length-force characteristics of EDL muscle obtained after proximal lengthening.	45
Figure 3.4	EDL proximo-distal force differences as a function of changing EDL relative muscle position.	46
Figure 4.1	Experimental design.	54
Figure 4.2	Stimulation artifact removal and signal reconstruction.	58
Figure 4.3	Sample brain section of double staining.	60
Figure 4.4	Response to mechanical stimuli.	61
Figure 4.5	Response to electrical stimuli.	63
Figure 4.6	Schematic illustration of MS afferent projections to Me5 in mice.	65
Figure A.1	An illustration of longer sarcomere effects.	76

LIST OF SYMBOLS

C	Celsius
cm	centimeter
g	gram
h	hour
Hz	hertz
kg	kilogram
mA	milliampere
mg	milligram
min	minute
ml	milliliter
mm	millimeter
ms	millisecond
N	Newton
nm	nanometer
P	probability value
R^2	coefficient of determination
s	second
U	unit
∘	degree
μg	microgram
μl	microliter
μm	micrometer
ρ	Spearman's rank correlation coefficient

LIST OF ABBREVIATIONS

ANOVA	Analysis of Variance
BTX-A	Botulinum Toxin Type-A
CNS	Central Nervous System
CP	Cerebral Palsy
DiI	1,1'-Dioctadecyl-3,3,3',3'-Tetramethylindocarbocyanine Perchlorate
ECM	Extracellular Matrix
EDL	Extensor Digitorum Longus
EDL_{dist}	Distal tendon of EDL muscle
EDL_{prox}	Proximal tendon of EDL muscle
EHL	Extensor Hallucis Longus
eM	Electrical stimulation condition of Masseter exclusively
EMFT	Epimuscular Myofascial Force Transmission
eMT	Electrical stimulation condition of Masseter and Temporalis
eT	Electrical stimulation condition of Temporalis exclusively
F_a	Active muscle force
$F_{EDLdistal}$	Active muscle force at the distal tendon of EDL muscle
$F_{EDLproximal}$	Active muscle force at the proximal tendon of EDL muscle
F_p	Passive muscle force
$F_{proximal}$	Total muscle force at the proximal tendon of EDL muscle
FR_{driven}	Driven firing rate
$FR_{Jaw\ Opening}$	Firing rate during jaw opening
$FR_{relative}$	Relative firing rate
FR_{spont}	Spontaneous firing rate
FT	Force Transducer
F_t	Total muscle force
$FT_{EDLdist}$	FT attached to the distal tendons of EDL muscle
$FT_{EDLprox}$	FT attached to the proximal tendon of EDL muscle
l_{range}	Length Range of Active Force Exertion

LSE	Longer Sarcomere Effect
Me5	Trigeminal Mesencephalic Nucleus
MS	Muscle Spindle
PBS	Phosphate-Buffered Saline
PFA	Paraformaldehyde
SD	Standard Deviation
TA	Tibialis Anterior
TB	True Blue chloride

$\Delta FR_{\text{Jaw Opening}}$	Relative firing rate in response to jaw opening condition
$\Delta FR_{\text{Masseter Pressure}}$	Relative firing rate in response to masseter pressure condition
$\Delta FR_{\text{Temporalis Pressure}}$	Relative firing rate in response to temporalis pressure condition
$\Delta l_{\text{mt TA}}$	TA muscle-tendon length relative to its optimum length
$\Delta l_{\text{mt EDLdistal}}$	EDL muscle-tendon length relative to its distal optimum length
$\Delta l_{\text{mt EDLproximal}}$	EDL muscle-tendon length relative to its proximal optimum length
$\Delta \text{position}_{\text{EDL}}$	Relative position of EDL muscle-tendon complex

1. INTRODUCTION

1.1 Related literature

1.1.1 Skeletal Muscle Anatomy and Physiology

Skeletal muscles are the motors of the human musculoskeletal system, maintaining body posture and serving as the primary drivers of bodily movement. They facilitate locomotion by generating force and exerting it on the skeleton. By incorporating specialized sensory receptors, they also play a crucial role in the sensorimotor network, enabling the body to adapt to varying demands and conditions. Together with the connective tissue that surrounds all the motor and sensory components, neuromusculoskeletal system works in harmony to facilitate daily movements.

At the microscopic level, skeletal muscles are composed of sarcomeres, the smallest force-producing units, aligned in series along the length of muscle fibrils. A bundle of myofibrils, surrounded by the sarcolemma, forms muscle fibers, which are single muscle cells. Muscle cells are embedded within an extracellular space, known as the extracellular matrix (ECM). Together they constitute a composite tissue that enables cells to function and resist stretching. Collagen, the most abundant protein in the ECM, forms a complex network of connective tissue by running in various directions, providing a structural framework within which muscle cells operate. The muscle fibers lie parallel to each other and are bundled together with endomysium to form muscle fascicles. The fascicles, encased by perimysium, come together and are surrounded by the epimysium, forming the entire muscle. These connective tissue layers (i.e., endomysium, perimysium, and epimysium) envelop the different muscle divisions and are mechanically interconnected, forming a continuous network (Figure 1.1).

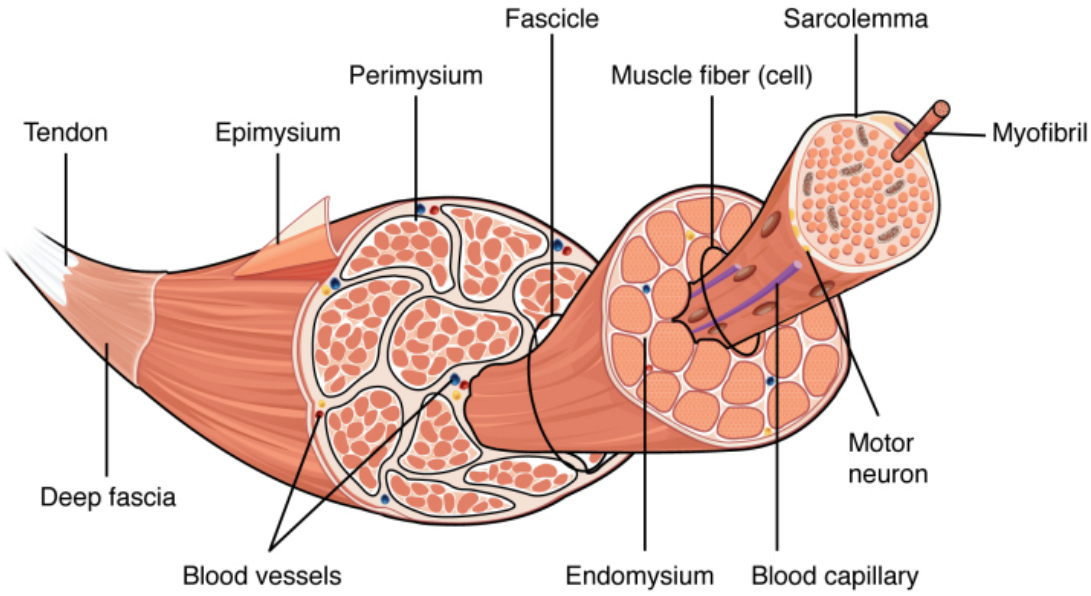

Figure 1.1 Skeletal muscle structure: the three connective tissue layers. Sarcomeres are aligned in series to constitute myofibrils, which are surrounded by the sarcolemma, forming muscle fibers. Muscle fibers come together with the endomysium to make up fascicles, which are encased by the perimysium. Fascicles are wrapped around by the epimysium, constituting the entire muscle. All the contractile elements (i.e., sarcomeres) and connective tissue layers (i.e., endomysium, perimysium, and epimysium) are mechanically integrated and function together. (adapted from Mohawk - PN Structure & Function of the Human Body, which is based on Anatomy & Physiology by OpenStax. Licensed under CC BY-SA; access for free at https://openstax.org/books/anatomy-and-physiology/pages/1-introduction; [1, 2]).

Muscle force varies depending on the specific demands of the task, as characterized by the isometric muscle length-force curve (Figure 1.2). In this context, total muscle force is the sum of the passive and active muscle forces. Active muscle force originates from the contraction of sarcomeres. On the other hand, passive muscle force results from the passive stretch of the muscle, attributed to the tension in the connective tissue layers surrounding the muscle fibers. As muscle length increases, active muscle force rises to a maximum at the muscle's optimum length before decreasing due to overstretching. The range of muscle length between the minimum and maximum active muscle force produced is known as the muscle's length range of active force exertion. Passive force is negligible in the ascending limb of the curve but increases dramatically in the descending limb of the muscle length force curve.

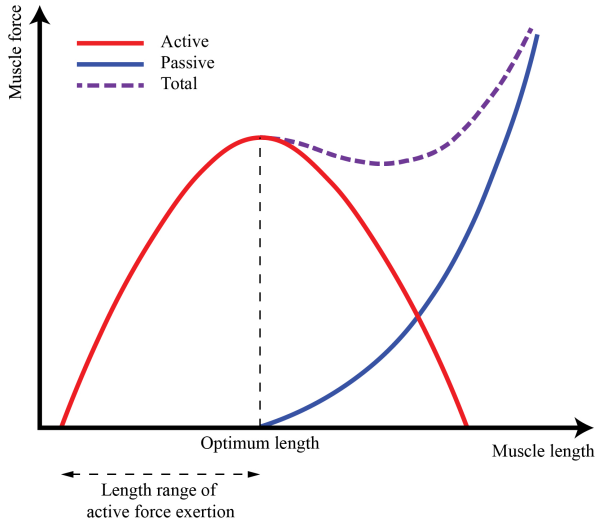

Figure 1.2 Skeletal muscle length-force relationship. Isometric muscle force is the sum of active and passive forces, varying with muscle length. Active force, produced by sarcomere contraction, peaks at the muscle's optimal length and decreases with overstretching. The length range of active force exertion is defined as the difference between the muscle length at which minimum and maximum active forces are generated. Passive force, arising from tension in connective tissues, is minimal at shorter lengths but increases significantly as the muscle stretches.

1.1.2 Epimuscular Myofascial Force Transmission (EMFT)

The tensional network of connective tissue extends along the layers that surrounds muscles, bones, nerves, and internal organs [3]. This structural framework integrates all the body components inside our skin and provides a highway for force transmission. In the last two decades, the consequences of the muscular force transmission through this connective tissue network have drawn significant attention [4]. Muscular activity influences the function of surrounding tissue both directly through the physical connections between muscles and their surroundings, and indirectly by changing the stiffness, elasticity, and orientation of the nearby connective tissue. With this view, muscle tendon units have been pictured to function together with their surroundings.

It has been shown that muscular force transmission is not limited to the myotendinous junction (Figure 1.3). Instead, muscle force is transmitted through ECM, which surrounds the muscle fibers and composed of layers called the endomysium, perimysium, and epimysium. This process is known as intramuscular myofascial force

transmission [5]. Beyond the muscle level, the muscle force transmission from one muscle to neighboring muscle through the connective tissues between them is called intermuscular myofascial force transmission [6]. Moreover, extramuscular myofascial force transmission describes the force transmission from the muscles' epimysium to non-muscular structures connections such as neurovascular tracts, compartmental connective tissues, and ligaments [7]. All these structures are in continuity with muscles' epimysium and ECM, hence with the entire fascia. Overall, the force produced in muscle fibers and transmitted through epimuscular connections (i.e., surrounding non-muscular and muscular structures) has been termed epimuscular myofascial force transmission (EMFT) [8, 9].

EMFT is the concept that describes the entire interplay between the smallest force producing units, i.e., sarcomeres, and their surroundings. In its core, this phenomenon emphasizes the importance of the muscle force transmitted beyond the boundaries of individual muscles to other neuromusculoskeletal system elements through specialized layers of connective tissues. EMFT looks beyond the traditional view of the muscles operating in isolation, which stem from the belief that muscles generate movement only by transferring forces to bones trough their tendons. The concept of EMFT highlights the interconnectedness of muscles and their surroundings through fascial network. This network enables the distribution of local forces generated by muscles, treating muscles and surrounding structures as the parts of an integrated neuromuscular system.

Research on EMFT has evolved our understanding of the neuromusculoskeletal system by underscoring its complexity and challenging the traditional view. Research on EMFT has impacted our understanding in various fields, including human biomechanics in health [10–13], sports [8, 14], physical therapy [3], rehabilitation [15], injury prevention [16] and neuromuscular diseases [17] such as spasticity. Several animal and human studies demonstrated that muscle forces can be transmitted to adjacent muscles and connective tissues, influencing and being influenced by the mechanical environment beyond the originating muscle. Yet, despite significant advancements, gaps remain in our understanding of both the mechanical and sensory implications

of EMFT. This indicates a pressing need for studies that can elucidate these aspects, laying the groundwork for a deeper understanding of neuromusculoskeletal system.

1.1.3 Mechanical Implications of EMFT

Mechanical implications of EMFT refer to the mechanical interactions that affect muscle's function and its contribution to joint movement. EMFT has two major mechanical implications that challenge classical muscle mechanics, which attempts to explain isometric muscle force solely based on muscle length but fails to capture the full complexity of muscle function.

(1) *Muscle's relative position is a co-determinant of the isometric muscle force.* Altering a muscle's relative position within the muscle compartment changes the tension and orientation of the epimuscular connections, leading to epimuscular loads with varying amplitudes and directions on different parts of the muscle. As a result, the force distribution across the musculoskeletal system changes, affecting the muscles' force production characteristics. This phenomenon has been demonstrated in rat leg muscles using specifically designed experiments. In these experiments, a muscle was kept at a constant length, and isometric muscle force at the muscle's tendon was measured at different lengths of its synergist [18] and antagonist [19] muscles. These experimental designs excluded the effects of muscle length, as the muscle was kept constant. However, the epimuscular connections were stretched due to changes in the muscle's position relative to other muscular and non-muscular structures. These studies established that, in addition to muscle length, muscle's force exerted at its tendon in an intact muscle compartment is also determined by the muscle's relative position within the compartment.

(2) *Bi-articular muscles exert unequal forces on its tendons.* Another characteristic effect of EMFT is that variations in the amplitude and distribution of epimuscular loads along the muscle belly leads to unequal forces exerted on the proximal and distal tendons of bi-articular muscles. This has been demonstrated in similar experimen-

tal settings, where epimuscular connections left intact. Experiments in the intact rat anterior crural compartments showed substantial proximo-distal differences for various EDL lengths [20]. When the bi-articular rat EDL muscle was kept at a constant length, while its synergist muscles were lengthened [6] and EDL's relative position was altered by equally moving its tendons in one direction [21], proximo-distal force differences were present. These differences exhibit that muscle force has been distributed on the surrounding structures via epimuscular connections. When researchers interfered with the connective tissues surrounding EDL muscle by removing its synergists [7], severing intermuscular connections [22], and performing fasciotomy [23], such effects of EMFT were diminished.

These studies revealed that EMFT plays a crucial role in defining the muscle's force production characteristics.

1.1.3.1 EMFT in the Use of BTX-A in Spasticity Management. Botulinum toxin type-A (BTX-A), is a neurotoxin that paralyzes the muscle fibers [24, 25]. Intramuscular BTX-A injections have been widely used to mitigate the debilitating effects of spasticity by paralyzing muscle fibers in conditions such as cerebral palsy [26]. The intended outcome of BTX-A administration is to alleviate joint stiffness by reducing hypertonia [27] and enhancing joint function [28], thereby improving muscle function [29] in the affected joints. Although BTX-A is effective in reducing hypertonia due to its paralyzing effects, its overall benefits have been questioned in clinical practice.

Animal experiments have provided objective measurements to investigate the impact of BTX-A on muscle mechanics. They revealed that its effects are not limited to muscle force reduction due to paralysis. Muscle paralysis was also accompanied by ECM adaptations, leading to stiffer mechanical properties in the muscle compartment. These tissue adaptations and the altered mechanical properties of the ECM were indicated by increased passive muscle forces [30–32] and elevated collagen content post-injection [30]. Moreover, studies have demonstrated that BTX-A crosses muscle fascia [24] and spread through vascular [33] and axonal [34] pathways, impacting not only

the target muscle but also non-targeted muscles [30, 35–39]. Such spread and changes in the soft tissue properties affect all muscles within the compartment and influences the EMFT mechanism. Specifically, experiments conducted in the rat anterior crural compartment [31, 32] and the rat posterior crural compartment [36, 39] demonstrated that the EMFT mechanism is significantly impacted by BTX-A exposure. However, it is important to note that these experiments were conducted acutely after BTX-A injection, when the muscle fibers were effectively paralyzed but the structural changes in the ECM composition had initiated but were not yet fully set.

The effects of EMFT in the therapeutic use of BTX-A in spasticity management are highly relevant, as evidenced by intraoperative experiments in patients with cerebral palsy. These experiments, in which *in vivo* muscle forces were directly measured at the muscle-tendon junction, revealed important relationships between spasticity and muscle co-activation (e.g., [40]). When individual spastic knee flexor muscles were activated, their force production profiles did not indicate a limited joint range of motion. For example, spastic gracilis, semitendinosus, and semimembranosus muscles did not indicate pathological condition, i.e., peak muscle force production at flexed knee positions [41–43]. However, when these muscles were co-activated with their synergistic and antagonistic counterparts, there was a notable shift in maximum muscle force toward the flexed knee positions [44–46]. These findings provide direct evidence that EMFT, elevated by co-activation, plays a crucial role in the mechanics of spastic muscles.

While the acute EMFT-reducing effects of BTX-A reported in animal studies [32, 39] could be favorable for spasticity management, clinical studies indicated that patients did not consistently benefit from BTX-A-induced improvements in joint range of motion [47, 48] or gait [49–51]. This could be due to the changes in both paralyzing effect of BTX-A and the resulting EMFT mechanism between the muscles exposed over the time course of spasticity management. Therefore, further research is required to investigate the long-term effects of BTX-A on intermuscular mechanics. This can be objectively tested by measuring the aforementioned mechanical implications of EMFT in both target muscle (i.e., BTX-A injected) and non-targeted muscles (i.e., exposed to BTX-A through leakage). Studying these experimental conditions provides opportunity

for understanding BTX-A effects on both the individual muscle level and compartment level (i.e., the mechanical interaction between muscles) to reveal its cumulative effect on spasticity management.

1.1.4 Sensory Implications of EMFT

The sensory implications of EMFT involve the integration of sensory feedback mechanisms in musculoskeletal system due to the intermuscular mechanical interactions. Specifically, this thesis focuses on how mechanoreceptors, particularly muscle spindles (MSs), are influenced by the transmission of local forces through epimuscular connections. While the mechanical aspects of EMFT have been extensively studied, the sensory dimension has not been thoroughly explored. However, understanding sensory dimension complements the mechanical implications of EMFT, facilitating the comprehensive understanding of overall muscle function, coordination and proprioception in health and disease. Because muscle force production and the sensation of the muscle force are not co-dependently occurring events in the mechanically integrated neuromusculoskeletal system (Figure 1.3).

EMFT studies showed that altering the relative muscle position in the compartment imposes changes in the orientation, amplitude, and distribution of epimuscular myofascial loads acting along the muscle length [8, 9]. Variations in epimuscular loads result in variations in strain along the muscle length, as demonstrated using various techniques. Utilizing experimental data obtained from the rat EDL muscle, Yucesoy et al. [7] modeled the interactions between EDL and its synergists, showing that EMFT leads to heterogeneous strain distribution along the muscle fibers. Later, magnetic resonance imaging techniques were employed to test whether the epimuscular loads introduce local length changes in human skeletal muscles. Yaman et al. [13] showed *in vivo* that local length changes are present in lower leg muscles despite no global muscle length changes. Moreover, substantial local length [53, 54] and stiffness [55] changes imposed by epimuscular connections have also been reported. Further studies using various microscopy techniques have provided direct experimental evidence for

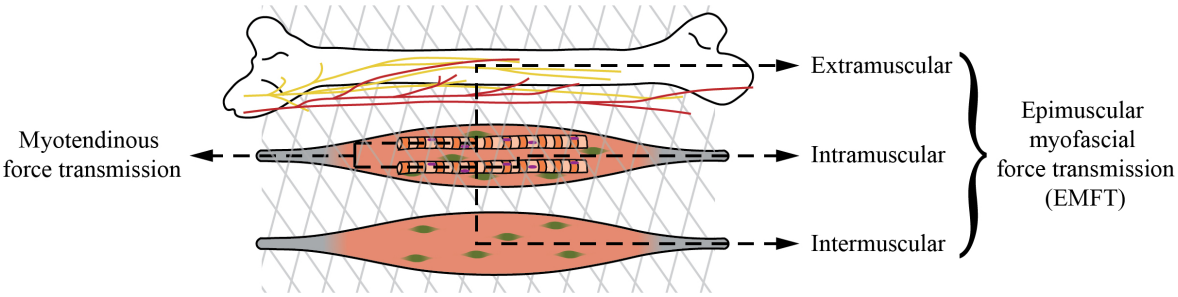

Figure 1.3 Mechanically integrated neuromusculoskeletal system. Muscle force produced in the muscle fibers is primarily transmitted to bones through the myotendinous junction (represented by the gray-colored ends of the muscle), known as myotendinous force transmission. However, a substantial amount of force can also be transmitted through connective tissue connections (depicted as a gray mesh structure). Muscle force transmitted through intramuscular connective tissue is referred to as intramuscular myofascial force transmission. Additionally, muscle force can be transmitted to neighboring non-muscular structures such as neurovascular tracts (shown as red and yellow tracts), termed extramuscular myofascial force transmission, and from one muscle to a neighboring muscle via intermuscular connections, termed intermuscular myofascial force transmission. Together, the transmission of muscle force through muscular and non-muscular structures is referred to as epimuscular myofascial force transmission (EMFT). Because muscle spindles (indicated as green spindle shapes inside the muscles) are mechanically integrated parts of this neuromusculoskeletal system, they are also subjected to EMFT. This figure was inspired from [52].

the variable sarcomere lengths across different muscle regions in both for rat [56, 57] and human [58] skeletal muscles. These studies demonstrated the context-dependent variability of sarcomere lengths. However, how exactly our sensory nervous system is informed about this variability, such as the variability of the muscle force despite being at a certain muscle length, is yet to be discovered.

1.1.4.1 EMFT in Muscle Spindle Function.

MSs are sensory receptors that convey sensory information related to muscle length and velocity to the central nervous system via the peripheral nervous system [59]. They are embedded in the muscle's intramuscular connective tissue [60], and are integral components of muscle bellies, where they are widely distributed [61]. Therefore, they are subject to epimuscular loads through connective tissues that wrap around the muscle intramuscularly and connect the muscle to its surroundings epimuscularly [17]. Thus, muscle force generation and the sensation of this force are interconnected processes. During force generation, mechanoreceptors, including MSs, adapt the muscle's output to enhance movement accuracy and efficiency [59]. This is achieved by integrating the neural information in

the sensorimotor system [62,63], with mechanoreceptors converting mechanical stimuli into neural signals [64].

Each MS comprises a group of intrafusal muscle fibers, distinct from the extrafusal fibers, and is encapsulated within a connective tissue sheath [65]. These intrafusal fibers run parallel to the extrafusal muscle fibers and are innervated by sensory neurons (group Ia and II afferents) and gamma motoneurons. Activation of stretch-sensitive ion channels on these sensory receptors, through the elongation or compression of intrafusal fibers, facilitates mechanotransduction, translating mechanical changes into neural signals [66]. Through this mechanism, motor actions shape into their context-dependent sensory representations in the central nervous system [67]. A fusion of parallel processing sensory units enables the active sensation of bodily movement. This complex interplay between muscle structure and function highlights the role of MSs in motor control and proprioception [59, 68, 69].

EMFT plays a crucial role in the muscle's output variability, influenced by its relative position. MSs, as primary receptors for muscular activity and movement, must detect EMFT to discern the purpose of the movement and accurately represent the muscle's contribution to desired actions. Moreover, their widespread distribution suggests that they function not only as global receptors, but also as local sensors, allowing the detection of mechanical interactions between the muscle fibers and ECM, as well as the muscle and its surroundings. Early studies have shown MS sensitivity to minute forces in the scale of single motor units [70], indicating their capability and role in sensing local length changes rather than solely overall muscle length. However, traditional studies using isolated receptor and muscle preparations, which involve the removal of epimuscular connections, do not fully capture the effects of varying epimuscular loads due to EMFT on MS neural feedback.

The impact of EMFT on MS feedback have been previously proposed [17] and studied. Researchers showed that imposing epimuscular loads by stretching the synergistic [71] and antagonistic [72] muscles changes the neural response in muscle afferent fibers. However, these studies do not include active muscle conditions, which more

accurately represent daily movements. Additionally, co-activation can eliminate slackness in connective tissue linkages between muscles and their surroundings [73], and co-activation has been directly demonstrated to increase EMFT [74]. These previous studies underlined the need for fundamental studies to better understand the effects of EMFT on MS neural feedback between activate muscles.

1.2 Thesis Outline

1.2.1 Aims

The concept of EMFT provides a holistic perspective on neuromuscular mechanics, emphasizing the interplay between muscles, connective tissues, and sensory receptors. This thesis investigated the impact of EMFT on both the mechanical and sensory aspects of muscle function. The mechanical dimension was explored with a particular focus on the complex effects of BTX-A exposure on the mechanical interactions between synergistic muscles. The research extended to the sensory dimension by revealing the fundamental effects of EMFT on muscle spindle neural feedback. The goal was to enhance understanding of EMFT's mechanical implications in the context of BTX-A use for spasticity management and to lay the groundwork for exploring its contribution on muscle spindle function in active muscles. This perspective highlighted the multifaceted role of EMFT in muscle function by integrating mechanical and sensory insights.

Three sets of animal experiments were planned in the scope of this thesis work. Specific aims were:

1. To assess how BTX-A-induced partial paralysis affects the EMFT mechanism and muscle force production characteristics of rat anterior crural compartment muscles in the long-term, particularly the targeted tibialis anterior muscle (i.e., the muscle injected with BTX-A) and the non-targeted bi-articular extensor digitorum longus and extensor hallucis longus muscles (i.e., those exposed to BTX-A via leakage).

2. To identify, for the first time, MS afferents from the masseter and temporalis muscles projecting to the trigeminal mesencephalic nucleus in mice, and to test whether MSs sense synergistic muscle activity mediated by EMFT.

Animal experiments were conducted using a range of techniques tailored to the study's objectives. *In vivo* muscle force measurements, nerve stimulation, and biochemical analysis were employed in rat experiments to investigate the mechanical implications of EMFT. Microsurgery, intramuscular electrical stimulation, *in vivo* electrophysiology, and histological analysis were used in mice experiments to examine the sensory implications of EMFT on MS feedback.

1.2.2 Overview

Chapter 2 *"BTX-A Affects Individual Muscle Mechanics but Sustains EMFT in the Long-Term"* investigated long-term changes in the EMFT mechanism and muscle force production in the rat anterior crural compartment following BTX-A administration, addressing the first aim of the thesis. The mono-articular tibialis anterior muscle was lengthened to examine the effects of BTX-A on its force production profile and EMFT by assessing the changes in muscle relative position on the forces of the extensor digitorum longus and extensor hallucis longus muscles. This study demonstrated that BTX-A-induced partial paralysis was sustained together with narrowed length range of active force exertion in the injected tibialis anterior and altered force production characteristics of all exposed muscles. However, BTX-A altered but—unlike previous acute reports—did not diminish EMFT. The findings provide valuable insights into changes in the EMFT mechanism during the time course of BTX-A exposure, with potential implications for spasticity management strategies in the clinical settings.

Chapter 3 *"Long-Term BTX-A Effects on Non-targeted Bi-Articular Muscle Mechanics and EMFT"* further explored the first aim of the thesis by testing the effects of EMFT between partially paralyzed rat anterior crural compartments imposed by long-term BTX-A exposure. The effects on proximal and distal forces were assessed

in the non-targeted bi-articular rat extensor digitorum longus muscle (i.e., exposed to BTX-A via leakage after the injection into tibialis anterior). It was shown that BTX-A exposure significantly altered the length range of active force exertion and passive forces, but these changes differed when measured at the distal and proximal tendons. However, no significant effects of BTX-A exposure on EMFT were observed. The results indicated that while the mechanics of the muscle spanning both joints were adversely affected, its mechanical interaction with its synergists remained unchanged. This study has important implications for BTX-A's effects on bi-articular muscles, potentially influencing the effectiveness of spasticity management strategies.

Chapter 4 *"Muscle Spindles Projecting to Mouse Me5 Sense Synergistic Muscle Activity Through EMFT"* focused on the second aim of thesis by exploring the sensory implications of EMFT. Mechanical and electrical stimuli were used to investigate how synergistic muscle activity affects MS sensory feedback. Mechanical conditions, provided muscle compartment intact, were used to identify MS afferents projecting to the mouse trigeminal mesencephalic nucleus for the first time in the literature, establishing the mouse as a viable model for studying MS function in this muscle group. It was then demonstrated that, selective stimulation of the synergistic temporalis muscle significantly increased sensory feedback from masseter MSs, through intermuscular myofascial interactions. The outcome of this work enhanced the contribution of EMFT on sensorimotor integration at the periphery level and addressed mechanisms mediated by MSs.

In Chapter 5 *"General Discussion"*, the key findings of this thesis on the mechanical and sensory aspects of EMFT were summarized, integrated, and discussed to draw holistic conclusions. This chapter highlighted the clinical and practical implications of this research and provided guidance for future studies.

1.3 List of Publications Resulting from the Thesis

1.3.1 Journal Articles

Kaya, C. S., **Yılmaz, E. O.**, Akdeniz-Doğan, Z. D., & Yucesoy, C. A. (2020). Long-Term Effects With Potential Clinical Importance of Botulinum Toxin Type-A on Mechanics of Muscles Exposed. *Frontiers in Bioengineering and Biotechnology*, 8, 738.

Yılmaz, E. O., Kaya, C. S., Akdeniz-Doğan, Z. D., & Yucesoy, C. A. (2021). Long-term BTX-A effects on bi-articular muscle: Higher passive force, limited length range of active force production and unchanged intermuscular interactions. *Journal of Biomechanics,* 126 (July).

1.3.2 Conference Proceedings

Yılmaz, E. O., Kaya, C. S., Akdeniz, Z. D., & Yucesoy, C. A. (2018, September). Comparison of short-term and long-term effects of BTX Type-A on mechanics of the rat tibialis muscle. Paper presented at the *International Biomechanics Congress*, Eskişehir, Turkey.

Kaya, C. S., **Yılmaz, E. O.**, Akdeniz, Z. D., & Yucesoy, C. A. (2019, July). Previously reported unintended acute botulinum toxin type-A effects persist also in the long-term. Paper presented by the first author at the *European Society of Biomechanics Conference*, Vienna, Austria.

2. BTX-A AFFECTS INDIVIDUAL MUSCLE MECHANICS BUT SUSTAINS EMFT IN THE LONG-TERM

2.1 Introduction

Epimuscular myofascial force transmission (EMFT) refers to the transfer of muscle force to surrounding muscular and non-muscular structures through connective tissues [8, 9]. A characteristic effect of EMFT is that despite a muscle is kept at a constant length, the lengthening of its synergist changes the force measured at its tendon, due to the changes in the distribution and orientation of epimuscular loads [75]. This challenges the classical view that attributes force production solely to muscle length. Yet, muscle's relative position within the muscle compartment is a co-determinant of its isometric muscle force, mediated by force transmission between muscle fibers and epimuscular connections with varying loads and orientations along them [7]. EMFT substantially influences the length-tension relationship in muscles, with high relevance to neuromuscular conditions.

Intraoperative experiments conducted in spastic muscles of the patients with spastic cerebral palsy showed important implications for the role of EMFT (e.g., [40]. Direct muscle force measurements at the tendons of the spastic hamstring muscles showed that when they are activated individually, they did not display apparent pathological conditions, i.e., they did not show a peak muscle force at a narrow knee joint angle [41–43]. However, when activated simultaneously together with their synergists and antagonists, the knee angle corresponds to the peak force shifted towards flexed knee angles [44–46]. Additionally, Tedroff et al. [76, 77] demonstrated that unintended co-activation of antagonistic and synergistic lower leg muscles occurs more frequently in children with spastic cerebral palsy than in typically developed children. These studies suggest that EMFT is an important factor contributing to the pathophysiology in conditions like spastic cerebral palsy, warranting attention in spasticity management strategies [17, 78].

Botulinum toxin type-A (BTX-A) is widely used in clinical settings to manage muscle spasticity observed in disorders such as cerebral palsy [27, 79, 80], spinal cord injuries [81, 82], multiple sclerosis [83, 84], and stroke [85, 86]. BTX-A therapy aims to reduce muscle tone [87] by temporarily paralyzing muscles, thereby lowering passive resistance at joints [88] and potentially improve the range of motion [89]. Animal experiments provided insights into how BTX-A affects muscle mechanics exposed muscles. Acute observations (i.e., five-days post-injection) have shown that BTX-A does not improve the muscle's length range of force exertion (l_{range}) and increases the passive forces of the target (i.e., BTX-A injected) tibialis anterior muscle [31]. Moreover, BTX-A also spreads through muscle fascia [24]. This diffusion changes the mechanical properties of other muscles exposed [30,31,35,36,38,39], modifying the length-force characteristics of both targeted (i.e., BTX-A injected) and non-targeted (i.e., exposed to BTX-A via diffusion) muscles. Furthermore, BTX-A exposure changes the composition of muscular and connective tissues [39], altering muscle force production characteristics.

Understanding the mechanical interactions between muscles is crucial, as they are clinically highly relevant and can impact the overall movement and limb stability in spasticity management. Animal experiments have provided valuable insight into how BTX-A affects the EMFT mechanism among exposed muscles. Studies in the intact rat anterior and posterior crural compartment muscles [31, 32, 36, 39] showed that acute exposure to BTX-A alters the inter-synergistic EMFT mechanism. Specifically, EMFT-diminishing effects of BTX-A reported in some animal studies [32, 39] could be advantageous for spasticity management considering clinical findings demonstrating abnormal and unintentional coupling of spastic muscles [44–46, 76, 77]. However, whether this effect is persistent in the long-term is not known. Therefore, it is critical to explore the mechanics of BTX-A-exposed muscles over the course of spasticity management in the context of EMFT.

The present study aimed to investigate the long-term effects of BTX-A on the mechanics of the rat anterior crural compartment muscles, with a particular focus on its effects on EMFT. We hypothesized that in the long-term, (1) BTX-A alters the force production characteristics of the injected tibialis anterior muscle, and the

other muscles exposed. Consequently, we expect that (2) BTX-A diminishes EMFT among the exposed muscles. These findings will provide insights into the mechanical implications of EMFT between partially paralyzed muscles and help inform BTX-A management strategies in clinical settings.

2.2 Materials and Methods

2.2.1 Subjects

All surgical and experimental procedures were approved by the Committee on the Ethics of Animal Experimentation at Boğaziçi University. Male Wistar rats were used in this study, divided into two groups: BTX-A (n = 7; body mass 394.7 ± 29.0 g and 404.3 ± 34.3 g at the times of injection and experiment, respectively) and control (n = 7; mean ± SD: body mass 386.3 ± 36.5 g and 406.9 ± 16.8 g at the times of injection and experiment, respectively).

A mild sedation was imposed using intraperitoneal ketamine (1 mg/kg). Subsequently, a region within approximately 15 mm of the patella's center was shaved and marked. The TA muscle was located by palpation after positioning the ankle in maximal plantarflexion and the knee at approximately a 90° angle. A second marker was placed 10 mm distal along the tibia. A line was drawn between the two markers, and the injection site was determined 5 mm lateral to the second marker over the TA muscle. The depth of the TA and the thickness of the skin at this site were approximately 5-5.5 mm and 0.7-1 mm, respectively. All injections were made exclusively into the superficial half of the TA, to a depth of 3 mm.

A 100 U vial of vacuum-dried BTX-A complex (BOTOX; Allergan Pharmaceuticals, Westport, Ireland) was reconstituted with 0.9% saline solution. The BTX-A group received a one-time intramuscular injection of BTX-A, with a total dose of 0.1 U in a 20 μl volume. The control group received a one-time intramuscular injection of the same volume of 0.9% saline solution. All injections were performed one month before

testing. The animals were housed separately in standard cages, in a temperature-controlled room with a 12-hour dark-light cycle and were allowed to engage in normal activities until the day of the experiment.

2.2.2 Surgical Procedures

The animals were anesthetized with an intraperitoneal injection of urethane solution (1.2 ml of 12.5% urethane per 100 g of body weight). Additional doses, up to a maximum of 0.5 ml, were administered when needed. After the experiments, the animals were euthanized with an overdose of the urethane solution.

To prevent hypothermia, they were kept on a heated pad (Homoeothermic Blanket Control Unit; Harvard Apparatus, Holliston, MA, United States) during surgery and data collection. The body temperature was maintained at 37°C by adjusting the pad's temperature using a feedback system connected to a rectal thermometer.

During the procedure, the skin and the biceps femoris muscle of the left hindlimb were removed. After exposing the anterior crural compartment, only a small distal fasciotomy was performed to remove the retinaculae (transverse crural ligament and crural cruciate ligament). Consequently, the connective tissues of the muscle bellies within the compartment (the tibialis anterior (TA), extensor digitorum longus (EDL), and extensor hallucis longus muscles (EHL)) remained intact.

A reference position was established with a knee joint angle of 120° and an ankle angle of 100°. This position corresponds to the knee and ankle positions the rat naturally attains during the stance phase of gait [90]. While maintaining this reference position, the following steps were taken. The four distal tendons of the EDL muscle were tied together using silk thread. Matching markers were placed on the distal tendons of the EDL, TA, and EHL muscles, as well as on a fixed point on the lower leg. Subsequently, the distal tendons of the EDL, TA, and EHL muscles were cut as distally as possible.

The femoral compartment was exposed for two main purposes: to access the proximal tendon of the EDL and to expose the sciatic nerve. A small piece of the lateral femoral condyle was kept attached while the tendon was cut from the femur. The sciatic nerve was then carefully dissected free from surrounding tissues. After severing all nerve branches to the muscles in the femoral compartment, the sciatic nerve was cut as proximally as possible.

The proximal tendon of the EDL, the tied distal tendons of the EDL, and the distal tendons of the TA and EHL muscles were then sutured to four separate Kevlar threads to connect them to force transducers.

2.2.3 Experimental Setup

To mount the animal in the experimental setup (Figure 2.1A), the following procedure was followed: (1) To prevent obstruction of the Kevlar threads connecting the distal tendons to their force transducers, the ankle was positioned at maximum plantar flexion (180°) and the foot was secured in a foot clamp. (2) The femur was fixed in a femur clamp to set the knee angle at 120°. (3) Ensuring proper alignment with the muscle's line of pull, each Kevlar thread was connected to a separate force transducer (BLH Electronics Inc., Canton, MA, United States). (4) The distal end of the sciatic nerve was placed on a bipolar silver electrode (Figure 2.1B).

2.2.4 Experimental Conditions and Procedure

Throughout the experiment, the room temperature was maintained at 26°C. To prevent dehydration, muscles and tendons were regularly irrigated with isotonic saline. The distal and proximal tendons of the EDL and the distal tendon of the EHL muscles were always kept in their reference positions, ensuring their lengths remained unchanged. However, the TA was adjusted to various muscle-tendon complex lengths by repositioning its force transducer. The isometric forces of all muscles were measured

simultaneously at each TA length. Measurements began at the active slack length of the TA and were taken in 1 mm increments until reaching 2 mm beyond its optimum length. The lengths of the TA muscle-tendon complex are expressed as deviations from its active slack length ($\Delta l_{mt\ TA}$). After setting the TA to the target muscle length, all studied muscles were maximally activated using a constant current of 2 mA (square pulse width 0.1 ms) delivered to the sciatic nerve (STMISOC; BIOPAC Systems, Goleta, CA, United States) with the following stimulation protocol: (1) two twitches were evoked, (2) 300 ms after the second twitch, the muscles were tetanized with a pulse train of 400 ms at a frequency of 100 Hz, and (3) 200 ms after the tetanic contraction, another twitch was evoked. Following each completion of this protocol, a recovery period of 2 mins was observed for all muscles, during which the TA was kept near its active slack length, while the lengths of the EDL and EHL remained unchanged.

2.2.5 Biochemical Analysis

In a separate set of male Wistar rats, the effects of BTX-A on intramuscular connective tissue content were assessed. The rats were divided into two groups (mean ± SD body mass): control (n = 6; 404.3 ± 31.0 g) and BTX-A (n = 6; 413.3 ± 46.2 g).

The collagen content of each muscle was quantified using a colorimetric analysis of hydroxyproline content [91] one month after the injections. Following the surgical procedures to expose the anterior crural muscles, biopsies were rapidly collected post-euthanasia. To ensure sample purity, all tendinous materials were carefully removed. The muscle biopsies were then flash-frozen in liquid nitrogen and stored at -80°C until analysis within four weeks. Each muscle sample was weighed and hydrolyzed at 130°C for 12 hours in 5 N HCl. The hydrolyzate samples were oxidized at room temperature with a chloramine-T solution for 25 mins. Impurities were removed by toluene extraction, and the remaining aqueous layer containing hydroxyproline products was heated in boiling water for 30 mins to convert them to pyrrole. The pyrrole reaction product was then extracted with toluene, and the final solution was mixed with Ehrlich's

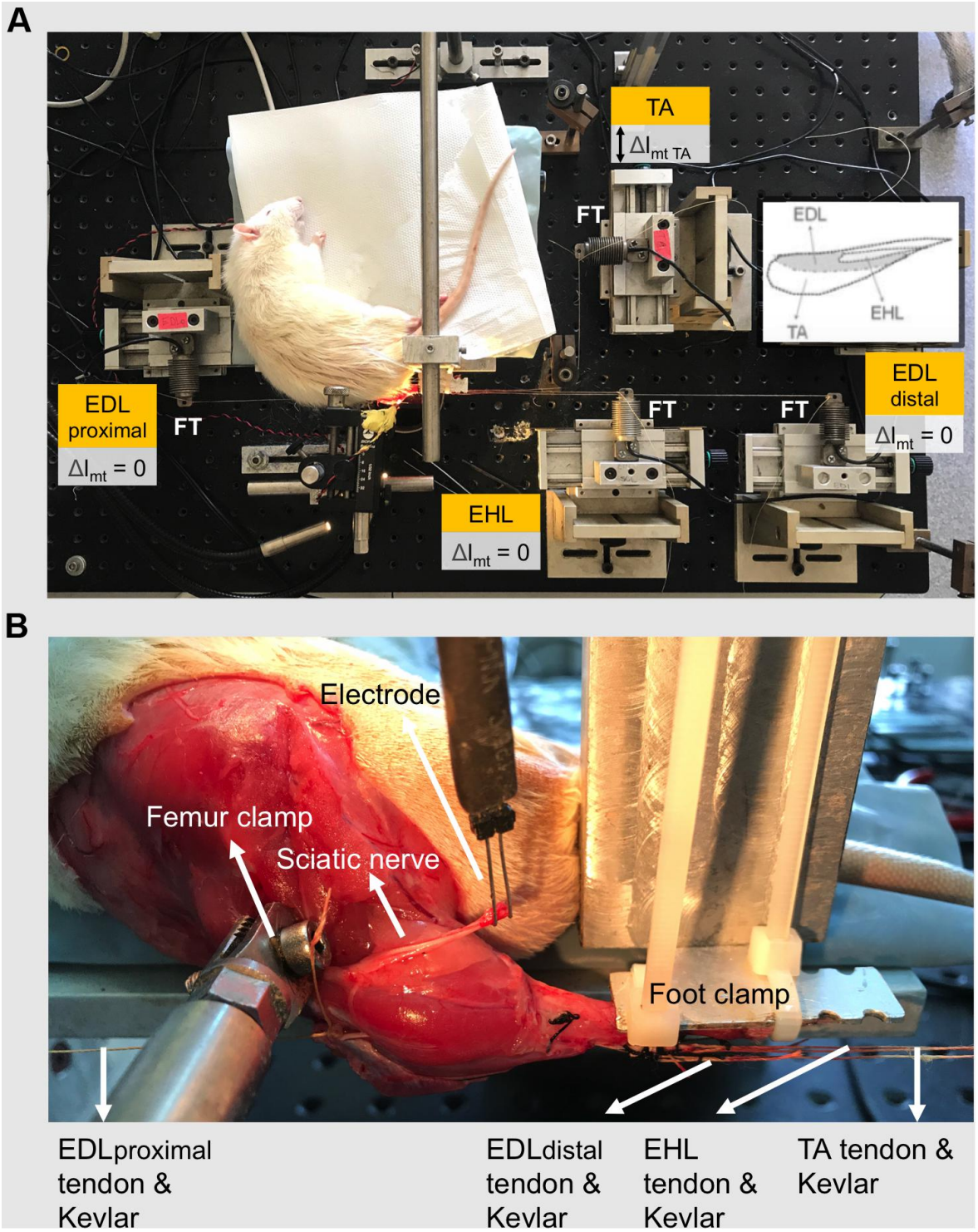

Figure 2.1 The animal experimental set-up. (A) The distal tendons of the tibialis anterior (TA) and extensor hallucis longus (EHL) muscles, along with the proximal and distal tendons of the extensor digitorum longus (EDL) muscle, were individually connected to separate force transducers using Kevlar threads. Throughout the experiment, the muscle-tendon complex lengths of the EDL and EHL muscles were maintained at a constant length. Only the TA muscle was gradually lengthened ($\Delta l_{mt\ TA}$) to increasing lengths, where isometric contractions were measured. The lengthening process, indicated by a double-headed arrow, began from the muscle's active slack length, increasing in 1-mm increments by adjusting the position of the TA force transducer. An inset shows the relative sizes and positions of the muscles in the anterior compartment of the lower leg. (B) The reference joint angles for the experiment were set at 120° for the knee and 100° for the ankle. The femur and foot were stabilized using metal clamps, and the distal end of the sciatic nerve was positioned on a bipolar silver electrode.

reagent for 30 mins. The absorbance of the samples was measured in triplicate at 560 nm using a UV-Visible spectrophotometer (UV1280; SHIMADZU, Kyoto, Japan).

2.2.6 Data Processing

The capacity of muscular tissues to resist mechanical stress at a specific muscle-tendon length is indicated by the muscle force in an unstimulated state, known as passive muscle force (F_p). Using force-time traces obtained from experiments: (i) F_p was measured 100 ms after the second twitch (Figure 2.2). (ii) The total muscle force was determined as the average force (over a 200 ms interval, 150 ms after inducing tetanic stimulation) during the tetanic plateau. The active muscle force (F_a) at each muscle-tendon complex length was calculated by subtracting F_p from the total muscle force.

A least squares criterion was applied to fit the data for F_p and F_a using a polynomial function (Eq. 3.1).

$$y = a_0 + a_1 x + a_2 x^2 + \cdots + a_n x^n \tag{2.1}$$

In the analysis, the isometric muscle forces (i.e., F_p or F_a) are represented by y, while the muscle-tendon complex length is represented by x. The coefficients $a_0, a_1, a_2, \ldots, a_n$ were determined during the fitting process.

A one-way analysis of variance (ANOVA) was used to determine the polynomial order [92]. The lowest order polynomial that still significantly improved the description of changes in muscle force data as a function of muscle-tendon complex length was selected. These polynomials were used to calculate the mean and standard deviations (SD) of data: for each muscle studied, muscle forces at different TA muscle-tendon complex lengths were obtained. The forces were averaged for each TA muscle-tendon complex length to determine the muscle force (mean ± SD) for the control and BTX-A groups.

Muscle length-force characteristics were assessed using four key determinants: (1) Muscle optimal force, the maximum isometric force exerted by an active muscle, indicating its force production capacity. (2) Muscle optimum length, the muscle length at which the optimal force (i.e., the maximum muscle force observed on the generic muscle length-force curve) is achieved. (3) Muscle active slack length, the shortest length at which an active muscle can still exert a non-zero force. (4) Muscle length range of force exertion, the range from active slack length to optimum length, indicating movement capability within the joint's potential range of motion.

These key determinants were processed using the fitted polynomials to determine the optimal TA force, the corresponding optimal muscle length, and the TA active slack length. The TA length range of active force exertion (l_{range}) was determined as the length range between muscle active slack length and muscle optimum length.

Hydroxyproline analysis quantified changes in intramuscular collagen content for muscles exposed to BTX-A. Using measured absorbance values of muscle samples, hydroxyproline contents of individual muscles were determined based on a standard regression curve (identifying known hydroxyproline amounts and their measured absorbance values) and expressed as μg hydroxyproline per mg of muscle tissue wet weight. The hydroxyproline content was converted into intramuscular collagen content using a constant (7.46), representing the number of hydroxyproline residues in one collagen molecule [93].

2.2.7 Statistical Analyses

After applying the Shapiro-Wilk test to check for normal distribution in the l_{range} data of the TA, either an unpaired t-test or the Mann-Whitney U test was used to assess the effects of BTX-A injection on this metric.

A two-way ANOVA for repeated measures (factors: TA muscle-tendon complex length and animal group) was separately conducted for the forces of each muscle. If

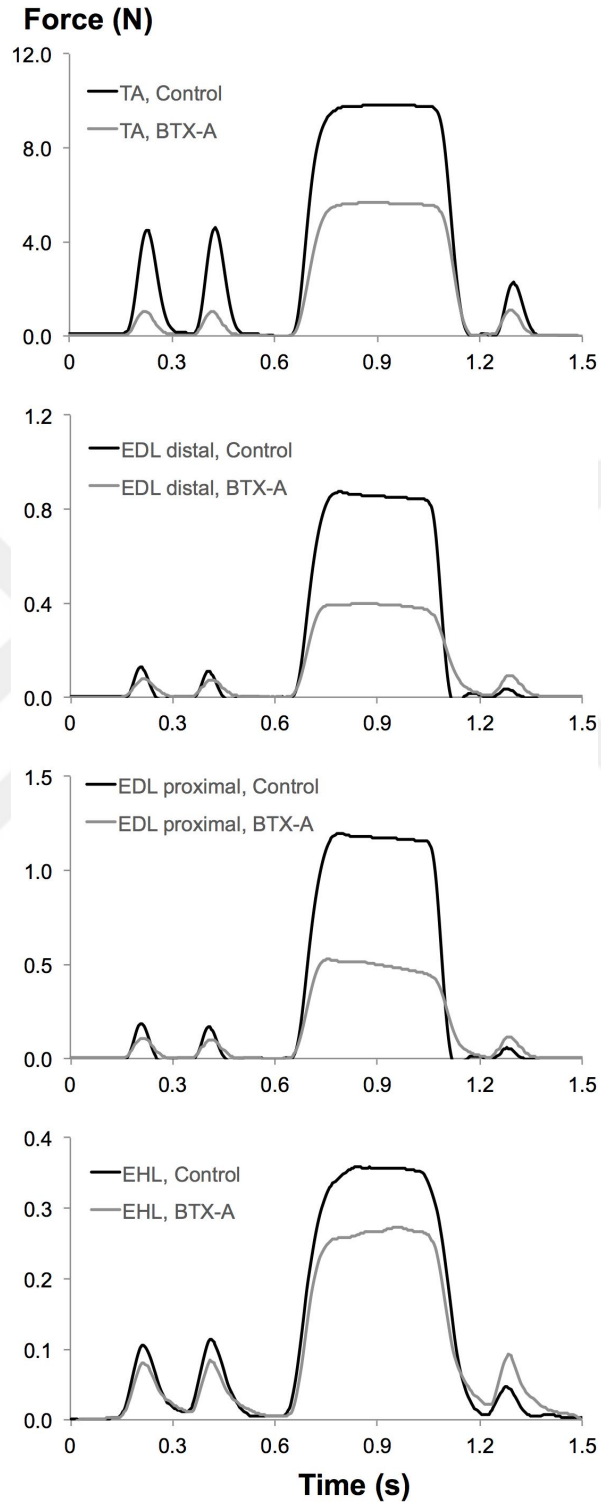

Figure 2.2 Representative force-time traces recorded at muscle tendons. Black traces represent the control group, while gray traces represent the BTX-A group. From the top to the bottom panels, the superimposed force-time traces of the TA, EDL distal, EDL proximal, and EHL muscles were recorded at the optimal length of the TA muscle.

significant main effects were identified, Bonferroni post hoc tests were performed to pinpoint specific within-factor differences.

The forces from both groups were normalized to their optimum length. The decrease in muscle active force was calculated per TA muscle-tendon complex length by comparing the mean force difference between the control and BTX-A groups, expressed as a percentage of the control group's mean force. The Spearman's rank correlation coefficient (ρ) was used to determine if reductions in TA active forces due to BTX-A injection correlated with TA muscle-tendon complex length, with significance set at $P < 0.05$.

The Shapiro-Wilk test was also used to assess the normality of the collagen content data. The collagen amount in the BTX-A group was compared to the control group using either an unpaired t-test or the Mann-Whitney U test, with differences considered significant at $P < 0.05$.

2.3 Results

2.3.1 Effects of BTX-A on Muscular Mechanics

2.3.1.1 TA Force-Length Characteristics. ANOVA (factors: TA length and animal group) revealed significant main effects on TA active forces and a significant interaction. Post hoc testing showed significant effects of BTX-A for most muscle lengths ($\Delta l_{mt\ TA} \geq$ -7 mm). TA active force reductions (e.g., 75.2%, 48.3%, and 52.8% at $\Delta l_{mt\ TA} =$ -7 mm, $\Delta l_{mt\ TA} = 0$ mm, and $\Delta l_{mt\ TA} = 2$ mm, respectively) were inversely correlated with increasing TA muscle length ($\rho =$ -0.94, $P < 0.001$). The l_{range} of the BTX-A group (8.56 ± 2.05 mm) was significantly narrower by 22.9% compared to the control group (11.10 ± 1.58 mm). ANOVA also showed significant main effects on TA passive forces, but no significant interaction. Compared to the control group, the passive forces in the BTX-A group were on average 12.3% higher (Figure 2.3).

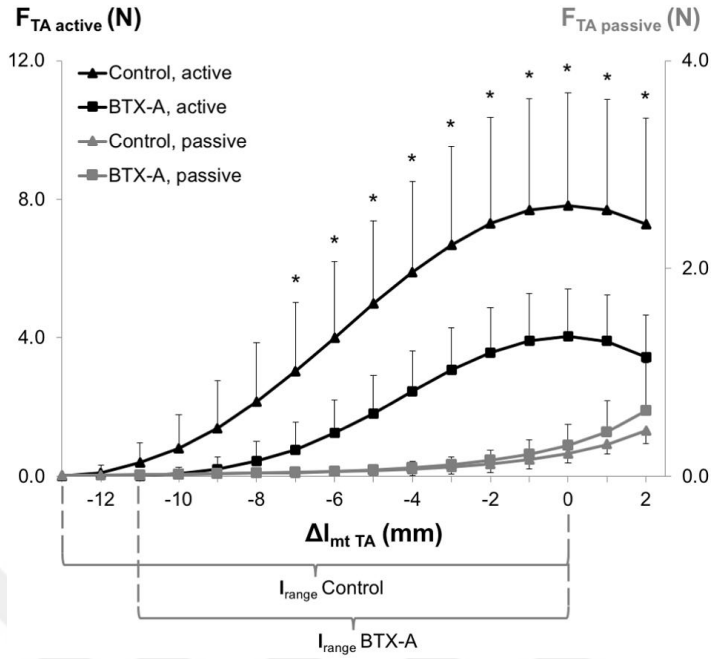

Figure 2.3 TA muscle forces as a function of TA muscle-tendon length. Active and passive muscle forces are presented as mean values with standard deviations for both the control and BTX-A groups. The length of the TA muscle-tendon complex is expressed as a deviation from its optimum length ($\Delta l_{mt\ TA}$). Significant differences in the TA active force between the control and BTX-A groups, identified using the Bonferroni post hoc test, are marked with an asterisk (*).

2.3.1.2 EDL Forces. ANOVA showed a significant effect of animal group on EDL active and passive forces, both distally and proximally, but no significant effects of TA length or interaction. BTX-A caused significant active force decreases (on average by 66.8% distally and 55.4% proximally) and passive force increases (on average by 62.5% distally and more than twice proximally) compared to the control group (Figures 2.4A, B).

ANOVA also showed significant main effects of both factors on the EDL proximo-distal active force differences (Figure 2.4C), but no significant interaction. In the control group, positive and negative proximo-distal active force differences were observed (distal EDL forces were higher than proximal ones for $\Delta l_{mt\ TA} \leq$ -7 mm and vice versa at longer TA lengths). For the BTX-A group, EDL proximal forces were higher than distal forces for most TA lengths ($\Delta l_{mt\ TA} \geq$ -11 mm). Bringing the TA to longer lengths significantly changed the proximo-distal active force difference measured at the shortest muscle length ($\Delta l_{mt\ TA}$ = -13 mm) for $\Delta l_{mt\ TA} \geq$ -8 mm and $\Delta l_{mt\ TA} \geq$ -9 mm for the control and BTX-A groups, respectively.

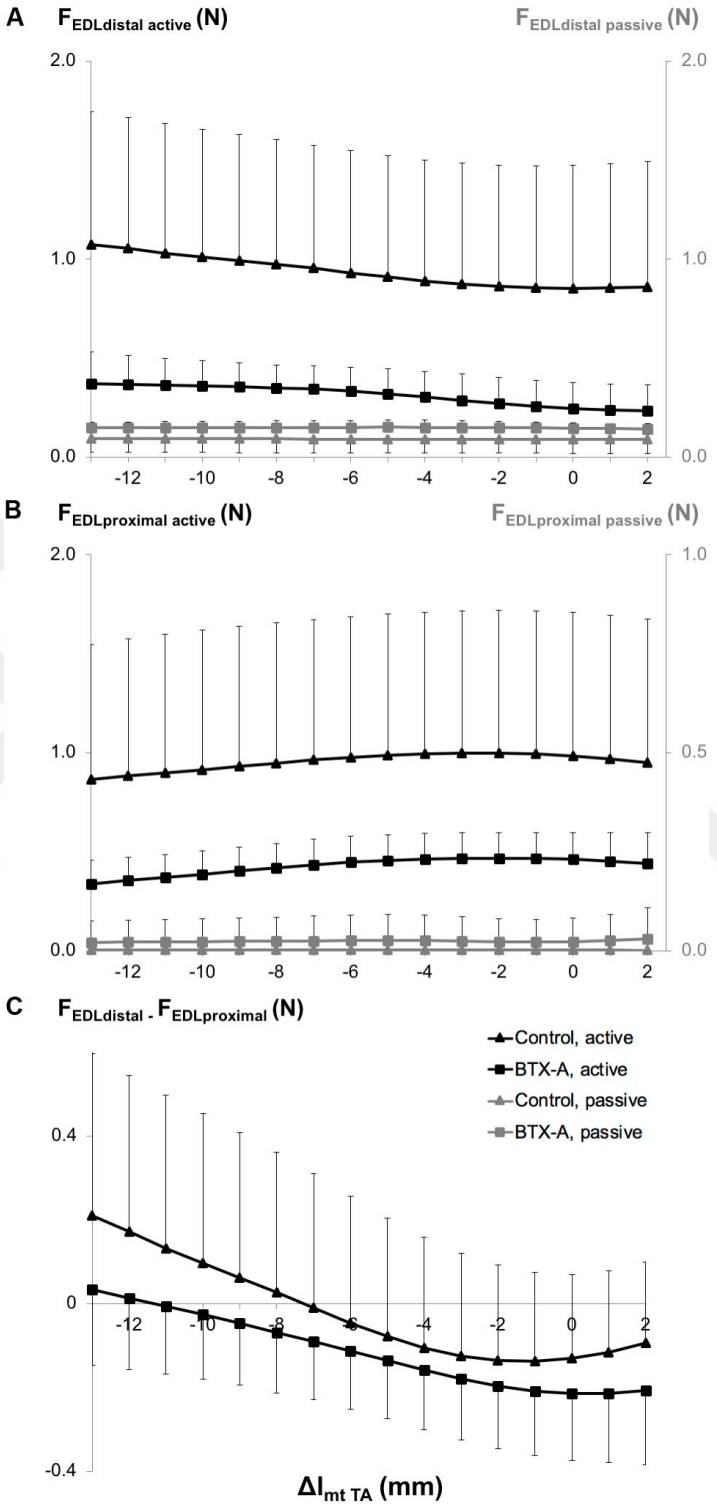

Figure 2.4 EDL muscle forces as a function of TA muscle-tendon length. The active and passive forces of the EDL were measured from (A) the distal tendon, (B) the proximal tendon, and (C) the difference in active force between the proximal and distal tendons of the EDL ($F_{EDLdistal}$ - $F_{EDLproximal}$). Isometric muscle forces are presented as mean values with standard deviations for both the control and BTX-A groups. The length of the TA muscle-tendon complex is expressed as a deviation ($\Delta l_{mt\ TA}$) from its optimum length.

2.3.1.3 EHL Forces. ANOVA showed significant main effects of both factors on EHL active forces, but no significant interaction, and only a significant effect of BTX-A on passive forces. BTX-A caused a significant active force decrease (on average by 28.8%) and passive force increase (on average by more than twice) compared to the control group (Figure 2.5).

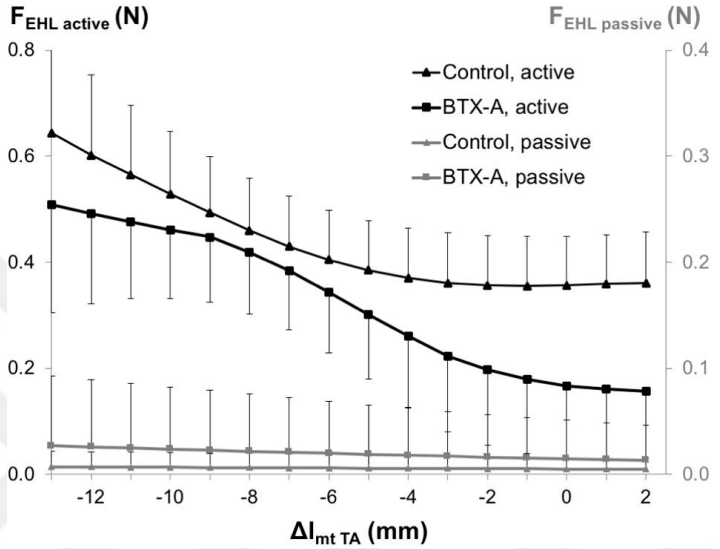

Figure 2.5 EHL muscle forces as a function of TA muscle-tendon length. Active and passive muscle forces are presented as mean values with standard deviations for both the control and BTX-A groups. The length of the TA muscle-tendon complex is expressed as a deviation ($\Delta l_{mt\ TA}$) from its optimum length.

2.3.2 Changes in Intramuscular Connective Tissue Content Due to BTX-A

For both the injected TA muscle and the non-injected EDL and EHL muscles, the intramuscular connective tissue contents (Figure 2.6) were significantly higher in the BTX-A group compared to the control group (BTX-A group: 21.61 ± 3.56, 14.94 ± 4.82, and 14.82 ± 4.32 μg collagen/mg muscle; Control group: 7.49 ± 2.08, 6.55 ± 2.55, and 7.05 ± 3.81 μg collagen/mg muscle; $P = 0.005$, 0.006, and 0.029 for the TA, EDL, and EHL, respectively). Additionally, muscle masses in the BTX-A group were lower than those of the control group (BTX-A group: 0.35 ± 0.04, 0.10 ± 0.01, and 0.01 ± 0.003 g; Control group: 0.65 ± 0.04, 0.16 ± 0.03, and 0.01 ± 0.01 g; $P < 0.001$, $P = 0.005$, and $P = 0.198$ for the TA, EDL, and EHL, respectively).

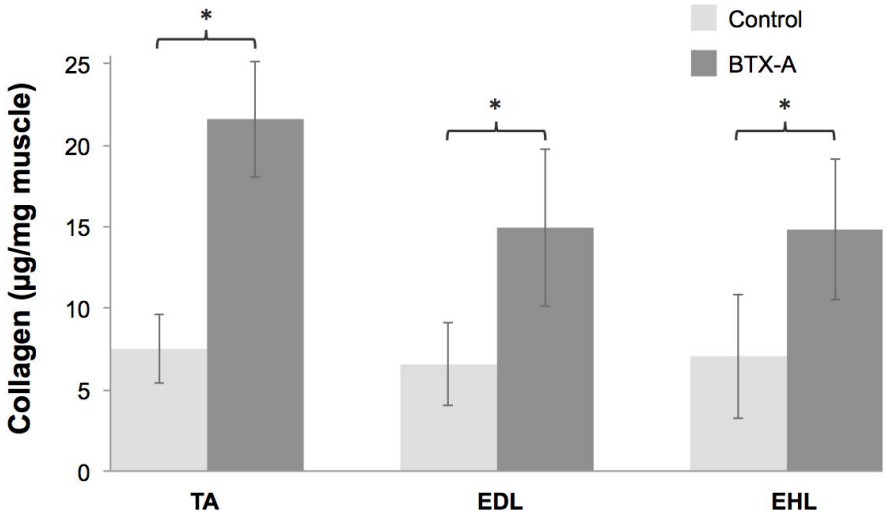

Figure 2.6 Collagen concentration in the TA, EDL, and EHL muscles. Collagen content for control (light gray bars) and BTX-A (dark gray bars) groups were shown. Data are presented as mean ± standard deviation. Significant differences between the control and BTX-A groups are marked with an asterisk (*).

2.4 Discussion

Our findings indicated that BTX-A, consistent with previous acute effects [31], significantly increases passive forces of all the muscles exposed. However, unlike earlier results, a significant decrease in the l_{range} of the targeted TA muscle was observed in the long-term. Moreover, BTX-A exposure through leakage affected the forces of the non-targeted EDL and EHL muscles resulting in a significant decrease in active forces and a significant increase in passive forces in both. Therefore, we accepted hypothesis (1) that BTX-A alters the force production characteristics of all anterior crural compartment muscles in the long-term. Previous acute reports also showed that BTX-A injections into the TA muscle caused EMFT effects to disappear for EDL muscle [31, 32]. In the present study, however, despite the changes in muscle tissue composition and observed muscle atrophy in all muscles supporting the alterations in EMFT, the findings do not indicate diminished EMFT due to BTX-A. Thus, hypothesis (2) was rejected.

2.4.1 Altered Mechanics of Muscles Exposed to BTX-A

Finite element modeling has been used to explore the effects of BTX-A on the mechanics of exposed muscles [94]. In their model, the researchers modeled the mechanical interactions between the BTX-A induced partially paralyzed muscle, in which some muscle fibers were inactive (representing paralyzed muscle fibers that do not shorten), and extracellular matrix (ECM) that wraps around the muscle fibers. They showed that the restricted shortening of the inactive muscle fibers also limits the shortening of active muscle fibers through muscle fiber-ECM interactions [8,37], an effect termed as the longer sarcomere effect (please see Appendix A for the illustration). Such effect results in the sarcomeres reaching their peak force production at a shorter length, in turn causing the muscle's optimum length to shift to a shorter length. They predicted that this effect would be more pronounced after long-term BTX-A exposure, which was characterized by increased ECM stiffness over time [95]. This potentially explains the narrowed l_{range} of the TA muscle due to BTX-A injection observed in the current results of this study, in contrast to previous findings reported acutely [31]. Increased passive forces, muscle atrophy, and higher collagen content, which is the primary load-bearing component of the ECM, further support the increased ECM stiffness in the muscles exposed to BTX-A. Studies specifically designed to explore longer sarcomere effects with *in vivo* imaging could enhance understanding of BTX-A-induced structural and mechanical changes.

2.4.2 Mechanical Interactions Between Partially Paralyzed Muscles

BTX-A-induced muscle paralysis alters EMFT mechanism in two ways:

2.4.2.1 Effects on individual muscles. BTX-A can affect individual muscle mechanics of both targeted and non-targeted muscles via spread through muscle fascia [24], bloodstream [33], or axonal pathways [34]. BTX-A-induced changes in force production characteristics due to the leakage in neighboring muscles [38], synergistic muscles

within a compartment [31, 32, 36, 39], and even across antagonistic compartments [39] have been documented in several animal studies. These effects included reduced active muscle force, increased collagen content, stiffness, and passive force, as well as reduced l_{range} in non-injected muscles acutely exposed to BTX-A. The present study confirmed a decrease in active forces across all synergistic muscles even long-term post-injection, suggesting that BTX-A spread persists. Even though BTX-A is clinically intended to improve agonist-antagonist force balance [96, 97], these findings may signal a complex imbalance between co- and/or counter-acting muscles. Considering children with spastic cerebral palsy struggling with the uncontrolled co-activation of their antagonistic and synergistic lower leg muscles [76, 77, 98], BTX-A's acute suppression of intermuscular interactions in animal studies [32] could benefit muscle coordination by mitigating co-contraction issues. However, it may also disturb the balance between the muscles, when uncontrolled.

2.4.2.2 Changes in collagenous and muscular tissue. BTX-A can alter the stiffness of the collagenous tissues and the composition of the muscular tissues. Epimuscular collagenous network includes the connections between the epimysia of neighboring muscles and collagen-reinforced neurovascular tracts that facilitates intermuscular mechanical interactions. Studies on BTX-A-free human muscles using various imaging techniques showed local length changes along muscle fibers despite global muscle length changes [13]. The direct effects of EMFT on muscle mechanics have been demonstrated [8, 9], including heterogeneous local length changes along muscle fibers after passive stretch [54], and submaximal activation [53] using magnetic resonance imaging techniques, as well as localized stiffness changes as shown by supersonic shear imaging [55]. Since BTX-A can alter muscles' length-force characteristics in response to changes in the mechanical conditions under which they operate, they should also be closely monitored in clinical interventions for spasticity. Because EMFT is highly relevant to spastic muscle's contribution to different joints. Intraoperative experiments on cerebral palsy patients showed that individually activated muscles display no apparent pathophysiological condition (e.g., exerting peak muscle force at narrow knee angle) that limits the joint angle [41–43]. However, when activated with synergists and

antagonists, this peak shifted towards flexed knee angles when activated with their synergists and antagonists [44–46, 99]. Considering these findings and the uncontrolled co-activation of antagonistic and synergistic muscles in children with spastic cerebral palsy [76, 77, 98], these intermuscular interactions should be clinically considered before intervention. Because, while BTX-A could have acute neurological benefits, co-existing mechanical consequences may not be favorable. The current results demonstrate that BTX-A exposure influences the force differences in the EDL muscle. At the shortest TA lengths, both animal groups exhibited higher distally exerted EDL active forces than those exerted proximally, suggesting proximally directed epimuscular myofascial loads. After lengthening TA further, they shifted distally, with the BTX-A group showing higher amplitudes. Although current findings suggest that long-term BTX-A exposure may increase stiffness in the connective tissue linkages between TA and EDL muscles, BTX-A did not diminish EMFT as reported acutely [31, 32]. Further investigation is needed to fully understand the effects of BTX-A on inter-muscular mechanics. Because BTX-A injection into TA showed significant effects on non-targeted EDL muscle. Experimental conditions, where the EDL muscle's length remains constant while its relative position changes, could exclusively reveal the complex BTX-A particularly for bi-articular muscles' contribution to joints it spans, as tested previously [32].

2.4.3 Limitations and Implications of the Study

The chosen time frame for assessing the long-term effects of BTX-A was based on the understanding of exocytosis, a process crucial for acetylcholine release at the neuromuscular junction. Any intervention, including BTX-A exposure, blocks this process presynaptically, leading to muscle paralysis [100–102]. According to de Paiva et al. [103], exocytosis at the parent nerve terminals ceases four weeks post BTX-A injection. However, this inhibition changes after one month, with exocytosis recovery and the formation of nerve-terminal sprouts increasing over time. Our decision to assess BTX-A effects one month post-injection avoided these complexities and aligns with earlier animal studies [38, 104–106]. Nevertheless, de Paiva et al. [103] indicated that the dynamic nature of exocytosis, influenced by parent terminals and nerve-terminal

sprouts, requires further study of BTX-A's longer-term effects for comprehensive understanding. This study contributes to such understanding by revealing novel mechanical effects that impact the exposed muscles' function.

There are notable differences between the injection protocols in terms of the BTX-A dosages, and volumes used in this animal study compared to common clinical practices. The TA muscle was manually located using anatomical landmarks, but clinical applications recommend using electrical stimulation, electromyography, or ultrasound-guided injections for greater accuracy, especially in deep or small muscles [29, 107–109]. Despite this, Picelli et al. [110] found that these advanced methods do not necessarily yield better outcomes for superficial muscles compared to manual placement. Consequently, we were confident in our ability to locate the superficial TA muscle and standardize the injection site and depth as per the protocol described in the 2.2. Materials and Methods. The optimal clinical dosage of BTX-A per muscle depends on factors such as muscle volume, spasticity degree, and the muscle's role in the patient's pathological joint movement [111]. Heinen et al. [29] reported a safe dosage range for children with cerebral palsy as 1 to 25 U/kg bodyweight, with clinical doses for lower extremity muscles typically ranging from 3 to 6 U/kg [35, 112]. In contrast, the dose used in this study was approximately 0.32 U/kg, significantly lower than clinical dosages. The volume injected (about 64 μl/kg) also differed from typical clinical volumes (2.5-8 ml/kg) used for lower limb muscles [35, 112]. Despite these differences, the study observed significant decreases in measured forces, suggesting that the dosage used was effective for the study's purposes. It is also important to note the variability in dosages and volumes used across different animal studies, making direct comparisons with clinical practice challenging. However, these animal studies, including the present one, have revealed significant new phenomena, suggesting previously unknown long-term effects of BTX-A on muscle mechanics, which warrant clinical testing.

Another consideration was the site of injection. Unlike common clinical practices that often involve multiple injection sites [27, 101], this study used a single site in the mid-target muscle belly. Given BTX-A's high diffusivity [24], dividing the total dose across multiple sites may help prevent the toxin from spreading to other muscles

[27, 111]. The single-site injection used here may have facilitated leakage to adjacent non-targeted muscles. Even with multiple injection sites, previous studies have shown that BTX-A can spread beyond the injection site [24], complicating the control of treatment effects, which has been considered a side effect [27, 83]. On the other hand, Frasson et al. [35] suggested that the spread of BTX-A from foot flexors to antagonists might improve gait in patients with CP. However, as indicated by earlier animal studies [39], such inter-compartmental spread can lead to uncontrolled effects in non-targeted muscles, necessitating specific long-term testing. Given BTX-A's potential to adversely affect muscle mechanics, controlling the leakage of the toxin is crucial for managing treatment outcomes. The spread of BTX-A into a bi-articular muscle can influence both proximal and distal joints, possibly affecting movements in non-targeted joints. Therefore, it is essential to evaluate the structural and functional effects of BTX-A on muscles exposed through diffusion in clinical settings.

2.5 Conclusion

This study investigated the long-term impact of BTX-A on the mechanics of exposed rat anterior crural compartment muscles, with a particular focus on its influence on EMFT. The findings demonstrated that BTX-A modifies the composition and force production characteristics of both the targeted TA muscle (injected) and the non-targeted EDL and EHL muscles (affected through diffusion). Though these changes indicate alteration in EMFT mechanism, acutely shown EMFT-reducing effect of BTX-A was not observed. These results provide valuable insights for clinical strategies for BTX-A management.

3. LONG-TERM BTX-A EFFECTS ON NON-TARGETED BI-ARTICULAR MUSCLE MECHANICS AND EMFT

3.1 Introduction

Botulinum toxin type-A (BTX-A) is a neurotoxic agent that prevents the discharge of acetylcholine-containing vesicles at the neuromuscular junction [101], leading to muscle paralysis [25]. BTX-A is widely used for spasticity management in patients with cerebral palsy (CP) [26]. The therapy aims at relieving the excessive stiffness at the patients' affected joints in order to improve function [29] by reducing hypertonia [27] and increasing range of motion [28]. However, clinical cohort studies showed that although BTX-A is successful in reducing hypertonia, it may not be as effective for improving joint range of motion [47, 48] and gait [49–51].

Animal experiments improve our understanding of how BTX-A affects muscular mechanics and provide an objective assessment of its role in joint function. Recent experiments showed two important acute effects. First, directly functional, BTX-A causes a narrower length range of active force exertion (l_{range}) [36] and an increased muscle passive force [31, 36]. Note that BTX-A leaks through muscle fascia [24] and can spread via vascular [33] and axonal [34] mechanisms. This leads to such functional effects to be also encountered in non-injected muscles [30,31,35,36,38,39,113]. Secondly, despite such spread affecting mechanics of several muscles in a compartment, BTX-A was shown to diminish epimuscular myofascial force transmission (EMFT) [32, 39].

The former, affecting muscles exposed is important because of the effects that contrast the expected functional outcome of BTX-A. The latter is also highly relevant as BTX-A is used in several bi-articular muscles in CP patients [114–116] and because EMFT has been shown to affect the mechanics of a bi-articular muscle differentially proximally and distally in BTX-A free muscles [8, 9, 20]. Note that intraoperative experiments allowing for direct force measurements at the muscle's tendon

showed interesting findings illuminating mechanical behavior of spastic muscles of CP patients with important implications for the role of EMFT (e.g., [40]). Spastic knee flexor muscles activated selectively, showed a peak force production only in extended knee joint positions (see [41–43] for spastic gracilis, semitendinosus, and semimembranosus muscles, respectively), indicating that their joint range of force production is not narrow. However, after being simultaneously co-activated with their synergistic and antagonistic muscles, their force production characteristics changed [44–46], featuring a shifting of high force production towards flexed knee positions. Such co-activation promotes EMFT [8,9]. Taking these issues into account, acute BTX-A effects limiting EMFT across muscles exposed may be a favorable asset during spasticity management. However, our understanding of both effects in the long-term is inadequate.

We aimed at devising specific animal experiments towards filling that gap and tested the following hypotheses: in the long-term, exposure to BTX-A (i) has no effects on l_{range} and passive forces of bi-articular muscle measured both distally and proximally and (ii) diminishes EMFT.

3.2 Materials and Methods

Surgical and experimental procedures were approved by the Committee on the Ethics of Animal Experimentation at Boğaziçi University.

3.2.1 Injection Protocol

Male Wistar rats were divided into two groups: BTX-A (n = 7, body mass = 405.3 ± 35.0 g) and control (n = 7, body mass = 395.7 ± 24.9 g). After imposing mild sedation with 1 mg kg^{-1} ketamine intraperitoneally, a circular region of approximately 15 mm radius at the center of the patella in the left hind limb was shaved. While the ankle was in maximal plantar flexion and the knee angle was 90°, the tibialis anterior (TA) muscle was located by palpation. From the center of the patella, a point 10 mm

distal along the tibia was marked. The injection point was marked 5 mm lateral to that over the TA. Considering the skin thickness (0.7-1 mm) and the diameter of the TA (5-5.5 mm), all injections were made to a depth of 3 mm into the superficial half of the TA.

The BTX-A group received injections of BTX-A (BOTOX; Allergan Pharmaceuticals, Westport, Ireland) reconstituted with 0.9% sodium chloride, at a total dose of 0.1U. The control group was injected with 0.9% saline solution. All animals received one-time intramuscular injection one-month prior to testing with injected volume = 20 μl. The animals were kept freely until the experiment day in separate, standard cages in a thermally regulated animal care room with 12 h dark-light cycles.

3.2.2 Surgical Procedure

The animals were anesthetized using intraperitoneally injected urethane solution (1.2 ml of 12.5% urethane solution/100 g body mass). Additional doses were given if necessary (maximally 0.5 ml). During surgery and data collection, the animals were placed on a heated pad (Harvard Apparatus, Homoeothermic Blanket Control Unit) to prevent hypothermia. A feedback system utilizing an integrated rectal thermometer allowed controlling body temperature at 37°C by adjusting the temperature of the heated pad. Immediately after the experiments, the animals were euthanized with an overdose of urethane solution.

The skin and the biceps femoris muscle of the left hind limb were removed and the anterior crural compartment muscles were exposed. Only limited distal fasciotomy was performed to remove the retinaculae. Connective tissues at the muscle bellies within the anterior crural compartment were left intact to maintain the physiological relations of intra- and epimuscular connections.

The combination of 120° knee and 100° ankle angles was selected as the reference position that corresponds to an *in vivo* position at the stance phase of the rat during

gait [90]. At the reference position, the four distal tendons of the extensor digitorum longus (EDL) were tied together using silk thread. Matching markers were placed on the distal tendons of the EDL, TA, extensor hallucis longus (EHL) and a fixed location on the lower leg. Subsequently, the distal EDL tendon complex and TA and EHL tendons were cut as distally as possible. The proximal EDL tendon was cut from the femur, with a small piece of the lateral femur condyle still attached. In order to provide connections to force transducers (FT; BLH Electronics Inc., Canton, MA, USA), Kevlar threads were sutured to the proximal tendon of the EDL, the tied distal tendons of the EDL, the distal tendon of the TA, the distal tendon of the EHL.

Within the femoral compartment, the sciatic nerve dissected free, and all nerve branches connected to the muscles of this compartment were cut. Finally, the sciatic nerve was cut as far proximally as possible.

3.2.3 Experimental Procedure

In the experimental setup (Figure 3.1), the femur and foot were fixed by metal clamps, such that the ankle was in maximal plantar flexion (180°) to allow for free passage of the Kevlar threads to the distal force transducers. The knee angle was set at 120°. Each Kevlar thread was connected to a separate FT. Care was taken to ensure the alignment of the Kevlar threads to be in the muscle line of pull. The distal end of the sciatic nerve was placed on a bipolar silver electrode. Room temperature was kept at 26°C. Muscle and tendon tissues were irrigated regularly by isotonic saline to prevent dehydration. The muscle lengths were set to their reference positions by adjusting their FTs. Before acquiring data, muscle-tendon complexes and their connective tissues were preconditioned by isometric contractions, alternatingly at long and short lengths until forces at short length were reproducible [117].

Three conditions were studied:

(1) EDL muscle was lengthened distally by moving its distal FT.

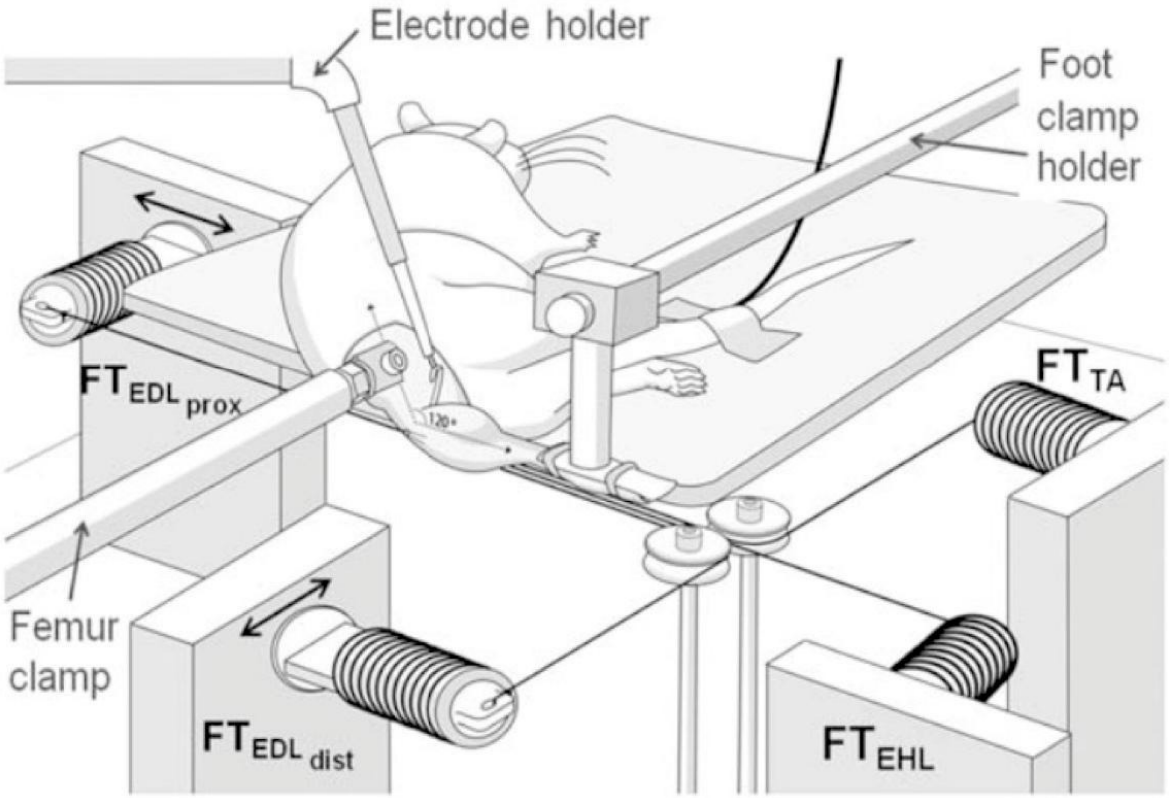

Figure 3.1 Schematic view of the experimental setup. The proximal and the tied distal tendons of the EDL (EDL_{prox} and EDL_{dist}, respectively) and the distal tendons of the tibialis anterior (TA) and extensor hallucis longus (EHL) muscles were each connected to a separate force transducer (FT). The femur and the foot were fixed by metal clamps. The distal end of the sciatic nerve was placed on a bipolar silver electrode. Throughout the experiment, the TA and the EHL were kept at constant muscle-tendon complex lengths. The EDL muscle was lengthened either proximally or distally to progressively increasing lengths, at which isometric contractions were performed. Lengthening (indicated by double-headed arrow) started from muscle active slack length at 1 mm increments by changing the position of the target EDL force transducer. During the proximal lengthening condition, EDL_{dist}, and during the distal lengthening condition, EDL_{prox} were kept in their reference positions. For the relative positioning condition, EDL_{dist} and EDL_{prox} were both moved in increments of 1 mm without changing EDL muscle length kept at its optimum length. This figure was adapted from [30].

(2) EDL muscle was lengthened proximally by moving its proximal FT.

Starting from muscle active slack length the EDL is lengthened to 2 mm over the optimum length in 1 mm increments. EDL muscle-tendon complex lengths were expressed as deviation from its optimum length ($\Delta l_{mt\ EDL}$).

(3) EDL muscle position was changed.

Initially, the EDL was set to its optimum length determined in (1). Subsequently, at a constant length, its position was altered ($\Delta position_{\ EDL}$) from proximal to distal positions by moving both proximal and distal FTs in 1 mm increments.

During the experiment, FTs other than those described above were kept in their reference positions. The isometric forces of all muscles were measured simultaneously after being activated by supramaximal stimulation of the sciatic nerve (STMISOC; Biopac Systems, Goleta, California), using a constant current of 2 mA (square pulse width 0.1 ms). After setting the EDL muscle to a target length/position, two twitches were evoked, and 300 ms after the second twitch, the muscles were tetanized (pulse train 400 ms, frequency 100 Hz). 200 ms after the tetanic contraction, another twitch was evoked. After each application of the stimulation protocol, 2 mins recovery was allowed for the EDL muscle at its active slack length.

3.2.4 Data processing

All muscle force measurements were done during isometric contraction of the anterior crural compartment muscles by following the stimulation protocol above. Muscle total force (F_t) was determined as the total force transmitted through myotendinous junction during the tetanic plateau (the mean force for a 200 ms interval, 150 ms after evoking tetanic stimulation). The muscle passive force (F_p) represents the mechanical resistance of the muscular tissue and was measured 100 ms after the second twitch. Muscle active force (F_a) was calculated by subtracting the F_p from the F_t. Data for F_p

and F_t were fitted with a polynomial function using a least squares criterion (Eq. 3.1):

$$y = a_0 + a_1 x + a_2 x^2 + \cdots + a_n x^n \tag{3.1}$$

where y represents isometric muscle forces (i.e., F_p or F_t) and x represents muscle-tendon complex length. a_0, a_1, ..., a_n are coefficients determined in the fitting process.

One-way analysis of variance (ANOVA) was used to select the lowest order of the polynomials that matched best with the measured muscle force data at different muscle-tendon complex lengths and positions [92]. Per muscle-tendon complex length, forces of each muscle were obtained by using these functions, averaged, and standard deviations were calculated to determine muscle force (mean ± SD). The range from active slack length to length at which optimal force is exerted (l_{range}) is taken as an indicator of movement capability with active force exertion within the potential range of motion of a certain joint.

3.2.5 Statistics

Shapiro-Wilk test was used to check if l_{range} data are normally distributed. Accordingly, unpaired-t or Mann-Whitney U test was used to test the effects of BTX-A injection on l_{range} of the EDL muscle.

For conditions (1) and (2), two-way ANOVA for repeated measures (factors: EDL muscle-tendon complex length and animal group) was performed. For condition (3), two-way ANOVA for repeated measures (factors: EDL muscle-tendon complex position and animal group) was performed. If significant main effects were found, Bonferroni post-hoc tests were performed to further locate within-factor differences.

Forces of both groups were aligned with their optimum length. Changes in active and passive forces are calculated as the difference in mean force between the control and the BTX-A groups, expressed as a percentage of the mean force of the control group. Statistical differences were considered significant at $P < 0.05$.

3.3 Results

3.3.1 Effects of BTX-A on Restrained Muscles

ANOVA showed a significant effect of BTX-A on TA active forces (on average 3 N), leading to a drop (by 34%). ANOVA also showed a significant effect of BTX-A on TA passive forces causing an increase (by 116%). ANOVA showed a significant effect of BTX-A on EHL active forces (on average 0.4 N), leading to a drop (by 20%). ANOVA also showed a significant effect of BTX-A on EHL passive forces causing a decrease (by 75%).

3.3.2 Effects of BTX-A on Mechanics of the Bi-articular Muscle

3.3.2.1 Distal Lengthening. *Distal Forces.* ANOVA (factors: EDL length and animal group) showed significant main effects of both factors on EDL distal active forces but no significant interaction (Figure 3.2A). On average, forces of the BTX-A group were lower by 51%. The difference between the distal l_{range} of the EDL of control and BTX-A groups was significant (9.04 ± 0.68 mm vs. 7.71 ± 1.38 mm, respectively, P = 0.049). ANOVA showed significant main effects of both factors on EDL distal passive forces and a significant interaction. Post-hoc testing showed that forces of the BTX-A group were higher than those of the control group for $\Delta l_{\text{mt EDLdistal}} \geq$ -1 mm (maximally approximating 2-fold).

Proximal Forces. ANOVA showed significant main effects of both factors on EDL proximal active forces, but no significant interaction (Figure 3.2B). On average, forces of the BTX-A group were lower by 34%. ANOVA showed significant main effects of both factors on EDL proximal passive forces and a significant interaction. Post-hoc testing showed that forces of the BTX-A group were higher than those of the control group for $\Delta l_{\text{mt EDLdistal}} \geq 1$ mm (approximating up to 4.5-fold).

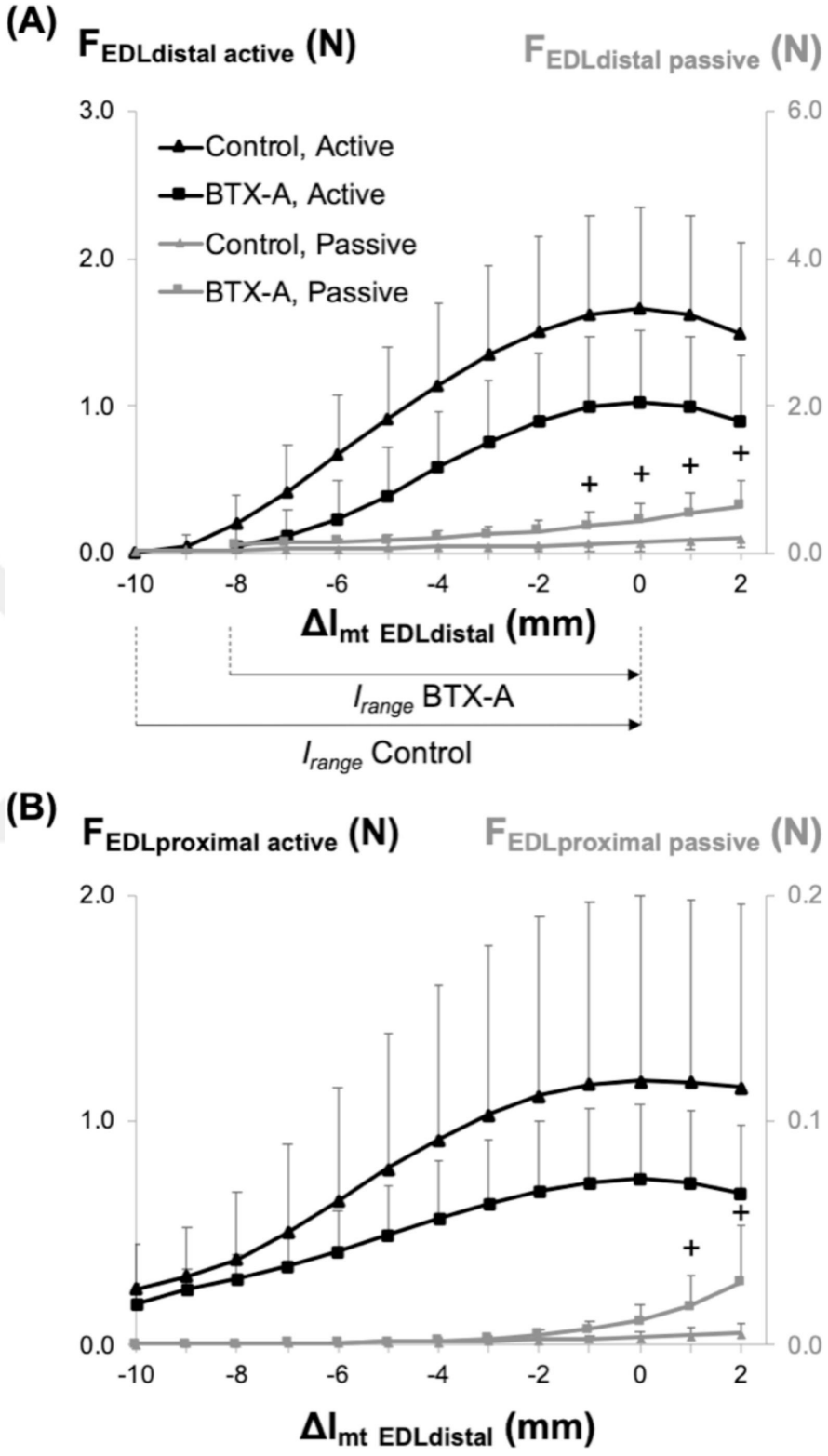

Figure 3.2 Length-force characteristics of EDL muscle obtained after distal lengthening. Distally (A) and proximally (B) exerted EDL active and passive isometric forces are shown as mean ± SD for the control and BTX-A groups. EDL muscle-tendon complex length is expressed as a deviation from its optimum length ($\Delta l_{mt\ EDLdistal}$). Distal l_{range} of BTX-A group (7.71 ± 1.38 mm) was significantly narrower compared to that of the control group (9.04 ± 0.68 mm), $P = 0.04864$ (A). Localized significant differences between the EDL forces of the BTX-A group and the control group (Bonferroni post-hoc test) are indicated by + (passive force).

3.3.2.2 Proximal Lengthening. *Proximal Forces.* ANOVA (factors: EDL length and animal group) showed significant main effects of both factors on EDL proximal active forces and a significant interaction (Figure 3.3A). Post-hoc testing showed that the forces of the BTX-A group were lower than those of the control group for $\Delta l_{\text{mt EDLproximal}} \geq$ -4 mm (e.g., at $\Delta l_{\text{mt EDLproximal}} =$ -4 mm and $\Delta l_{\text{mt EDLproximal}} = 2$ mm by 76% and 56%, respectively). The difference between the distal l_{range} of the EDL of control and BTX-A groups was significant (7.36 ± 1.98 mm and BTX-A 4.99 ± 1.44 mm, respectively, P = 0.027). ANOVA showed significant main effects of both factors on EDL proximal passive forces and a significant interaction. Post-hoc testing showed that forces of the BTX-A group were higher than those of the control group for $\Delta l_{\text{mt EDLproximal}} \geq 1$ mm (up to 3-fold).

Distal Forces. ANOVA showed significant main effects of both factors on EDL distal active forces and a significant interaction (Figure 3.3B). Post-hoc testing showed that forces the of the BTX-A group were lower than those of the control group for $\Delta l_{\text{mt EDLproximal}} \geq$ -5 mm (e.g., at $\Delta l_{\text{mt EDLproximal}} =$ -5 mm and $\Delta l_{\text{mt EDLproximal}} = 2$ mm by 76% and 63%, respectively). ANOVA showed significant main effects of both factors on EDL distal passive forces but no significant interaction. On average, forces of the BTX-A group were higher by 122%.

3.3.3 Effects of BTX-A on EMFT

ANOVA (factors: EDL relative position and animal group) showed only a significant main effect of EDL relative position on EDL proximo-distal total force differences (Figure 3.4). For both groups, EDL muscle positions altered from proximal to distal locations, force differences changed from negative but smaller amplitudes to positive greater amplitudes (e.g., for the BTX-A group from -0.49 ± 0.41 N at $\Delta\text{position}_{\text{EDL}} =$ -5 mm to 1.97 ± 0.82 N at $\Delta\text{position}_{\text{EDL}} = +5$ mm).

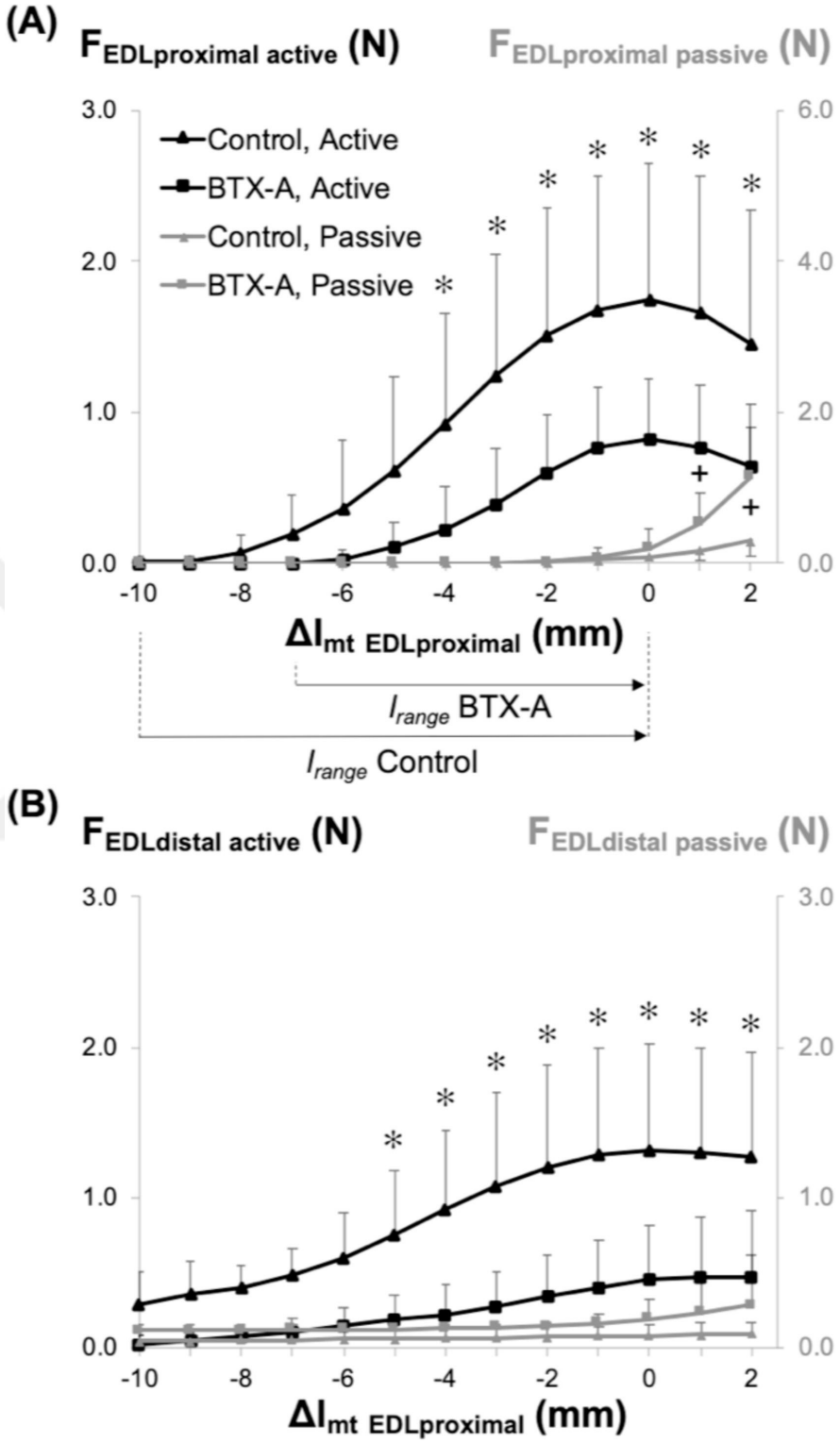

Figure 3.3 Length-force characteristics of EDL muscle obtained after proximal lengthening. Proximally (A) and distally (B) exerted EDL active and passive isometric forces are shown as mean ± SD for the control and BTX-A groups. EDL muscle-tendon complex length is expressed as a deviation from its optimum length ($\Delta l_{mt\ EDLproximal}$). Proximal l_{range} of BTX-A group (4.99 ± 1.44 mm) was significantly narrower compared to that of the control group (7.36 ± 1.98 mm), $P = 0.02676$ (A). Localized significant differences between the EDL forces of the BTX-A group and the control group (Bonferroni post-hoc test) are indicated by P (active force) and by + (passive force).

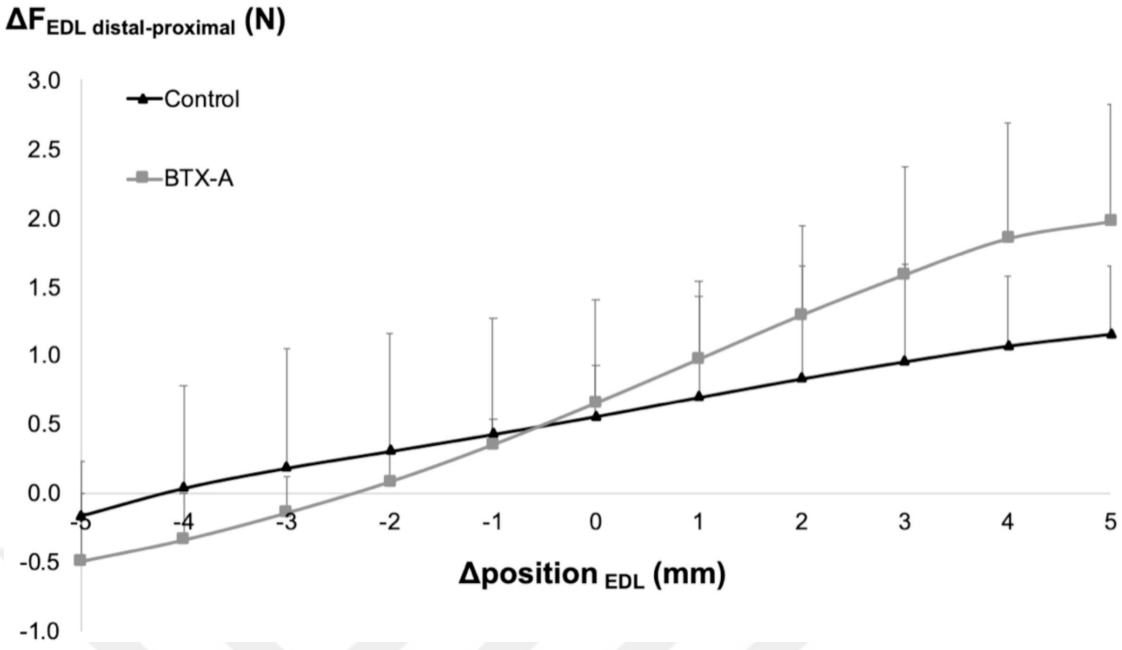

Figure 3.4 EDL proximo-distal force differences as a function of changing EDL relative muscle position. Total force differences, calculated as $F_{distal} - F_{proximal}$ for the BTX-A group and the control group are shown as mean ± SD. EDL muscle-tendon complex relative position changes (Δposition $_{EDL}$) are expressed as a deviation from the proximal starting position (Δposition $_{EDL}$ = -5 mm) to the distal end position (Δposition $_{EDL}$ = 5 mm).

3.4 Discussion

Our results showed that in the long-term, exposure of bi-articular muscle to BTX-A caused a significant narrowing of its l_{range} and increasing of its passive forces measured both distally and proximally. Additionally, no significant effects on EMFT were found. Therefore, both hypotheses are rejected, indicating that BTX-A affects the mechanics of the muscle adversely for both joints it spans, while not affecting its mechanical interaction with the surrounding muscles and other tissues.

Spasticity management aims at limiting exaggerated resistance to stretch, which has neural and non-neural components [118]. The neural component involves an excessive motoneuron drive, which is related to the velocity dependent stretch hyperreflexia and non-velocity dependent involuntary background activation. Stretch reflex threshold is decreased in patients with spasticity explained by abnormal afferent signaling [119]. BTX-A paralyzes both extrafusal and intrafusal muscle fibers and decreases the active muscle force and the sensitivity of muscle spindles. Therefore, BTX-A helps

to suppress the neural component via limiting muscle activation. However, in CP or stroke, the contribution of the neural component to movement abnormalities can be limited (e.g., [120, 121], whereas the non-neural component is dominant [122, 123].

Non-neural component involves elevated passive stiffness due to alterations in intra- and extracellular muscular connective tissues [124]. Animal studies provide an objective assessment for BTX-A effects on connective tissue properties via passive muscle forces. Consistent with acute BTX-A effects [30,31], the present results sustain increased passive forces for one-month after injection, with two plausible reasons: (1) An increase in the extracellular matrix (ECM) collagen content. In the rat anterior crural compartment, exposure to BTX-A yielded an increase (at least two fold) of collagen content for the short-term [30], and of hydroxyproline amount for the long-term [113]. Yet, for a comprehensive understanding of BTX-A induced structural changes in the muscle exposed, collagen isoforms and other elastic proteins such as titin should be studied. (2) Elevated ECM stiffness. Thacker et al. [106] reported that for isolated rat muscle fiber bundles exposed to BTX-A suggesting that collagen orientation and cross-linking may also get affected. In the whole muscle level, steeper slope of the length-passive force curve of muscles exposed supports that [30,31,39,113].

Turkoglu et al. [94] modeled partially activated rat EDL to study the mechanical mechanism of effects of exposure to BTX-A. This showed that the lack of shortening in paralyzed muscle fibers limits the shortening of also activated ones, referred to as the "longer sarcomere effect (LSE)". Modeling of the time course of treatment indicated that LSE is characterized and manipulated by increased ECM stiffness [95]. Such LSE yields a higher force production at shorter muscle lengths resulting in a narrower l_{range}. This mechanism can explain the proximally and distally narrower EDL l_{range} shown presently. Note that muscle l_{range} cannot be directly correlated with the joint range of motion, but it is an indicator of individual muscles' function within the potential range of motion at the joint. A narrower l_{range} suggests that joint movement can be limited by the muscles before physical constraints provided by other tissues such as ligaments and bones. Therefore, exposure to BTX-A of their muscles may contribute to the limited joint range in patients suffering from spastic CP. However, clinical testing for

that should be done.

Collagenous connections between the epimysia of adjacent muscles and neurovascular tracts form intermuscular connections and facilitate EMFT. Previously, [32] reported diminished EMFT short-term after BTX-A administration. This may have relevant implications for the mechanics of spastic muscle and spasticity management using BTX-A. Regarding the former, [76, 77] showed more pronounced co-activation of unintended antagonist and synergist lower leg muscles in CP than in typically developing children. Intra-operative experiments in spastic CP patients directly testing effects of co-activation of spastic hamstrings with their synergistic ([44] and/or antagonistic muscles [40, 45, 46] reported higher muscle force production in flexed knee positions. Differently than spastic muscles activated alone [41–43] mechanical interaction between upper leg muscles appears to affect the pathological condition in the knee. This is characterized by EMFT [8, 9]. Regarding the latter, exposure to BTX-A eliminates muscle spindle discharge [125, 126], yielding a decrease in the stretch reflex activity of the muscle. Yet, recall the LSE, finite element modeling shows [94, 95] suggesting that activatable muscle parts in muscle exposed to BTX-A may have an elevated muscle spindle firing which may compromise spasticity management. That is why diminished EMFT reported for the short-term exposure to BTX-A [32] appeared beneficial. However, the present results do not sustain that for the long-term. Smilde et al. [71] showed that muscle stretch could change the discharging of muscle spindles in neighboring muscles, which effect is ascribed to EMFT. Since muscles' afferent inputs are impaired in spastic CP [127], the interaction between BTX-A and EMFT effects requires further attention. The present findings suggest that BTX-A may compromise not only the mechanical but also the neural outcome of muscles exposed. This may be highly important, but differences between the present experimental BTX-A protocols and the clinical practice exist (see Appendix B for more details), and the viewpoints developed here should be specifically tested in spastic CP patients.

In conclusion, the present study showed that long term exposure to BTX-A affects the contribution of bi-articular muscle to both joints it spans such that both in the active state via narrowed range of force production and in the passive state via in-

creased passive resistance, the muscle's contribution to joint motion gets compromised. Moreover, unlike shown earlier for the short term, the muscle's mechanical interaction with the surroundings is unaffected. These findings suggest that for bi-articular muscles exposed, BTX-A may differentially and adversely affect the mechanics of both joints, which may compromise long-term spasticity management. The effects of BTX-A shown in present experiments should be studied in CP patients.

4. MUSCLE SPINDLES PROJECTING TO MOUSE Me5 SENSE SYNERGISTIC MUSCLE ACTIVITY THROUGH EMFT

4.1 Introduction

Muscle fibers, composed of sarcomeres, i.e. the smallest force generating units, contract and develop forces. They are attached to and pull on the bones via tendons to generate bodily movement. However, because of the muscle fibers' arrangement inside the extracellular matrix and their connections along the longitudinal length of the muscle [5], the force transmission is not limited to the myotendinous junction but also epimuscular myofascial force transmission (EMFT) occurs [8]. The mechanical interaction between muscle and surrounding connective tissues leads to variability in local lengths along muscle fibers even when the muscle is kept at constant muscle length. Because intramuscular connective tissues are an integral part of the fascial system [128], the muscle's connectivity extends beyond the muscle belly through epimuscular connections that include neurovascular tracts, compartmental tissues and direct collagenous links between the epimysia of adjacent muscles [9]. Therefore, mechanical interactions between a muscle and its surroundings occur and lead to varying amplitudes of myofascial loads that act on the muscle with effects down to individual muscle fibers [129]. Resulting from such EMFT, substantial local length [53, 54] and stiffness [55] changes have been reported in human muscles *in vivo*, in conditions involving no global muscle length changes [13]. Further studies using various microscopy techniques have reported experimental evidence for the variable sarcomere lengths across different muscle regions both for rat [56, 57] and human [58] skeletal muscles.

Muscle force production and sensation are interdependent within the mechanically integrated neuromusculoskeletal system. The motor actions shape into their context-dependent sensory representations in the nervous system through the integration of sensory information from the parallel processing of multiple sensory units

[59, 62, 63]. This sensory integration is a dynamic process that continually adapts to sensory input from muscle spindles (MSs) and fine-tuning motor actions accordingly [130].MSs are essential for the sensory aspect of this integration at two levels. First, as primary mechanoreceptors, they capture the variations in local lengths along muscle fibers due to their widespread distribution within the muscle belly. Second, embedded in a collagenous capsule within the perimysium, they are influenced by forces transmitted through connective tissues, allowing them to encode myofascial force transmission across the entire muscle compartment. Even though research on the mechanical implications of EMFT is extensive, the sensory implications are understudied. Studies showed that imposing epimuscular loads by stretching synergistic [71] and antagonistic [72] muscles affects neural responses in MS afferents. However, these studies lack active muscle conditions, which are more representative of daily movements, highlighting the need for fundamental research to understand MS' proprioceptive feedback between active muscles.

Investigating the sensory aspects of EMFT requires specialized experimental designs and techniques. We used a modernized protocol designed to identify MS afferents, applying mechanical stimuli while preserving the connective tissues around the muscles. This approach included recording neuronal activity from the trigeminal mesencephalic nucleus (Me5) in mice for the first time, which contains first-order sensory neurons for the masseter and temporalis muscles [131, 132]. Based on the established anatomical and physiological characteristics of the mouse model, we hypothesize that (1) mice are a suitable model for studying the neural dynamics of MSs projecting to the Me5 nucleus in the brainstem, and (2) activity in the synergistic muscle alters the MS feedback in the target muscle, influenced by EMFT. Findings of this study will improve the understanding of how intermuscular mechanical interactions influence sensorimotor integration in active muscle state.

4.2 Materials and Methods

4.2.1 Animals

Animals (6 female and 5 male mice; body mass 23.12±3.26 g, n = 11; age at experiment = 12±2 weeks; F1 generation of crossing between B6J (JAX stock #000664) x SSTs-Cre (JAX stock #013044)) were used for the experiments, however, without making use of optogenetic modulation. Immediately after the experiments, animals were sacrificed by cervical dislocation. A subset of the animals (n = 3) and an extra animal was perfused for histological analysis. The animals were kept implanted until the experiment day, housed in pairs in a thermally regulated animal care room illuminated with reversed 12 h dark-light cycles. All experiments were performed under working protocols from the welfare body (project number 2017-0041). Experimental procedures were approved by the Dutch central commission for animal research (Centrale Commissie Dierproeven) and supervised by the Animal Welfare Body of the Radboud University Medical Center.

4.2.2 Surgical procedures

4.2.2.1 Headpost implantation. After anesthetizing the mice using isoflurane (1.5 to 2% dosage; E-Z Anesthesia, E-Z Systems Corporation), a dose of Rimadyl (5 mg/kg; carprofen Rimadyl cattle, Zoetis, USA) and Dexamethasone (2 mg/kg; Centrafarm B.V., The Netherlands) were injected intraperitoneally. The animals were placed onto the surgery setup using a mouthpiece to semi-stabilize the head. An incision was made after cleaning the skin with ethanol and betadine, and the connective tissue over the skull was cleared using 3% hydrogen peroxide. The skull was marked using a permanent marker at AP = -5.5 mm, ML = -1 mm. Then, an aluminum headpost was placed facing anteriorly at the bregma level. Before waking up the animals for recovery, the stability of the headpost was tested and fluorescence dye injections were made (please see 4.2.5. Histology section below). Starting from 24 h before to 48 h after the operation, the animals received analgesic medication in their water (1 ml/liter).

4.2.2.2 Recording session. Each animal was anesthetized with urethane (1.7 g/kg body mass) and supplementary doses were given if needed (maximum total dose of 2.1 g/kg). The animal received an analgesic dissolved in water (1 ml/liter; Rimadyl cattle, Zoetis) on the day prior to the surgery. After the induction of anesthesia, an additional dose of Rimadyl (5 mg/kg) was subcutaneously injected as well as Dexamethasone (2 mg/kg) to reduce brain swelling. The left side of the animal's face was shaved, and the masseter and temporalis muscles were marked. The animal's head was secured to a horizontal platform using the previously attached headpost, which was anteriorly located on the animal's cranium. After the top of the cranium was positioned flat, a ground screw was implanted over the right frontal cortex. Then, a craniotomy with a diameter of 3 mm was performed over inferior colliculus (previously marked on the skull at 5.5 mm post bregma, 1 mm lateral from the midline and confirmed via intrinsic optical imaging of noise burst sequences) to record from the trigeminal mesencephalic nucleus (Me5) located 3.4-3.7 mm underneath (Allen CCF mouse atlas).

4.2.3 Electrophysiological recordings

Recordings were performed using silicon electrode arrays (NeuroNexus, USA) with 64 channels attached to a piezoelectric micromanipulator (SMX series, Sensapex, Finland) in a Faraday cage. The distribution of recording sites was arranged in two different configurations: (1) A4x16-6mm-tet/lin-600/125-333-121/177 and (2) A4x16-6mm-50-200-177. The electrode array was advanced at a speed of 1 mm/min to a total depth of 3-4 mm with into the brainstem orthogonally to the brain surface to record extracellularly from the left Me5, which contains the muscle spindle afferents belong to Masseter and Temporalis muscles (Figure 4.1A). Recordings were digitized at 30 kHz and synchronized to that stimulation using a custom-made experimental control system (Controller) in Matlab (The Mathworks, Natick, USA) via a data acquisition board (PCIe-6321, National Instruments), which acquired synchronization signal at 10 kHz.

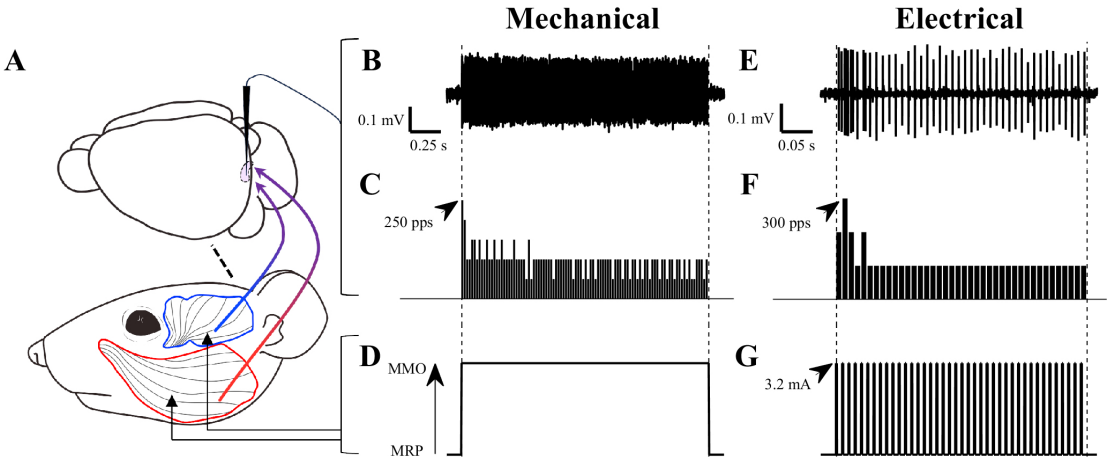

Figure 4.1 Experimental design. (A) Electrophysiological recordings were performed from the trigeminal mesencephalic nucleus (purple), which contains the muscle spindle afferents of masseter (red) and temporalis (blue) muscles, in mice. While mechanical and electrical stimuli delivered to masseter and temporalis muscles, neuronal activity (B, E) was recorded using microelectrode arrays. Firing rates (spikes/s; C, F) were calculated using a bin size of 0.02 s and 0.01 s, respectively for mechanical and electrical stimuli. Mechanical stimuli consisted of jaw opening (D) using a Kevlar thread and muscle surface pressure applied via solenoid. Electrical stimulation consisted of two single square pulses separated by 1 s, followed by a pulse train consisting of forty pulses (G) and another single pulse delivered after 1 second. (MMO: Maximum mouth opening, MRP: Mandibular resting position).

4.2.4 Experimental design

The activity was monitored using the Open Ephys GUI and the experimental protocol was initiated when single-unit neural activity of putative muscle spindles (MSs) was detected and stable using the jaw opening condition (see below). We used two types of muscular stimulation to probe MS activity: (1) mechanical and (2) electrical stimulation (see Figure 4.1 for the overview).

4.2.4.1 Mechanical stimulation trials. Mechanical stimulation conditions included 3-6 times ramp-hold-releases for jaw opening (2 s hold phase, lengthening speed $>$ 10 mm/s, intertrial duration = 1 min) and muscle surface pressure to masseter and temporalis (per muscle, 2-4 times 0.25-0.5 s hold). Jaw opening condition consisted of moving the mandible from resting position to maximum mouth opening using a Kevlar thread attached to solenoid, holding for 2 s and releasing. Then, using a blunt plastic tip attached to another solenoid, pressure was applied superficially to the center of

the masseter and temporalis muscles three times. After the preliminary experiments, in which such muscle pressure imposition process was established using three animals, the muscle pressure period was set to 0.5 s and repeated two times per trial. After completing the electrical stimulation trials, if the animal's vital signs were stable, the mechanical stimulation conditions were repeated to confirm stability of the recordings after the long recording sessions.

First, mechanical stimuli were applied to identify MSs afferents and their muscle of origin. Conventionally, this could be done by isolating the muscle from its surroundings and lengthening the muscles from its tendon. However, because we were interested in studying the effects of force transmission through the connective tissues between muscles, we used another approach to identify MSs to avoid interfering with the connective tissues. Previous electrophysiological studies (e.g., [133–136]) reported that there are only MS afferents and periodontal mechanoreceptors, and no strong evidence indicating the existence of GTOs afferents projecting to Me5. MS afferents belonging to mastication muscles can be distinguished from the periodontal mechanoreceptors on the basis of two criteria [134, 135, 137–139]: (1) increased firing response to jaw lowering and (2) response to perturbation on individual muscles.

4.2.4.2 Electrical stimulation trials. Intramuscular electrical stimulation was used to impose isometric twitch and tetanic muscle contractions to stretch intermuscular connections between masseter and temporalis muscles. For each animal, three electrical stimulation conditions (each has 10 trials with an inter-trial duration of 1 min) per recording session were studied (i) masseter stimulation exclusively, (ii) temporalis stimulation exclusively and (iii) masseter and temporalis stimulation simultaneously. Electrical stimuli consist of two single pulses and a 400 ms pulse train, followed by another single pulse. Positive square pulses with 3.2 mA amplitude and 1 ms pulse width were intramuscularly delivered using a bipolar silver electrode. In line with our expertise in previous animal experiments (e.g., [30–32, 36, 39, 113, 140], single pulses were delivered to remove the slackness of the muscle and 100 Hz pulse trains yielded visually confirmed isometric tetanic muscle contractions.

In order to prevent muscle fatigue and potentiation, inter-stimulus duration was kept at 1 min. Each of the overall recording sessions including all conditions lasted for 60-90 mins depending on the vital signs of the animal.

4.2.5 Histology

To our knowledge, this is the first study conducting electrophysiological recordings from Me5 in mice. Presently, we used a double staining technique to confirm our recording probe location. Because interpreting cellular architecture of such a small structure as Me5 (appr. 0.4x0.4 mm2 in the transverse and 0.6x0.3 mm2 in the median plane) using regular cell membrane staining is challenging, double staining offers more accurate results. masseter and temporalis muscles were injected using a micro syringe (Nanofil 10 μl microsyringe w/33G beveled needle, World Precision Instruments) and pump (Micro4 Microsyringe Pump, injection speed: 250 nl/min) during headpost implantation surgery (7 days prior to recording) with 0.5 μl True Blue Chloride solution (TB; Santa Cruz Biotechnology, prepared 1% in sterile water) at 5 and 2 different locations for masseter and temporalis muscles, subsequently. Before each penetration in the recording day, the shanks of the electrode array were dipped into DiI solution (1 μg/μL in 99% ethanol) and allowed to dry for 5-10 mins. After the recording, animals were perfused by injection of 20 ml PBS (150 ml/hour) followed by 20 ml PFA (4% solution in PBS, kept at 4°C) into the left ventricle while the right atrium was cut. Then, the brains were extracted and kept in 4% PFA at 4°C fridge, followed by 30% sucrose until the brain sinks at the bottom of the container before the slice preparation. The brains were freeze-sectioned into 40 and 50 μm slices using a microtome (HM 440 E, Microm, Germany) and the slices were mounted into 0.17 mm glass coverslips using FluorSave^{TM} as the mounting reagent. Then slices were imaged using a light microscope (Thunder, Leica, Germany) using selective filters for DiI: excitation (549 nm) and emission (565 nm) as well as TB: excitation (386 nm) & emission (420 nm) with 20x/0.80 Air (0.40 mm) objective.

4.2.6 Neural Data Analysis

Data were digitized using a 64-channel headstage (Intan Technologies) connected to a neurophysiology recording system (Open Ephys, Cambridge, USA). During electrical stimulation, 1 ms square pulses were set on the continuous knob of the stimulator, but they effectively generated artifacts that last 1-2 ms in the recording electrodes, during which no spiking activity was expected. Thus, the raw signal was preprocessed to remove the stimulation artifacts using a custom-made template subtraction method, a variation of the ones in the literature [141–146]. The stimulation artifact length was too variable to allow for a reliable analysis within a 2 ms window from stimulus start (Figure 4.2A). Hence, this period was excluded (zeroed out) from analysis for each stimulus (Figure 4.2B). A custom algorithm was utilized to separate the neural data from the artifact in between the single pulses (Figure 4.2C). Specifically, exponential, polynomial, and robust local regression methods were employed to construct the average pattern template, with the best fit determined by the highest coefficient of determination (R^2) to maximize signal quality. Then after subtracting the template from the parts in between the single pulses, the signal is reconstructed. Data were band-pass filtered (0.3-6.0 kHz; Figure 4.2), and spike sorted to collect single-unit responses using the custom-written autosortC from the Controller package. The average number of cells/electrode in a single session was 0.49 after the spike-sorting and curation.

For a fair comparison between the firing rates during electrical stimulation (tetanus period) and spontaneous firing rates, we excluded a 2 ms interval around each single pulse from both periods. Specifically, from the tetanus period, which consisted of 40 pulses over 400 ms, we excluded a total of 80 ms (2 ms for each pulse). Using the stimulation period as a template, we excluded the corresponding parts from the spontaneous firing period, ensuring consistency in the comparison. This way, we avoided the use of multiplication constants, which could introduce bias in representing the resting firing rate.

Mechanical stimulation conditions were used to identify MS afferents (ramp-hold-release and muscle surface pressure). Opening the jaw joint using a Kevlar thread

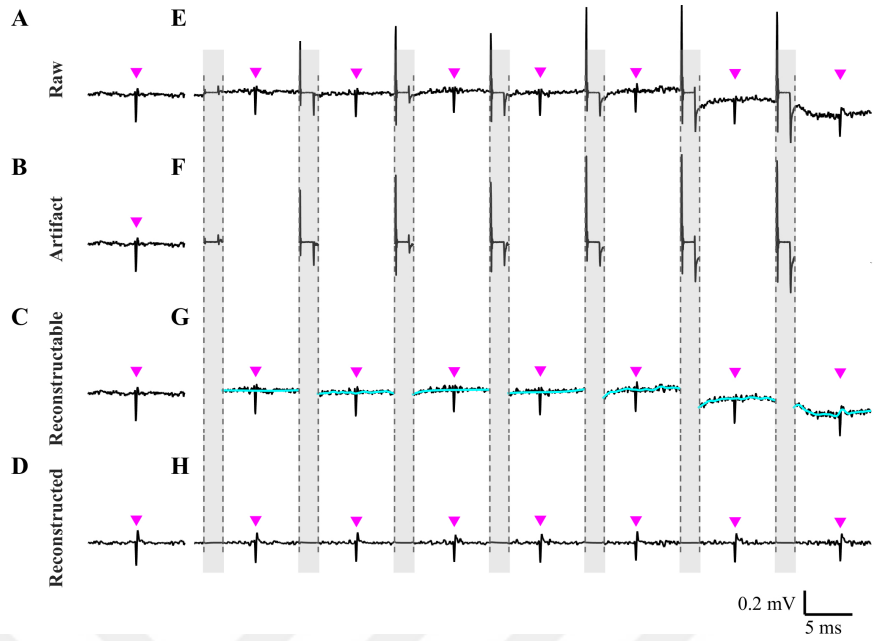

Figure 4.2 Stimulation artifact removal and signal reconstruction. (A) Raw signal (black) and stimulation artifact detection (dashed gray) of eight consecutive pulses, recorded from a muscle spindle afferent. (B) Signal divided into artifact (gray areas) and (B) reconstructable (artifact-free) segments. (C) A curve (i.e. template) was fit to reconstructable segments and the artifact segments were replaced with zero and subtracted the template from the raw artifact-free segments to reconstruct the signal. (D) Then, the signal was band-pass filtered to capture the underlying spikes indicated with downward magenta arrows across the figure.

attached to a solenoid lengthened masseter and temporalis muscles and resulted in a significant increase in MS firing rate. Imposed muscle pressure allowed the identification of MSs that belong to each muscle, as their response was more sensitive to the perturbation of one muscle than the other [134,135]. The neurons that did not respond significantly to both jaw opening and either of the muscle perturbation were excluded. Out of the total of 1344 cells identified after spike sorting, 51 cells were identified as MS afferents that belong to masseter and temporalis muscles. The inclusion criteria were a significant response to both jaw opening and muscle surface pressure conditions (see 4.3. Results section for details).

4.2.7 Statistical analyses

Statistical analyses were conducted using MATLAB (R2019b). Each recording session included 3-6 mechanical trials for each mechanical condition and 10 trials for electrical conditions. Therefore, in order to prevent time- and stimulus-dependent

variations in the spontaneous firing rate, we sampled the spontaneous firing rate in each trial in the first 30 s and last 20 s. Bin sizes were equal to the stimulus duration in each trial. It was 2 s for jaw opening conditions. For imposed muscle pressure conditions, the bin size was 0.25 s for two animals and 0.5 s for the rest.

4.2.7.1 Single-cell analysis. Significant response to each stimulation was tested using the following statistical approach. For each cell, cumulative histograms were calculated from the sampled spontaneous firing rate. Then, the driven firing rates for each trial were compared against the distribution. For each trial, p-values were calculated and the mean value per each cell was used to conclude whether that cell showed a significant response to a stimulus. Statistical differences were considered significant if $P < 0.05$.

4.2.7.2 Population analysis. To test our hypothesis, the MS afferents were divided into two groups based on their muscle of origin: masseter MSs and temporalis MSs. First, the Shapiro-Wilk normality test was applied. Based on the results, either paired t-test or Wilcoxon Signed-Rank test was conducted between the spontaneous and driven firing rates to test the effect of each stimulation on different MSs. Furthermore, spontaneous firing rates of masseter and temporalis MSs were compared in different electrical stimulation conditions with either repeated measures ANOVA or Friedman test based on the normality tests and Mauchly's test for sphericity to reveal the time-dependent differences. If no significant difference was found, the relative firing rate was calculated as the difference between the driven and spontaneous firing rates, but if a difference was found, this difference was divided by the standard deviation. Then, based on the results of the normality and sphericity tests, either repeated measures ANOVA or Friedman test followed by post hoc analyses with Bonferroni correction were used to compare relative firing rates and highlight the effects of added activation of a synergist on MS feedback.

4.3 Results

We recorded from the trigeminal mesencephalic nucleus (Me5) in urethane anesthetized mice (n = 11) using extracellular recordings via 64-channel multi-shank electrodes (Figure 4.1A). We extracted 1433 units using spike sorting. In the analysis, we first identify muscle spindle (MS) afferents located in the masseter and temporalis muscles in response to mechanical stimuli (jaw opening and muscle surface pressure, Figure 4.1B-D). Then, we use electrical stimuli (Figure 4.1E-G) to test our hypothesis that synergistic muscle contraction alters the feedback from MS afferents. In a subset of animals, we used a double staining technique to verify the location of the probe in relation to the Me5 in mice (Figure 4.3).

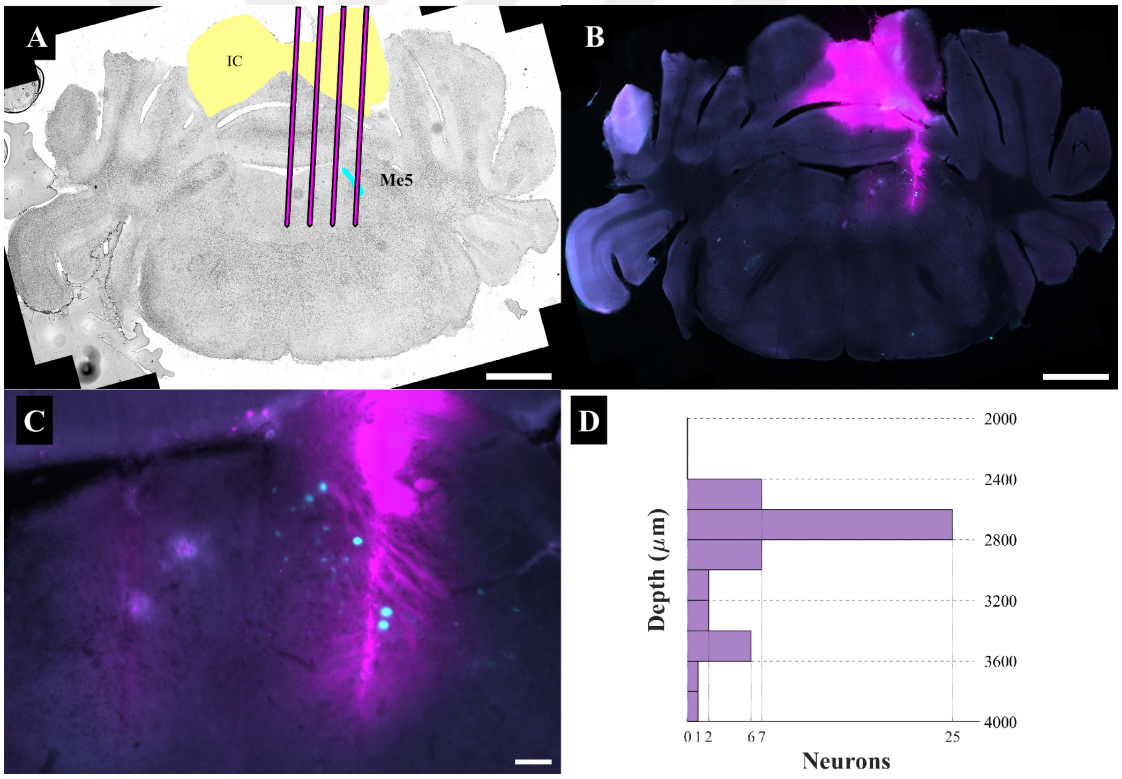

Figure 4.3 Sample brain section of double staining. (A) Four-shank electrode array (magenta in A) was advanced into the brainstem using the inferior colliculus (IC; yellow in A) as a reference to target the trigeminal mesencephalic nucleus (Me5; cyan in A). (B) Electrode array was stained with DiI (magenta in B and C) and stained the brain. (C) True blue chloride dye (cyan in B and C) injected into skeletal muscles lead to staining of muscle spindle afferents projecting to the trigeminal mesencephalic nucleus in the brainstem in mice. (D) Distribution of muscle spindle afferents identified in Me5 across different depths in the brainstem. Note that, there was a difference between the penetration plane of the probe and the imaging angle. Therefore, only one shank of the electrode array is visible. All these results confirmed our success in landing the probe into the right location. While scale bars in Panel A and B show 1 mm, the scale bar in Panel C shows 100 μm.

4.3.1 MS afferent and origin identification

4.3.1.1 Jaw opening condition. With this condition, we aimed to identify neurons that are responding to muscle stretch. We used four inclusion criteria to confidently identify the cells responding to jaw opening: signal-to-noise ratio threshold of 3.5, minimum modulation ratio of 2 and minimum firing rate of 20 Hz during the stimulus. Out of the 154 cells significantly responding to jaw opening, 67 exceeded the signal-to-noise ratio threshold. From the remaining cells, 33 were excluded based on the modulation ratio, 25 based on the firing rate threshold, and 11 after visual inspection of spike waveforms. After accounting for cells excluded by multiple criteria, 51 cells were included in total. The included and excluded cells are shown in Figure 4.4A.

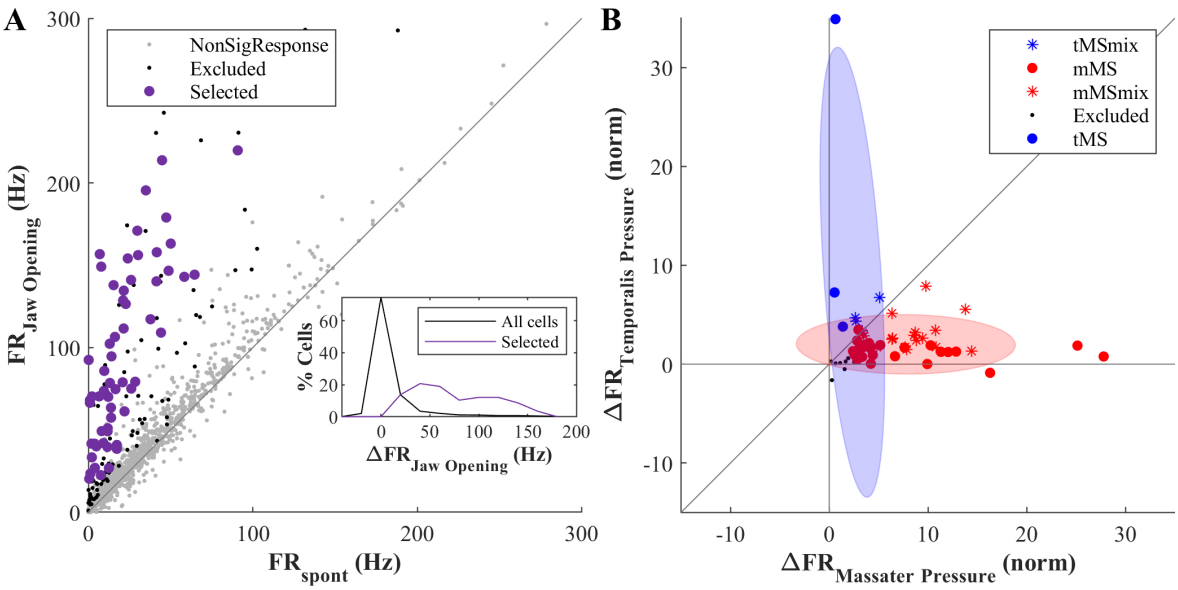

Figure 4.4 Response to mechanical stimuli. (A) Cells' response to jaw opening condition. Scatter plot shows the mean spontaneous (FR_{spont}) and driven firing rate during jaw opening ($FR_{Jaw\ Opening}$) condition of all the cells recorded from the trigeminal mesencephalic nucleus. Inset figure shows the distribution of the relative firing rates ($\Delta FR_{Jaw\ Opening}$) in all the cells recorded (black) and identified muscle spindle afferents (purple). (B) Relative firing rate of the muscle spindle afferents in response to masseter ($\Delta FR_{Masseter\ Pressure}$) and temporalis ($\Delta FR_{Temporalis\ Pressure}$) surface pressure conditions. The ellipses show the 95% confidence intervals of masseter (red) and temporalis (blue) muscle spindles.

4.3.1.2 Muscle surface pressure condition. After identifying the neurons that respond to muscle stretch (putative MSs), we applied muscle surface pressure to both

masseter and temporalis muscles to identify the MSs located specifically in these muscles. Moreover, although the jaw opening condition was the primary criterion to reliably identify MS afferents in Me5 [134, 135], we used the muscle surface pressure conditions as a control to verify the MS identity. Even though we aimed to place Kevlar loop to diastema, where there is no tooth, jaw opening using a Kevlar loop might stimulate periodontal mechanoreceptors. By applying muscle surface pressure using a solenoid, we identified MS afferents that belong to either masseter or temporalis muscles. Another possibility is that some MS afferents identified with jaw opening condition can originate from deeper parts of the mastication muscles which cannot be stimulated with the application of muscle surface pressure or from pterygoid muscle, a small muscle located underneath the masseter muscle. Therefore, those MS afferents could be the cells that are significantly responding to jaw opening but not muscle surface pressure of masseter or temporalis muscles (n = 8). On the other hand, for the cells that are significantly responding to jaw opening and both muscle surface pressure conditions, the muscle of origin is determined by the effect size (i.e., quantified as Cohen's d), the muscle of origin being more sensitive to muscle pressure than the other [134, 135]. Relative responses to masseter and temporalis were calculated as the mean firing rate during stimulation period - mean firing rate during spontaneous activity divided by the standard deviation of the spontaneous activity. This approach aimed to minimize the inter-trial and time-dependent differences (Figure 4.4B). In the end, we identified a total of 51 MS afferents belonging to masseter and temporalis muscles. Out of these, 44 of these were masseter MSs and 7 were temporalis MSs.

4.3.2 The effects of synergistic muscle stimulation

We tested the hypothesis that the activity of a synergistic muscle changes the MS response. For this purpose, we analyzed the effect of electrical stimulation of masseter (eM), temporalis (eT) and both muscles (eMT) on MS afferents located in masseter and temporalis muscles (see Figure 4.5).

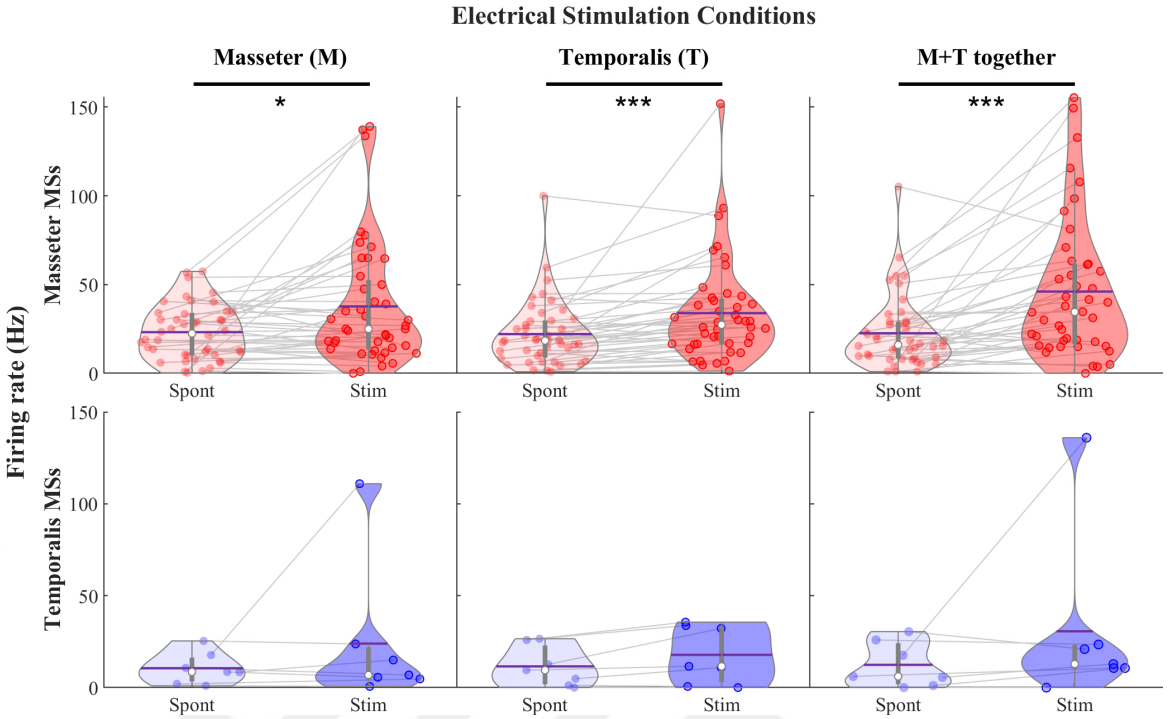

Figure 4.5 Response to electrical stimuli. Firing rates of masseter (red) and temporalis (blue) muscle spindle afferents to electrical stimulation of masseter (M), temporalis (T) and both muscles (M+T) simultaneously. The horizontal solid purple lines indicate the mean of the distribution, the white circles indicate the median, and the inner gray boxes indicate the interquartile range. Asterisks under horizontal lines indicate significant differences ($*P < 0.05$, and $***P < 0.001$) between the spontaneous and driven firing rates during pulse train stimulation in each condition.

4.3.2.1 Masseter MSs. First, we tested whether the masseter MSs' spontaneous (FR_{spont}) and driven (FR_{driven}) firing rates under electrical stimulation conditions meet the normality assumption for parametric tests (Shapiro-Wilk normality test; $P < 0.001$ for FR_{driven} in eM, eT, eMT, and for FR_{spont} in eT, eMT; $P = 0.074$ for FR_{spont} in eM). Next, we examined how electrical tetanic stimulation of the masseter, temporalis, and both muscles together affects the masseter MSs' neural signal by comparing the FR_{spont} and FR_{driven} in each condition (Wilcoxon Signed-Rank test; $P = 0.029$ for eM, $P < 0.001$ for eT and eMT). On average, the firing rate of masseter MSs increased by 62.70% from $FR_{spont} = 23.17$ Hz to $FR_{driven} = 37.69$ Hz for eM, by 53.50% from $FR_{spont} = 22.09$ Hz to $FR_{driven} = 33.91$ Hz for eT, by 103.90% from $FR_{spont} = 22.59$ Hz to $FR_{driven} = 46.06$ Hz for eMT.

Since the electrical stimulation of masseter, temporalis, and both muscles occurred sequentially during the experiments, this could introduce time-dependent effects on MS response. Indeed, testing for differences between the FR_{spont} in each condition yielded a significant difference (Friedman test; $P = 0.029$). Accordingly, we normalized the relative firing rate ($FR_{relative}$) based on the standard deviation of the FR_{spont} for each condition. To identify the effect of added activation of synergistic muscle stimulation, we compared $FR_{relative}$ in each condition, yielding a significant difference (Friedman test; $P = 0.007$). The significant difference was found between eM and eMT (multiple comparisons with Bonferroni correction; $P = 0.006$ between eM and eMT, $P = 0.128$ between eM and eT, and $P = 0.859$ between eT and eMT), indicating that added activation of synergistic temporalis muscle significantly increased the $FR_{relative}$ of the masseter MSs.

4.3.2.2 Temporalis MSs. Initially, we tested whether the FR_{spont} and FR_{driven} of temporalis MSs under electrical stimulation conditions meet the normality assumption for parametric tests (Shapiro-Wilk normality test; $P = 0.002$, $P = 0.101$, $P = 0.001$ for FR_{driven} and $P = 0.511$, $P = 0.205$, $P = 0.225$ for FR_{spont} in eM, eT, eMT conditions, respectively). Then, we examined how electrical tetanic stimulation of the masseter, temporalis, and both muscles together affects the neural signal of temporalis MSs by comparing the FR_{spont} and FR_{driven} in each condition (Wilcoxon Signed-Rank test; $P = 0.813$, $P = 0.313$ for eM, eMT, respectively, and paired t-test; $P = 0.055$ for eT). On average, the firing rate of temporalis MSs increased by 127.18% from $FR_{spont} = 10.53$ Hz to $FR_{driven} = 23.93$ Hz for eM, by 54.44% from $FR_{spont} = 11.53$ Hz to $FR_{driven} = 17.81$ Hz for eT, by 147.32% from $FR_{spont} = 12.38$ Hz to $FR_{driven} = 30.63$ Hz for eMT.

After confirming that the sphericity assumption holds (Mauchly's test for sphericity; $P = 0.466$), no significant time-dependent difference was found between the FR_{spont} in different conditions (repeated measures ANOVA; $P = 0.885$). We then checked the normality assumption for parametric tests between $FR_{relative}$ in each condition (Shapiro-Wilk normality test; $P < 0.001$, $P = 0.311$, $P = 0.001$ for eM, eT, eMT, respectively).

Subsequently, no significant effect of added activation of the synergist muscle was found for temporalis MSs (Friedman test; $P = 0.618$).

4.4 Discussion

In this study, we investigated how the activation of neighboring muscles affects muscle spindle (MS) afferent feedback in the mouse trigeminal mesencephalic nucleus (Me5). Using mechanical stimuli, we identified MS afferents originating from masseter and temporalis muscles. Our findings demonstrated that masseter MSs firing rates increase in response to temporalis muscle contraction, induced by electrical stimulation (Figure 4.6).

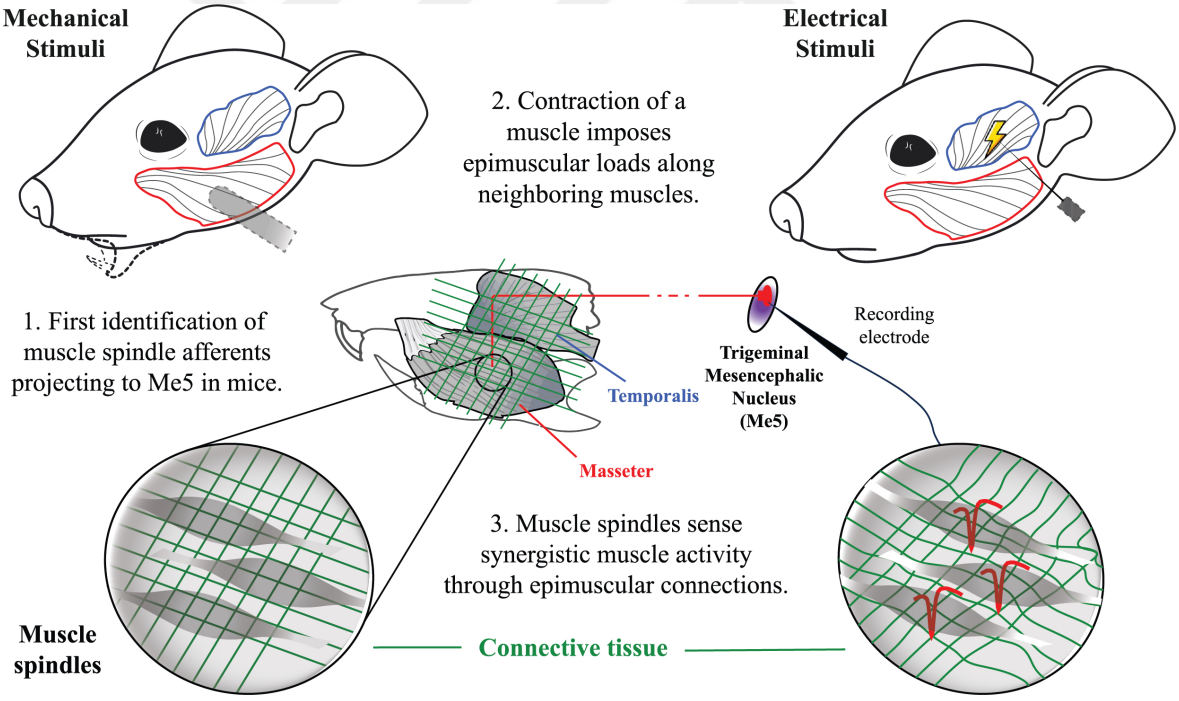

Figure 4.6 Schematic illustration of MS afferent projections to Me5 in mice. MSs located in the masseter and temporalis muscles, along with their afferent fibers projecting to Me5, are illustrated. Panel 1 depicts the identification of muscle spindle afferents using mechanical stimuli. Panel 2 demonstrates how muscle contraction imposes epimuscular loads along neighboring muscles via connective tissue structures (green lines). In panel 3, magnified views highlight the changes in connective tissue structures due to imposed epimuscular loads during stimulation of the synergistic temporalis muscle. Muscle spindles in the masseter, embedded in connective tissue, sense synergistic activity from the temporalis muscle through these epimuscular connections.

The observed increase in MS afferent activity could be attributed to two potential mechanisms: mechanical and neural. The mechanical mechanism involves the direct stretching of intermuscular connective tissue between the two muscles, which in turn stretches the intrafusal muscle fibers and activates the masseter MSs. Additionally, the neural mechanism may involve gamma motor neurons activating masseter MS afferents in response to the activation of the synergistic temporalis muscle. Despite no supporting evidence, it could have been possible that electrical stimulation might depolarized MS sensory endings in temporalis muscle and triggered reflexive response in synergistic masseter muscle. However, the influence of anesthesia must be taken into account. Because, the deep general anesthesia induced by urethane in this study suppresses central nervous system (CNS) and brainstem activities, including gamma motor drive. Maggi and Meli [147] reported dose-dependent muscle relaxation in rats under urethane anesthesia, with complete muscle relaxation occurring by 3 hours at a dose of 1.2 g/kg. The dose of 1.7 g/kg used in this study was considerably higher, producing faster-acting, deeper muscle relaxation and indicating stronger suppression of gamma motor activity. Additionally, the absence of visible contraction in other muscles during electrical stimulation suggests a lack of reflexive activity through alpha motor neurons, making alpha-gamma co-activation in these muscles highly unlikely. Nevertheless, this phenomenon occurs to adjust MS sensitivity to length changes typically during voluntary movements.

Moreover, the differences between the masticatory muscles (which project to Me5) and limb muscles (which project to spinal ganglia) must be acknowledged. For example, MS function during eating may differ from during limb movements. Studies on awake monkeys targeting the Me5 nucleus during voluntary contractions reported that MS activity decreases during jaw-closing movements, despite the active shortening of extrafusal fibers [135]. This difference was probably observed because decreased MS discharge during chewing prevents reflexive contractions against hard objects, aided by the integration of sensory information from periodontal receptors. On the other hand, MS activity in limb muscles often increases with gamma motor modulation during voluntary movements, enhancing proprioceptive feedback. Nonetheless, the present experiments were under anesthesia and yielded compatible responses to the MSs pro-

jecting to the spinal cord. Note that, researchers also indicated that although MSs contribute to muscle force regulation, MS afferent signals alone were insufficient to activate motor neurons. In addition, sympathetic stimulation has also been shown to reduce MS sensitivity to stretching, as demonstrated by Roatta et al. [137] in rabbits. However, these studies did not examine neither the contribution of synergistic muscle activity to MS responses under anesthesia nor selectively stimulated individual muscles. Therefore, direct comparisons with our findings were limited due to differences in experimental protocols.

A more substantiated explanation for the observed changes in MS activity in response to the synergistic muscle activity is intermuscular interactions. In mice, masseter and temporalis muscles are interconnected by dense connective tissues, including deep and superficial fascia, which facilitate myofascial force transmission. These structural linkages allow the contraction of one muscle to impose local forces and length changes to the other, contributing to structural integrity and movement coordination. Since MSs are highly sensitive receptors capable of detecting small local forces from individual motor units [70], they can sense these local forces acting on their collagenous capsule. The transfer of local forces occurs through the perimysium of the muscle of origin, where MSs are located [148, 149], and the epimysium of the neighboring muscle. This has been demonstrated between synergistic muscles in rats [71] and antagonist muscles in frogs [72] under passive conditions. Force transmission through these connective pathways are likely amplified by the stimulation of a neighboring muscle, which preloads the collagenous structures within the compartment [73, 74].

Although our results showed a significant overall increase in firing rate, notable a variability was observed at the individual MS level (Figure 4.5). This variability aligns with finite element modeling studies based on experimental data from rat skeletal muscles [7, 20, 150] and the observed variability in sarcomere lengths across different parts of rat [56, 57] and human [58] skeletal muscles. Variable local length [53, 54] and stiffness [55] changes have been reported in human muscles *in vivo* even under conditions without global muscle length changes [13]. Epimuscular interactions cause such variability, down to the level of individual muscle fibers [129]. These studies show

that EMFT within an intact muscle compartment can cause both local lengthening and shortening in different muscle regions. Consequently, depending on the location of MSs within the muscle, EMFT effects may enhance or reduce MS activity. Therefore, our findings suggest that MSs are distributed strain receptors embedded in the skeletal muscles, detecting the local variations within the muscle compartment.

Sensorimotor integration at the peripheral level involves the encoding of sensory information by MSs to generate motor outputs through peripheral neural pathways. Under awake, *in vivo* conditions, CNS modulates gamma motor neurons to adjust the tension in intrafusal muscle fibers, thus incorporating changes in MS signals. The sensory information across all MSs within a muscle incorporates the distribution of myofascial load along the muscle. This allows CNS to form an internal prediction of expected movement, known as temporal template [151]. This template enables the CNS to integrate and adjust for myofascial force transmission [71]. Animal studies have demonstrated such adaptations to altered intermuscular interactions, such as experimentally induced enhanced connectivity between synergistic muscles [152]. When intermuscular interactions align with expected patterns, MSs show no unusual activity, and MS feedback remains independent of the activity in synergistic muscles. However, any deviation between actual and expected movement triggers MS output, prompting compensatory adjustments in motor output. Thus, EMFT plays a crucial role in sensorimotor integration, enabling the CNS to maintain an integrated system that accounts for the local length changes within the muscle belly that reflects the myofascial force transmission within the muscle compartment. The encoding of sensory feedback about these muscular interactions is essential for maintaining healthy muscle mechanics, with disruptions in this process potentially exacerbating neuromuscular conditions (discussed in Chapter 5).

4.4.1 Limitations

One limitation of this study was related to histological procedures, which were required to verify recording locations during acute experimental sessions. To identify

the electrode sites, the electrode array was dipped into a dye solution before recordings. However, the ethanol-based DiI solution used was highly diffusive within brain tissue, resulting in a cloudy appearance at the electrode insertion site under the microscope. This made it difficult to clearly identify the original insertion tracks in most brain slices. However, sections prepared with a different cutting angle relative to the electrode insertion angle successfully captured the electrode array location (Figure 4.3A). Additionally, histological analysis on animals that underwent long recording sessions was challenging, requiring quick termination of the experiment with perfusion. Therefore, one animal was used exclusively for histological analysis, as it was lost before the recordings could be completed. Consequently, from a total of 51 MSs recorded, 12 units were recorded from the three animals that underwent successful histological analysis. Figure 4.3 shows 3 of the MS units obtained from the displayed histologically-verified recording. Although histological data were limited, the consistency of electrophysiological recordings and functional confirmations across all animals supports the reliability of our electrode placements.

It was a challenging task to identify MSs' origin without exposing and thus interfering with the connective tissues. However, jaw opening condition served as a reliable method to identify MSs. Following approaches in the studies that utilize larger animals, we applied inclusion criteria by combining jaw opening with muscle surface pressure to enhance accuracy. Apart from the masseter and Temporalis muscles studied here, there is another muscle called Pterygoid, whose MS afferents project to Me5. Yet, due to its deep location beneath the masseter, it was formidable to confidently identify MSs located in the pterygoid solely using surface pressure techniques, precluding its inclusion in this study. Although we potentially recorded MS activity in the pterygoid during jaw opening (Figure 4.4A), those units did not respond to muscle surface pressure, hence were excluded (please see 4.3. Results section and Figure 4.4B). Moreover, our findings regarding MSs being responsive to muscle surface pressure were aligned with previous studies demonstrating that small local length changes along muscle fibers can activate MSs in the target muscle (e.g., [71, 72]). Notably, as observed in other studies [134, 135], MSs showing higher responses to a specific muscle, imposed by passive over-the-skin muscle perturbations, than the other provided a reliable means

to identify the muscle of origin.

Recording electrical activity during stimulation without artifacts is challenging when the recording and stimulating electrodes are in close proximity. To address this, we implemented offline processing strategies to manage these artifacts effectively. While online hardware solutions could potentially offer more professional handling, integrating such a solution would have required a dedicated project beyond the scope of our study and likely would not have significantly improved our results. Artifact removal technique used in this study resulted in minimal data loss and found successful.

4.4.2 Conclusion

To our knowledge, this is the first study to report in vivo electrophysiological recordings from the Me5 nucleus in mice, identifying MS afferents located in masseter and temporalis muscles. This is significant for two reasons. First, we demonstrate that Me5 can be successfully targeted for acute recordings in mice, establishing it as a suitable model for studying this nucleus. Thus, our electrophysiological and histological findings confirmed hypothesis (1). Because mice are commonly used in genetic research, this opens up new opportunities to study Me5 in genetically modified mouse models.

Second, Me5 is a unique nucleus containing the first-order MS afferent fibers in the CNS, making it ideal for studying MS function without disrupting muscle architecture. This setup facilitates the investigation of both neural and mechanical mechanisms underlying intermuscular interactions that modulate MS feedback. Our results showed that activity in neighboring muscles significantly influences sensory feedback from MSs, highlighting the role of EMFT in this process and supporting hypothesis (2). This study lays the foundation for further exploration of EMFT's effects on sensorimotor integration and CNS's regulation of MS function. However note that, while nerve-crushing techniques could have made sure to eliminate the contribution of neural pathways to synergistic MS activity, they are challenging to execute due to the small anatomy that should be acknowledged when using mice.

5. INTEGRATED DISCUSSION

This thesis investigates the mechanical and sensory implications of epimuscular myofascial force transmission (EMFT) within the neuromusculoskeletal system, focusing on interactions between skeletal muscles, connective tissues, and sensory receptors. Chapters 2 and 3 addressed the mechanical aspects of EMFT, utilizing rat models alongside traditional experimental methodologies, such as in vivo muscle force measurements, nerve stimulation, and biochemical analysis. By examining how long-term exposure to Botulinum Toxin Type A (BTX-A) influences the intermuscular mechanical interactions among synergistic muscles, this work filled a critical knowledge gap in the field. Shifting focus to the sensory domain, Chapter 4 employed mouse models, microsurgical techniques, histological analysis, and in vivo electrophysiology to explore the impact of mechanical interactions between synergistic muscles on muscle spindle (MS) neural feedback in active muscle state. Representing the first in vivo acute electrophysiological recordings from mouse Me5, this work opened new avenues for studying MS afferent signals within the scope of EMFT. Beyond informing BTX-A applications for spasticity management, these findings also provided insights into how EMFT contributes to sensorimotor by influencing MSs' encoding of local length changes.

5.1 EMFT in Spasticity Management Using BTX-A

Neuromuscular therapeutic interventions, especially for managing conditions like spasticity, require considerations of biomechanical and neurological factors. While BTX-A is commonly employed to manage spasticity, concerns persist regarding its long-term efficacy. Animal experiments have greatly advanced understanding of BTX-A's impact on muscle mechanics, offering essential insights even with inherent limitations in clinical translation such as the differences between species and the use of healthy animals. Nonetheless, these preclinical findings remain critical for shaping clinical strategies; hence, this thesis relied on animal models to explore the biomechanical

impact of BTX-A.

Even though animal research showed that BTX-A changes the individual muscle mechanics, these changes do not consistently yield functional improvements in the clinic. As a neurotoxin, BTX-A reduces abnormal positive motor drive by paralyzing the exposed muscles. However, because skeletal muscles are essential for motor function, BTX-A's side effects—such as muscle atrophy, reduced contractile material, and connective tissue stiffening—raise significant concerns about its long-term impact on muscle function. Therefore, understanding how BTX-A affects individual and intermuscular mechanics, along with its influence on pathological neural drive, is crucial to optimize clinical use.

In the first part of this thesis, rat experiments were conducted to investigate the long-term mechanical implications of EMFT in the context of BTX-A intervention. While Chapter 2 focused on direct intermuscular interactions between the target (i.e., BTX-A injected) mono-articular muscle and its synergists [113], Chapter 3 examined the differential effects on the tendons of a non-targeted bi-articular muscle exposed through leakage [140]. Findings indicated that adverse effects of BTX-A (e.g., narrowed length range of force exertion and increased passive force) persisted at the individual muscle level for all the muscles exposed. However, BTX-A's diminishing effect on EMFT did not appear to be sustained long-term.

Clinical observation consistently documented frequent unintentional co-activation of spastic muscles [76, 77] and limited muscle range due to the co-activation with synergists in spastic muscles [44–46]. These findings highlighted EMFT's substantial role in spastic muscle mechanics, underscoring two critical implications: First, BTX-A's effects should be evaluated beyond individual muscles, incorporating patient-specific intermuscular interactions. Second, BTX-A may effectively reduce abnormal muscle tone arising from abnormal afferent firing due to abnormal spastic muscle coupling, potentially linked to the intermuscular mechanical interactions.

The second part of this thesis, presented in Chapter 4, investigated EMFT's sen-

sory implications in mice. Prior studies have only examined how inter-antagonistic [72] and inter-synergistic [71] muscular interactions impact MS sensory feedback under passive conditions, showing that passive neighboring muscle stretch affects MS responses. However, limited research existed on EMFT's effects among active muscles, which better replicates functional muscle mechanics. Addressing this gap, how inter-synergistic force transmission affects MS responses during synergistic muscle activation was explored. In this study, unlike the rat experiments, we employed a selective muscle stimulation methodology as in the intraoperative measurements unveiling the effects of EMFT among spastic muscles. Results indicated that the average firing rate of MSs increased in response to stimulation of synergistic muscles. This increase showed variability, with firing rates reflecting location-specific differences in local length changes along muscle fibers during contraction. This study is currently under revision for publication.

BTX-A indiscriminately paralyzes muscle fibers, reducing MS activity by paralyzing intrafusal fibers, a mechanism generally viewed favorably in the literature [126]. However, BTX-A's impact on MS activity is complex due to its influence on EMFT. In patients with spasticity, pathological synergistic or antagonistic activation can already result in disruptions to MS feedback through intermuscular interactions, a critical consideration for spastic cerebral palsy patients. Although abnormal MS firing (i.e., sensorimotor noise) may not directly cause disability—instead arising as a reflection of the abnormal downward propagation of neural signals from an upper motor neuron lesion—it can still exacerbate symptoms by increasing tonic firing in the peripheral nervous system. Additionally, while the research on BTX-A's direct effects on CNS still in the preclinical stage, BTX-A-induced structural changes in both muscular and connective tissue can impair peripheral nervous system activity, including MS feedback. This impairment could lead to plastic changes and reorganization in the CNS, potentially worsening the pathology over time.

On the other hand, BTX-A injections for patients with such MS afferent signaling abnormalities [119, 153] may help suppress unintended intermuscular mechanical coupling, reduce sensory coupling and alleviate associated symptoms. After all, as Gi-

ladi noted [154], BTX-A performs a "sensory trick" by partially paralyzing muscles and silencing sensory feedback without addressing the underlying pathology. Consequently, BTX-A's uncontrolled and variable effects over time can lead to mixed outcomes once the toxin wears off. Moreover, BTX-A-induced atrophy of both extra- and intrafusal fibers further weakens the muscle, complicates EMFT mechanisms and affects the sensory representation of the muscle by altering MS feedback. These limitations underscore the need for refined interventions in the clinic. For instance, selective targeting of intrafusal fibers might allow clinicians to harness BTX-A's benefits by suppressing MS firing while preserving extrafusal fiber function, thereby reducing abnormal motor drive in spasticity. Alternatively, modifying BTX-A with C3-transferase, an enzyme that reduces muscle stiffness, has shown potential for reducing adverse effects at the individual muscle level [155]. Nevertheless, there is no doubt that gaining better control over EMFT-related effects will improve the outcome of the intervention.

5.2 EMFT's Contribution to Sensorimotor Integration

Sensorimotor integration at the peripheral level refers to the process of dynamically generating motor responses based on sensory inputs from receptors responsible for proprioception in the peripheral nervous system. In this context, sensory information encoded by MS provides data on the distribution of local length changes along muscle fibers, offering a lower-resolution read-out of the sarcomere length distribution across muscle bellies. Moreover, through a continuum of collagenous structures at intra-, inter-, and extra-muscular levels, the nervous system can detect changes in the mechanical equilibrium among muscles within the entire compartment, allowing fine-tuning of muscles' output. Integrating such proprioceptive data offer the ability to incorporate factors like the stiffness and orientation of myofascial connective tissues, as well as the epimuscular loads acting through them, that significantly influence muscles' force-production characteristics. During muscular activity, CNS constantly creates a spatiotemporal template for the anticipated movement, relying on MS sensory feedback. Therefore, EMFT's contribution to such sensorimotor integration through MS signals is vital for CNS to adapt to external disturbances, refine motor predictions and

thereby supporting coordinated balance, posture, and movement in harmony.

5.3 Final Remarks and Future Directions

Several alternative approaches could improve the perspective of this thesis. In Chapter 4, we used mouse models to leverage the capabilities of *in vivo* acute electrophysiological recording techniques to study how EMFT affects MS activity. This research led to the development of new methods to study MS activity in the mouse Me5, directly targeting MS sensory afferents—similar to spinal sensory ganglia—which represents, from available records, the first instance in the literature. Although there could be functional differences between MSs located in masticatory muscles and limb muscles, the present experiments were under anesthesia and yielded compatible responses to the MSs projecting to spinal cord. Moreover, significant experimental advantages existed for working this muscle group, including the ability to keep nervous tissue intact. In contrary, experimental preparations to record from spinal ganglia require laborious preparations to keep the nerves functional and stable while susceptible to the interferences during recording. Studying EMFT in mouse Me5 offers further advantages, such as enabling genetically modified strains. This is particularly useful when advanced experimental techniques such as neuronal marking together with nerve crushing will be utilized to manipulate specific sensory and motor neurons as well as muscle fibers. Note that however, when such techniques are employed, it is essential to confirm they do not alter signaling in the neuronal circuitry or interfere with collagenous structures in a way to deviate from *in vivo* physiology. Furthermore, the selective application of intramuscular electrical stimulation in EMFT studies warrants elaborate exploration but, fine-tuning and standardization of such technique requires further attention and should be more extensively documented in the literature. These methodological improvements would definitely deepen the understanding of EMFT's role in modulating MS feedback.

APPENDIX A. ILLUSTRATION OF LONGER SARCOMERE EFFECT

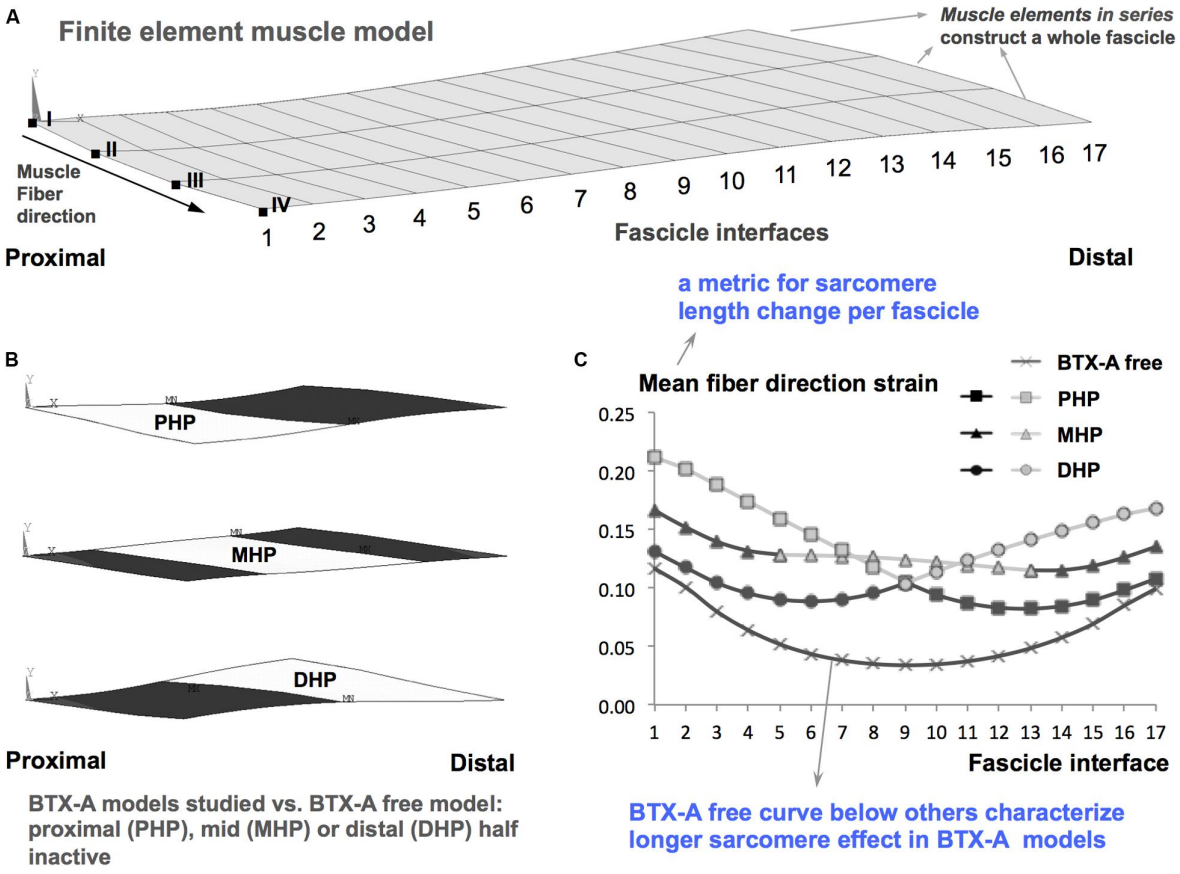

Figure A.1 An illustration of longer sarcomere effects. (A) Turkoglu et al. [94] modeled a skeletal muscle comprising a series of interconnected muscle elements that form entire fascicles. Each set of model nodes along one side of a fascicle was called a fascicle interface. For example, the most proximal fascicle interface combines nodes indicated by Roman numerals from I to IV. Each fascicle interface is sequentially numbered from 1 to 17. Local length changes along the muscle fiber direction, i.e., fiber direction strain, are analyzed. (B) Schematic representation of the BTX-A models analyzed. These models simulate partial muscle paralysis by inactivating muscle elements in the proximal half (PHP), middle half (MHP), or distal half (DHP) of the muscle. Paralyzed areas are shown in white, while black regions represent maximally activated sections. These models are compared against a control model without BTX-A (in which the entire muscle is maximally activated). (C) The characteristic longer sarcomere effect of BTX-A, as previously shown [94], is exemplified here. The mean fiber direction strain reflects the average local length changes across nodes I to IV at each fascicle interface, representing sarcomere length change per fascicle. The mean fiber direction strain curve for the BTX-A-free muscle localized below those of the BTX-A models, indicating that sarcomeres in BTX-A-exposed muscle attains longer lengths. This figure is adapted from [94].

APPENDIX B. BTX-A INJECTION PROCEDURES IN ANIMAL EXPERIMENTS VS. CLINICAL PRACTICE

By facilitating controlled interventions, animal experiments help to successfully develop fundamental knowledge about the effects of BTX-A injection on muscular mechanics. Yet, BTX-A injection procedures for spastic CP patients differ in common clinical practice with regard to mainly injection dose, volume and available guiding technology. In the lower extremity, clinical injection dosage ranges between 3 to 6 U kg^{-1} body weight [35, 112], which is much higher than the dosage we used presently (approximately 0.32 U kg^{-1}). However, consistent with previous studies that explored the effects of BTX-A on rat skeletal muscle [30–32, 36, 39, 113], the dosage used in this study did impose a substantial decrease in the measured active muscle forces, hence it was effective. The present single injection volume (approximately 64 μl kg^{-1}) was also well below injection volumes typically used in human lower limb muscles (2.5-8 ml kg^{-1}) [35, 112] which, is administered by dividing the total volume between several injection sites [27, 111]. Considering a single injection protocol employed, we may have provoked the leakage of the toxin into non-injected muscle although such spread of the BTX-A beyond the injection site was also shown to be possible after multiple injections [24]. Lastly, unlike the present experiments, although assistive techniques such as ultrasound imaging are used to localize the injection site in clinics, Picelli et al. [110] showed that such guidance is not significantly superior to the injections made by manual placement methods for superficial muscles. Nevertheless, the differences between BTX-A injection conventions applicable in animal experiments and clinical protocols are clear. However, the present findings do provide new insights for ultimately obtaining an improved outcome of BTX-A treatment provided that they are tested in specific clinical trials.

REFERENCES

1. Betts, J. G., K. A. Young, J. A. Wise, E. Johnson, and et al., *Anatomy and Physiology / OpenStax*, OpenStax, apr 25 2013.

2. Biga, L. M., S. Bronson, S. Dawson, A. Harwell, and et al., *Mohawk - PN Structure & Function of the Human Body*, OpenStax/Oregon State University, sep 26 2019.

3. Schleip, R., C. Stecco, M. Driscoll, and P. Huijing, *Fascia: The Tensional Network of the Human Body Expert Consult: Fascia: The Tensional Network of the Human Body - E-Book*, Elsevier Health Sciences, dec 8 2021.

4. Huijing, P. A., "Muscle as a collagen fiber reinforced composite: A review of force transmission in muscle and whole limb," *Journal of Biomechanics*, Vol. 32, no. 4, pp. 329–345, 1999.

5. Purslow, P. P., "The Structure and Role of Intramuscular Connective Tissue in Muscle Function," *Frontiers in Physiology*, Vol. 11, 2020.

6. Maas, H., G. C. Baan, and P. A. Huijing, "Intermuscular interaction via myofascial force transmission: Effects of tibialis anterior and extensor hallucis longus length on force transmission from rat extensor digitorum longus muscle," *Journal of Biomechanics*, Vol. 34, no. 7, pp. 927–940, 2001. PMID: 11410176.

7. Yucesoy, C., B. Koopman, G. Baan, H. Grootenboer, and P. Huijing, "Extramuscular myofascial force transmission: Experiments and finite element modeling," *Archives of Physiology and Biochemistry*, Vol. 111, no. 4, pp. 377–388, 2003.

8. Yucesoy, "Epimuscular myofascial force transmission implies novel principles for muscular mechanics," *Exercise and Sport Sciences Reviews*, Vol. 38, no. 3, pp. 128–134, 2010.

9. Huijing, P. A., "Epimuscular myofascial force transmission: A historical review and implications for new research. International society of biomechanics Muybridge award lecture, Taipei, 2007," *Journal of Biomechanics*, Vol. 42, no. 1, pp. 9–21, 2009.

10. Bojsen-Møller, J., S. Schwartz, K. K. Kalliokoski, T. Finni, and et al., "Intermuscular force transmission between human plantarflexor muscles in vivo," *Journal of Applied Physiology*, Vol. 109, no. 6, pp. 1608–1618, 2010. PMID: 20884838.

11. Carvalhais, V. O. d. C., J. d. M. Ocarino, V. L. Araújo, T. R. Souza, and et al., "Myofascial force transmission between the latissimus dorsi and gluteus maximus muscles: An in vivo experiment," *Journal of Biomechanics*, Vol. 46, no. 5, pp. 1003–1007, 2013.

12. Oda, T., R. Himeno, D. C Hay, K. Chino, and et al., "In vivo behavior of muscle fascicles and tendinous tissues in human tibialis anterior muscle during twitch contraction," *Journal of Biomechanics*, Vol. 40, no. 14, pp. 3114–3120, 2007.

13. Yaman, A., C. Ozturk, P. A. Huijing, and C. A. Yucesoy, "Magnetic resonance imaging assessment of mechanical interactions between human lower leg muscles in vivo," *Journal of Biomechanical Engineering*, Vol. 135, no. 9, 2013.

14. Yucesoy, C. A., E. Pontén, F. J. Valero-Cuevas, M. Smeulders, and et al., "Editorial: Muscle Mechanics, Extracellular Matrix, Afferentation, Structural, and Neurological Coupling and Coordination in Health and Disease," *Frontiers in Physiology*, Vol. 12, pp. 1–6, 2021.

15. Yucesoy, C., and P. Huijing, "Substantial effects of epimuscular myofascial force transmission on muscular mechanics have major implications on spastic muscle and remedial surgery," *Journal of Electromyography and Kinesiology*, Vol. 17, no. 6, pp. 664–679, 2007. PMID: 17395489.

16. Zügel, M., C. N. Maganaris, J. Wilke, K. Jurkat-Rott, and et al., "Fascial tissue research in sports medicine: From molecules to tissue adaptation, injury and diagnostics: Consensus statement," *British Journal of Sports Medicine*, Vol. 52, no. 23, p. 1497, 2018. PMID: 30072398.

17. Huijing, P. A., "Epimuscular myofascial force transmission between antagonistic and synergistic muscles can explain movement limitation in spastic paresis," *Journal of Electromyography and Kinesiology*, Vol. 17, no. 6, pp. 708–724, 2007.

18. Huijing, P. A., and G. C. Baan, "Myofascial force transmission: Muscle relative position and length determine agonist and synergist muscle force," *Journal of Applied Physiology*, Vol. 94, no. 3, pp. 1092–1107, 2003.

19. Huijing, P. A., and G. C. Baan, "Myofascial force transmission via extramuscular pathways occurs between antagonistic muscles," *Cells Tissues Organs*, Vol. 188, no. 4, pp. 400–414, 2008. PMID: 18349517.

20. Yucesoy, B. H. Koopman, G. C. Baan, H. J. Grootenboer, and et al., "Effects of inter- and extramuscular myofascial force transmission on adjacent synergistic muscles: assessment by experiments and finite-element modeling," *Journal of Biomechanics*, Vol. 36, pp. 1797–1811, 12 2003.

21. Maas, H., G. C. Baan, P. A. Huijing, C. A. Yucesoy, and et al., "The Relative Position of EDL Muscle Affects the Length of Sarcomeres within Muscle Fibers: Experimental Results and Finite-Element Modeling," *Journal of Biomechanical Engineering*, Vol. 125, no. 5, pp. 745–753, 2003. PMID: 14618935.

22. Maas, H., H. J. Meijer, and P. A. Huijing, "Intermuscular interaction between synergists in rat originates from both intermuscular and extramuscular myofascial force transmission," *Cells Tissues Organs*, Vol. 181, no. 1, pp. 38–50, 2005. PMID: 16439817.

23. Huijing, P. A., H. Maas, and G. C. Baan, "Compartmental fasciotomy and isolating a muscle from neighboring muscles interfere with myofascial force transmission within the rat anterior crural compartment," *Journal of Morphology*, Vol. 256, no. 3, pp. 306–321, 2003.

24. Shaari, C. M., E. George, B. Wu, H. F. Biller, and et al., "Quantifying the spread of botulinum toxin through muscle fascia," *The Laryngoscope*, Vol. 101, pp. 960–964, 9 1991.

25. Shaari, C. M., and I. Sanders, "Quantifying how location and dose of botulinum toxin injections affect muscle paralysis," *Muscle & Nerve*, Vol. 16, no. 9, pp. 964–969, 1993.

26. Calderon-Gonzalez, R., R. Calderon-Sepulveda, M. Rincon-Reyes, J. Garcia-Ramirez, and et al., "Botulinum toxin a in management of cerebral palsy," *Pediatric Neurology*, Vol. 10, no. 4, pp. 284–288, 1994.

27. Graham, H. K., K. R. Aoki, I. Autti-Rämö, R. N. Boyd, and et al., "Recommendations for the use of botulinum toxin type A in the management of cerebral palsy," *Gait and Posture*, Vol. 11, no. 1, pp. 67–79, 2000.

28. Ozcakir, S., and K. Sivrioglu, "Botulinum toxin in poststroke spasticity," *Clinical Medicine and Research*, Vol. 5, no. 2, pp. 132–138, 2007.

29. Heinen, F., K. Desloovere, A. S. Schroeder, S. Berweck, I. Borggraefe, and et al., "The updated European Consensus 2009 on the use of Botulinum toxin for children with cerebral palsy," *European Journal of Paediatric Neurology*, Vol. 14, no. 1, pp. 45–66, 2010. PMID: 19914110.

30. Ateş, F., and C. A. Yucesoy, "Effects of botulinum toxin type A on non-injected bi-articular muscle include a narrower length range of force exertion and increased passive force," *Muscle and Nerve*, Vol. 49, no. 6, pp. 866–878, 2014.

31. Yucesoy, C. A., Ö. Emre Arikan, and F. Ateş, "Btx-A administration to the target muscle affects forces of all muscles within an intact compartment and epimuscular myofascial force transmission," *Journal of Biomechanical Engineering*, Vol. 134, no. 11, 2012.

32. Yucesoy, C. A., A. N. Turkoğlu, S. Umur, and F. Ateş, "Intact muscle compartment exposed to botulinum toxin type a shows compromised intermuscular mechanical interaction," *Muscle and Nerve*, Vol. 51, no. 1, pp. 106–116, 2015.

33. Ansved, T., T. Odergren, and K. Borg, "Muscle fiber atrophy in leg muscles after botulinum toxin type a treatment of cervical dystonia," *Neurology*, Vol. 48, no. 5, pp. 1440–1442, 1997.

34. Antonucci, F., C. Rossi, L. Gianfranceschi, O. Rossetto, and et al., "Long-distance retrograde effects of botulinum neurotoxin A," *Journal of Neuroscience*, Vol. 28, no. 14, pp. 3689–3696, 2008. PMID: 18385327.

35. Frasson, E., E. Dall'Ora, M. Bordignon, F. Brigo, P. Tocco, and et al., "Spread of botulinum neurotoxin type A at standard doses is inherent to the successful treatment of spastic equinus foot in cerebral palsy: Short-term neurophysiological and clinical study," *Journal of Child Neurology*, Vol. 27, no. 5, pp. 587–593, 2012. PMID: 22114218.

36. Yucesoy, C. A., and F. Ateş, "Btx-A has notable effects contradicting some treatment aims in the rat triceps surae compartment, which are not confined to the muscles injected," *Journal of Biomechanics*, Vol. 66, pp. 78–85, 2018.

37. Yucesoy, C. A., and P. A. Huijing, "Specifically Tailored Use Of The Finite Element Method To Study Muscular Mechanics Within The Context Of Fascial Integrity: The Linked Fiber-Matrix Mesh Model," *International Journal for Multiscale Computational Engineering*, Vol. 10, no. 2, 2012.

38. Yaraskavitch, M., T. Leonard, and W. Herzog, "Botox produces functional weakness in non-injected muscles adjacent to the target muscle," *Journal of Biomechanics*, Vol. 41, no. 4, pp. 897–902, 2008.

39. Ateş, F., and C. A. Yucesoy, "Botulinum toxin type-A affects mechanics of non-injected antagonistic rat muscles," *Journal of the Mechanical Behavior of Biomedical Materials*, Vol. 84, pp. 208–216, 2018.

40. Ateş, F., Y. Temelli, and C. A. Yucesoy, "Intraoperative experiments show relevance of inter-antagonistic mechanical interaction for spastic muscle's contribution to joint movement disorder," *Clinical Biomechanics*, Vol. 29, no. 8, pp. 943–949, 2014. PMID: 25001327.

41. Ateş, F., Y. Temelli, and C. A. Yucesoy, "Human spastic Gracilis muscle isometric forces measured intraoperatively as a function of knee angle show no abnormal muscular mechanics," *Clinical Biomechanics*, Vol. 28, no. 1, pp. 48–54, 2013. PMID: 23021616.

42. Ateş, F., Y. Temelli, and C. A. Yucesoy, "The mechanics of activated semitendinosus are not representative of the pathological knee joint condition of children with cerebral palsy," *Journal of Electromyography and Kinesiology*, Vol. 28, pp. 130–136, 2016.

43. Yucesoy, Y. Temelli, and F. Ateş, "Intra-operatively measured spastic semimembranosus forces of children with cerebral palsy," *Journal of Electromyography and Kinesiology*, Vol. 36, pp. 49–55, 2017.

44. Kaya, C. S., Y. Temelli, F. Ates, and C. A. Yucesoy, "Effects of inter-synergistic mechanical interactions on the mechanical behaviour of activated spastic semitendinosus muscle of patients with cerebral palsy," *Journal of the Mechanical Behavior of Biomedical Materials*, Vol. 77, pp. 78–84, 2018.

45. Kaya, C. S., F. Bilgili, N. E. Akalan, Y. Temelli, and et al., "Intraoperative experiments combined with gait analyses indicate that active state rather than passive dominates the spastic gracilis muscle's joint movement limiting effect in cerebral palsy," *Clinical Biomechanics*, Vol. 68, pp. 151–157, 2019.

46. Kaya, C. S., F. Bilgili, N. E. Akalan, and C. A. Yucesoy, "Intraoperative testing of passive and active state mechanics of spastic semitendinosus in conditions involving intermuscular mechanical interactions and gait relevant joint positions," *Journal of Biomechanics*, Vol. 103, p. 109755, 2020. PMID: 32204891.

47. Reddihough, D. S., J. A. King, G. J. Coleman, A. Fosang, and et al., "Functional outcome of botulinum toxin A injections to the lower limbs in cerebral palsy," *Developmental Medicine & Child Neurology*, Vol. 44, pp. 820–827, dec 5 2002. PMID: 12455858.

48. Tedroff, K., F. Granath, H. Forssberg, and Y. Haglund-Akerlind, "Long-term effects of botulinum toxin A in children with cerebral palsy," *Developmental Medicine & Child Neurology*, Vol. 51, pp. 120–127, 2 2009. PMID: 19191845.

49. Hastings-Ison, T., M. Sangeux, P. Thomason, B. Rawicki, M. Fahey, and et al., "Onabotulinum toxin-A (Botox) for spastic equinus in cerebral palsy: a prospective kinematic study," *Journal of Children's Orthopaedics*, Vol. 12, no. 4, pp. 390–397, 2018.

50. Rutz, E., E. Hofmann, and R. Brunner, "Preoperative botulinum toxin test injections before muscle lengthening in cerebral palsy," *Journal of Orthopaedic Science*, Vol. 15, no. 5, pp. 647–653, 2010.

51. Tamás, T., D. Gyula, H. D. H. Nikoletta, K. Sándor, and et al., "Botulinum toxin treatment in children with cerebral palsy," *Orvosi Hetilap*, Vol. 160, no. 28, pp. 1105–1111, 2019. PMID: 31280598.

52. Maas, H., and T. G. Sandercock, "Force transmission between synergistic skeletal muscles through connective tissue linkages," *Journal of Biomedicine and Biotechnology*, Vol. 2010, 2010.

53. Karakuzu, A., U. Pamuk, C. Ozturk, B. Acar, and et al., "Magnetic resonance and diffusion tensor imaging analyses indicate heterogeneous strains along human medial gastrocnemius fascicles caused by submaximal plantar-flexion activity," *Journal of Biomechanics*, Vol. 57, pp. 69–78, 2017.

54. Pamuk, U., A. Karakuzu, C. Ozturk, B. Acar, and et al., "Combined magnetic resonance and diffusion tensor imaging analyses provide a powerful tool for in vivo assessment of deformation along human muscle fibers," *Journal of the Mechanical Behavior of Biomedical Materials*, Vol. 63, pp. 207–219, 2016.

55. Ateş, F., R. J. Andrade, S. R. Freitas, F. Hug, and et al., "Passive stiffness of monoarticular lower leg muscles is influenced by knee joint angle," *European Journal of Applied Physiology*, Vol. 118, no. 3, pp. 585–593, 2018. ISBN: 0123456789.

56. Moo, E. K., R. Fortuna, S. C. Sibole, Z. Abusara, and et al., "In vivo sarcomere lengths and sarcomere elongations are not uniform across an intact muscle," *Frontiers in Physiology*, Vol. 7, pp. 1–9, 2016.

57. Tijs, C., J. H. van Dieën, and H. Maas, "Effects of epimuscular myofascial force transmission on sarcomere length of passive muscles in the rat hindlimb," *Physiological Reports*, Vol. 3, no. 11, 2015.

58. Llewellyn, M. E., R. P. Barretto, S. L. Delp, and M. J. Schnitzer, "Minimally invasive high-speed imaging of sarcomere contractile dynamics in mice and humans," *Nature*, Vol. 454, no. 7205, pp. 784–788, 2008. PMID: 18600262.

59. Proske, U., and S. C. Gandevia, "The proprioceptive senses: Their roles in signaling body shape, body position and movement, and muscle force," *Physiological Reviews*, Vol. 92, no. 4, pp. 1651–1697, 2012. PMID: 23073629.

60. Xie, P., Y. Jiang, X. Zhang, and S. Yang, "The Study of Intramuscular Nerve Distribution Patterns and Relative Spindle Abundance of the Thenar and Hypothenar Muscles in Human Hand," *PLOS ONE*, Vol. 7, p. e51538, dec 10 2012.

61. Banks, R. W., "An allometric analysis of the number of muscle spindles in mammalian skeletal muscles," *Journal of Anatomy*, Vol. 208, no. 6, pp. 753–768, 2006. PMID: 16761976.

62. Riemann, B. L., and S. M. Lephart, "The sensorimotor system, part I: The physiologic basis of functional joint stability," *Journal of Athletic Training*, Vol. 37, no. 1, pp. 71–79, 2002. PMID: 16558670.

63. Riemann, B. L., and S. M. Lephart, "The sensorimotor system, Part II: The role of proprioception in motor control and functional joint stability," *Journal of Athletic Training*, Vol. 37, no. 1, pp. 80–84, 2002. PMID: 16558671.

64. Jaalouk, D. E., and J. Lammerding, "Mechanotransduction gone awry," *Nature Reviews Molecular Cell Biology*, Vol. 10, no. 1, pp. 63–73, 2009. PMID: 19197333.

65. Kandel, E. R., J. D. Koester, S. H. Mack, and S. A. Siegelbaum, *Principles of Neural Science, Sixth Edition*, McGraw Hill Professional, apr 5 2021.

66. Bewick, G. S., and R. W. Banks, "Mechanotransduction in the muscle spindle," *Pflugers Archiv European Journal of Physiology*, Vol. 467, no. 1, pp. 175–190, 2014.

67. Adams, R. A., S. Shipp, and K. J. Friston, "Predictions not commands: Active inference in the motor system," *Brain Structure and Function*, Vol. 218, no. 3, pp. 611–643, 2013. PMID: 23129312.

68. Houk, J., and W. Simon, "Responses of Golgi tendon organs to forces applied to muscle tendon.," *Journal of Neurophysiology*, Vol. 30, no. 6, pp. 1466–1481, 1967.

69. Kistemaker, D. A., A. J. Knoek van Soest, J. D. Wong, I. Kurtzer, and P. L. Gribble, "Control of position and movement is simplified by combined muscle spindle and Golgi tendon organ feedback," *Journal of Neurophysiology*, Vol. 109, no. 4, pp. 1126–1139, 2013. PMID: 23100138.

70. Cameron, W. E., M. D. Binder, B. R. Botterman, R. M. Reinking, and et al., "Motor unit-muscle spindle interactions in active muscles of decerebrate cats," *Neuroscience Letters*, Vol. 19, no. 1, pp. 55–60, 1980.

71. Smilde, H. A., J. A. Vincent, G. C. Baan, P. Nardelli, and et al., "Changes in muscle spindle firing in response to length changes of neighboring muscles," *Journal of Neurophysiology*, Vol. 115, no. 6, pp. 3146–3155, 2016. PMID: 27075540.

72. Arıkan, Ö. E., B. Güçlü, and C. A. Yucesoy, "Altered afferent response of restrained antagonistic muscles after passive stretching of Gastrocnemius indicate a remarkable role of epimuscular myofascial force transmission in the sensory level (Abstract)," *Neuroscience 2009.*, no. October 2019, pp. 1–2, 2009.

73. Maas, H., and T. G. Sandercock, "Are skeletal muscles independent actuators? Force transmission from soleus muscle in the cat," *Journal of Applied Physiology*, Vol. 104, no. 6, pp. 1557–1567, 2008. PMID: 18339889.

74. Tijs, C., J. H. van Dieën, G. C. Baan, and H. Maas, "Synergistic co-activation increases the extent of mechanical interaction between rat ankle plantar-flexors," *Frontiers in Physiology*, Vol. 7, pp. 1–8, 2016.

75. Maas, H., G. C. Baan, and P. A. Huijing, "Muscle force is determined also by muscle relative position: Isolated effects," *Journal of Biomechanics*, Vol. 37, no. 1, pp. 99–110, 2004.

76. Tedroff, K., L. M. Knutson, and G. L. Soderberg, "Synergistic muscle activation during maximum voluntary contractions in children with and without spastic cerebral palsy," *Developmental Medicine and Child Neurology*, Vol. 48, no. 10, pp. 789–796, 2006.

77. Tedroff, K., L. M. Knutson, and G. L. Soderberg, "Co-activity during maximum voluntary contraction: A study of four lower-extremity muscles in children with and without cerebral palsy," *Developmental Medicine and Child Neurology*, Vol. 50, no. 5, pp. 377–381, 2008. PMID: 18371092.

78. Smeulders, M. J., M. Kreulen, J. J. Hage, P. A. Huijing, and et al., "Spastic muscle properties are affected by length changes of adjacent structures," *Muscle and Nerve*, Vol. 32, no. 2, pp. 208–215, 2005. PMID: 15937875.

79. Criswell, S. R., B. E. Crowner, and B. A. Racette, "The use of botulinum toxin therapy for lower-extremity spasticity in children with cerebral palsy.," *Neurosurgical focus*, Vol. 21, no. 2, pp. 1–7, 2006.

80. Lukban, M. B., R. L. Rosales, and D. Dressler, "Effectiveness of botulinum toxin A for upper and lower limb spasticity in children with cerebral palsy: A summary of evidence," *Journal of Neural Transmission*, Vol. 116, no. 3, pp. 319–331, 2009. PMID: 19142573.

81. Adams, M. M., and A. L. Hicks, "Spasticity after spinal cord injury," *Spinal Cord*, Vol. 43, pp. 577–586, 10 2005.

82. Marciniak, C., L. Rader, and C. Gagnon, "The use of botulinum toxin for spasticity after spinal cord injury," *American Journal of Physical Medicine and Rehabilitation*, Vol. 87, no. 4, pp. 312–317, 2008. PMID: 18356622.

83. Hyman, N., S. Glickman, A. Sayer, A. Richardson, and et al., "Botulinum toxin (Dysport®) treatment of hip adductor spasticity in multiple sclerosis: A prospective, randomised, double blind, placebo controlled, dose ranging study," *Journal of Neurology Neurosurgery and Psychiatry*, Vol. 68, no. 6, pp. 707–712, 2000.

84. Van Der Walt, A., S. Sung, T. Spelman, M. Marriott, and et al., "A double-blind, randomized, controlled study of botulinum toxin type A in MS-related tremor," *Neurology*, Vol. 79, pp. 92–99, jul 3 2012. PMID: 22753445.

85. Bakheit, A. M., A. F. Thilmann, A. B. Ward, W. Poewe, J. Wissel, and et al., "A randomized, double-blind, placebo-controlled, dose-ranging study to compare the efficacy and safety of three doses of botulinum toxin type A (Dysport) with placebo in upper limb spasticity after stroke," *Stroke*, Vol. 31, pp. 2402–2406, 10 2000. PMID: 11022071.

86. Bhakta, B. B., J. A. Cozens, M. A. Chamberlain, and J. M. Bamford, "Impact of botulinum toxin type A on disability and carer burden due to arm spasticity after stroke: A randomised double blind placebo controlled trial," *Journal of Neurology Neurosurgery and Psychiatry*, Vol. 69, no. 2, pp. 217–221, 2000. PMID: 10896696.

87. Grazko, M. A., K. B. Polo, and B. Jabbari, "Botulinum toxin A for spasticity, muscle spasms, and rigidity," *Neurology*, Vol. 45, pp. 712–717, 4 1995. PMID: 7723960.

88. Sheean, G. L., "Botulinum treatment of spasticity: Why is it so difficult to show a functional benefit?," *Current Opinion in Neurology*, Vol. 14, no. 6, pp. 771–776, 2001.

89. Koman, L. A., J. F. Mooney, B. P. Smith, F. Walker, and J. M. Leon, "Botulinum toxin type A neuromuscular blockade in the treatment of lower extremity spasticity in cerebral palsy: a randomized, double-blind, placebo-controlled trial. BOTOX Study Group," *Journal of Pediatric Orthopedics*, Vol. 20, no. 1, pp. 108–115, 2000. PMID: 10641699.

90. Gruner, J. A., J. Altman, and N. Spivack, "Effects of arrested cerebellar development on locomotion in the rat - Cinematographic and electromyographic analysis," *Experimental Brain Research*, Vol. 40, no. 4, pp. 361–373, 1980.

91. Carlson, C. G., and M. A. Rüegg, "Determination of hydroxyproline content as a measure of fibrosis in nondystrophic and dystrophic skeletal muscle," 2009.

92. Barnett, V., J. Neter, and W. Wasserman, "Applied Linear Statistical Models.," *Journal of the Royal Statistical Society. Series A (General)*, Vol. 138, no. 2, p. 258, 1975.

93. Neuman, R. E., and M. A. Logan, "The Determination Of Collagen And Elastin In Tissues," *Journal of Biological Chemistry*, Vol. 186, pp. 549–556, oct 1 1950.

94. Turkoglu, A. N., P. A. Huijing, and C. A. Yucesoy, "Mechanical principles of effects of botulinum toxin on muscle length-force characteristics: An assessment by finite element modeling," *Journal of Biomechanics*, Vol. 47, no. 7, pp. 1565–1571, 2014.

95. Turkoglu, A. N., and C. A. Yucesoy, "Simulation of effects of botulinum toxin on muscular mechanics in time course of treatment based on adverse extracellular matrix adaptations," *Journal of Biomechanics*, Vol. 49, no. 7, pp. 1192–1198, 2016.

96. Elvrum, A.-K. G., S. M. Brændvik, R. Sæther, T. Lamvik, and et al., "Effectiveness of resistance training in combination with botulinum toxin-A on hand and arm use in children with cerebral palsy: a pre-post intervention study," *BMC Pediatrics*, Vol. 12, p. 91, jul 2 2012.

97. Gracies, J. M., B. Singer, and J. Dunne, "The role of botulinum toxin injections in the management of muscle overactivity of the lower limb," *Disability and Rehabilitation*, Vol. 29, no. 23, pp. 1789–1805, 2007.

98. Ikeda, A. J., M. F. Abel, K. P. Granata, and D. L. Damiano, "Quantification of co-contraction in spastic cerebral palsy," *Electromyography and clinical neurophysiology*, Vol. 38, pp. 497–504, dec 1 1998. PMID: 9842485.

99. Ateş, F., Y. Temelli, and C. A. Yucesoy, "Effects of antagonistic and synergistic muscles' co-activation on mechanics of activated spastic semitendinosus in children with cerebral palsy," *Human Movement Science*, Vol. 57, no. 2017, pp. 103–110, 2018.

100. Blasi, J., E. R. Chapman, E. Link, T. Binz, S. Yamasaki, and et al., "Botulinum neurotoxin A selectively cleaves the synaptic protein SNAP-25," *Nature*, Vol. 365, pp. 160–163, sep 9 1993. PMID: 8103915.

101. Brin, M. F., "Botulinum Toxin : Chemistry , Pharmacology , Toxicity , and Immunology Pharmacology of BTX," pp. 146–168, 1997.

102. Kareem, A. A., *Use of Botulinum Toxin A in Cerebral Palsy*. IntechOpen, nov 5 2018.

103. de Paiva, A., F. A. Meunier, J. Molgó, K. R. Aoki, and et al., "Functional repair of motor endplates after botulinum neurotoxin type A poisoning: Biphasic switch of synaptic activity between nerve sprouts and their parent terminals," *Proceedings of the National Academy of Sciences*, Vol. 96, pp. 3200–3205, mar 16 1999.

104. Longino, D., T. A. Butterfield, and W. Herzog, "Frequency and length-dependent effects of Botulinum toxin-induced muscle weakness," *Journal of Biomechanics*, Vol. 38, no. 3, pp. 609–613, 2005.

105. Minamoto, V. B., J. B. Hulst, M. Lim, W. J. Peace, and et al., "Increased efficacy and decreased systemic-effects of botulinum toxin A injection after active or passive muscle manipulation," *Developmental Medicine and Child Neurology*, Vol. 49, no. 12, pp. 907–914, 2007.

106. Thacker, B. E., A. Tomiya, J. B. Hulst, K. P. Suzuki, and et al., "Passive mechanical properties and related proteins change with botulinum neurotoxin A injection of normal skeletal muscle.," *Journal of orthopaedic research : official publication of the Orthopaedic Research Society*, Vol. 30, no. 3, pp. 497–502, 2012.

107. Chin, T. Y., G. R. Nattrass, P. Selber, and H. K. Graham, "Accuracy of intramuscular injection of botulinum toxin A in juvenile cerebral palsy: A comparison between manual needle placement and placement guided by electrical stimulation," *Journal of Pediatric Orthopaedics*, Vol. 25, no. 3, pp. 286–291, 2005.

108. Walter, U., and D. Dressler, "Ultrasound-guided botulinum toxin injections in neurology: technique, indications and future perspectives," *Expert Review of Neurotherapeutics*, Vol. 14, pp. 923–936, aug 1 2014. PMID: 25046267.

109. Wissel, J., A. B. Ward, P. Erztgaard, D. Bensmail, and et al., "European consensus table on the use of botulinum toxin type a in adult spasticity," *Journal of Rehabilitation Medicine*, Vol. 41, no. 1, pp. 13–25, 2009.

110. Picelli, A., S. Tamburin, P. Bonetti, C. Fontana, and et al., "Botulinum toxin type a injection into the Gastrocnemius muscle for spastic Equinus in adults with stroke," *American Journal of Physical Medicine and Rehabilitation*, Vol. 91, no. 11, pp. 957–964, 2012.

111. Molenaers, G., A. van Campenhout, K. Fagard, J. de Cat, and et al., "The use of botulinum toxin A in children with cerebral palsy, with a focus on the lower limb," *Journal of Children's Orthopaedics*, Vol. 4, no. 3, pp. 183–195, 2010.

112. Koman, L. A., J. F. Mooney, B. Smith, A. Goodman, and et al., "Management of Cerebral Palsy with Botulinum-A Toxin," *Journal of Pediatric Orthopaedics*, Vol. 13, no. 4, pp. 489–495, 1993.

113. Kaya, C. S., E. O. Yılmaz, Z. D. Akdeniz-Doğan, and C. A. Yucesoy, "Long-Term Effects With Potential Clinical Importance of Botulinum Toxin Type-A on Mechanics of Muscles Exposed," *Frontiers in Bioengineering and Biotechnology*, Vol. 8, p. 738, jun 30 2020.

114. Al-Khodairy, A. T., C. Gobelet, and A. B. Rossier, "Has botulinum toxin type A a place in the treatment of spasticity in spinal cord injury patients?," *Spinal Cord*, Vol. 36, no. 12, pp. 854–858, 1998. PMID: 9881735.

115. Lampire, N., N. Roche, P. Carne, L. Cheze, and et al., "Effect of botulinum toxin injection on length and lengthening velocity of rectus femoris during gait in hemiparetic patients," *Clinical Biomechanics*, Vol. 28, no. 2, pp. 164–170, 2013.

116. Tedroff, K., K. Löwing, Y. Haglund-ÅKerlind, E. M. Gutierrez-Farewik, and et al., "Botulinumtoxin A treatment in toddlers with cerebral palsy," *Acta Paediatrica, International Journal of Paediatrics*, Vol. 99, no. 8, pp. 1156–1162, 2010.

117. Huijing, P. A., and G. Baan, "Extramuscular myofascial force transmission within the rat anterior tibial compartment: Proximo-distal differences in muscle force," *Acta Physiologica Scandinavica*, Vol. 173, no. 3, pp. 297–311, 2001. PMID: 11736692.

118. van den Noort, J. C., L. Bar-On, E. Aertbeliën, M. Bonikowski, and et al., "European consensus on the concepts and measurement of the pathophysiological neuromuscular responses to passive muscle stretch," *European Journal of Neurology*, Vol. 24, no. 7, pp. 981–e38, 2017. PMID: 28557247.

119. Stampacchia, G., E. Bradaschia, and B. Rossi, "Change of stretch reflex threshold in spasticity: effect of botulinum toxin injections.," *Archives italiennes de Biologie*, Vol. 142, pp. 265–273, 2004.

120. Willerslev-Olsen, M., J. B. Andersen, T. Sinkjaer, and J. B. Nielsen, "Sensory feedback to ankle plantar flexors is not exaggerated during gait in spastic hemiplegic children with cerebral palsy," *Journal of Neurophysiology*, Vol. 111, no. 4, pp. 746–754, 2014. PMID: 24225545.

121. Willerslev-Olsen, M., M. Choe Lund, J. Lorentzen, L. Barber, and et al., "Impaired muscle growth precedes development of increased stiffness of the triceps surae musculotendinous unit in children with cerebral palsy," *Developmental Medicine and Child Neurology*, Vol. 60, no. 7, pp. 672–679, 2018.

122. Alhusaini, A. A., J. Crosbie, R. B. Shepherd, C. M. Dean, and et al., "No change in calf muscle passive stiffness after botulinum toxin injection in children with cerebral palsy," *Developmental Medicine and Child Neurology*, Vol. 53, no. 6, pp. 553–558, 2011.

123. Dietz, V., and T. Sinkjaer, "Spastic movement disorder: impaired reflex function and altered muscle mechanics," *Lancet Neurology*, Vol. 6, no. 8, pp. 725–733, 2007. PMID: 17638613.

124. Bar-On, L., K. Desloovere, G. Molenaers, J. Harlaar, and et al., "Identification of the neural component of torque during manually-applied spasticity assessments in children with cerebral palsy," *Gait and Posture*, Vol. 40, no. 3, pp. 346–351, 2014.

125. Abbruzzese, G., and A. Berardelli, "Neurophysiological effects of botulinum toxin type a," *Neurotoxicity Research*, Vol. 9, no. 2-3, pp. 109–114, 2006. PMID: 16785106.

126. Hallett, M., "Mechanism of action of botulinum neurotoxin: Unexpected consequences," *Toxicon*, Vol. 147, pp. 73–76, 2018. PMID: 28803760.

127. Dietz, V., "Proprioception and locomotor disorders," *Nature Reviews Neuroscience*, Vol. 3, no. 10, pp. 781–790, 2002. PMID: 12360322.

128. Adstrum, S., G. Hedley, R. Schleip, C. Stecco, and et al., "Defining the fascial system," *Journal of bodywork and movement therapies*, Vol. 21, no. 1, pp. 173–177, 2017.

129. Pamuk, U., A. O. Cankaya, and C. A. Yucesoy, "Principles of the Mechanism for Epimuscular Myofascial Loads Leading to Non-uniform Strain Distributions Along Muscle Fiber Direction : Finite Element Modeling," Vol. 11, pp. 1–15, 2020.

130. Wasaka, T., and R. Kakigi, *Sensorimotor Integration: The Somatosensory System and Voluntary Movement*, pp. 957–975. Cham: Springer International Publishing, 2019.

131. Hinrichsen, C. F., and L. M. Larramendi, "Features of trigeminal mesencephalic nucleus structure and organization. I. Light microscopy," *American Journal of Anatomy*, Vol. 126, no. 4, pp. 497–505, 1969. PMID: 5369112.

132. Hinrichsen, C. F. L., and L. M. H. Larramendi, "The trigeminal mesencephalic nucleus. II. Electron microscopy," *American Journal of Anatomy*, Vol. 127, pp. 303–319, 3 1970.

133. Jerge, C. R., "Organization and function of the trigeminal mesencephalic nucleus," *Journal of Neurophysiology*, Vol. 26, pp. 379–392, may 1 1963.

134. Cody, F. W. J., R. W. H. Lee, and A. Taylor, "A functional analysis of the components of the mesencephalic nucleus of the fifth nerve in the cat," *The Journal of Physiology*, Vol. 226, pp. 249–261, oct 1 1972.

135. Goodwin, G. M., and E. S. Luschei, "Discharge of spindle afferents from jaw closing muscles during chewing in alert monkeys," *Journal of Neurophysiology*, Vol. 38, no. 3, pp. 560–571, 1975.

136. Passatore, M., M. L. Lucchi, G. M. Filippi, E. Manni, and et al., "Localization of neurons innervating masticatory muscle spindle and periodontal receptors in the mesencephalic trigeminal nucleus and their reflex actions," *Archives Italiennes De Biologie*, Vol. 121, pp. 117–130, 4 1983. PMID: 6615117.

137. Roatta, S., U. Windhorst, M. Ljubisavljevic, H. Johansson, and et al., "Sympathetic modulation of muscle spindle afferent sensitivity to stretch in rabbit jaw closing muscles," *Journal of Physiology*, Vol. 540, no. 1, pp. 237–248, 2002. PMID: 11927683.

138. Passatore, M., and G. M. Filippi, "A dual effect of sympathetic nerve stimulation on jaw muscle spindles," *Journal of the Autonomic Nervous System*, Vol. 6, no. 3, pp. 347–361, 1982. PMID: 6221044.

139. Filippi, G. M., P. Errico, R. Santarelli, B. Bagolini, and et al., "Botulinum a toxin effects on rat jaw muscle spindles," *Acta Oto-Laryngologica*, Vol. 113, no. 3, pp. 400–404, 1993.

140. Yılmaz, E. O., C. S. Kaya, Z. D. Akdeniz-Doğan, and C. A. Yucesoy, "Long-term BTX-A effects on bi-articular muscle: Higher passive force, limited length range of active force production and unchanged intermuscular interactions," *Journal of Biomechanics*, Vol. 126, 2021. PMID: 34293603.

141. Hashimoto, T., C. M. Elder, and J. L. Vitek, "A template subtraction method for stimulus artifact removal in high-frequency deep brain stimulation," *Journal of Neuroscience Methods*, Vol. 113, no. 2, pp. 181–186, 2002. PMID: 11772439.

142. Bar-Gad, I., S. Elias, E. Vaadia, and H. Bergman, "Complex locking rather than complete cessation of neuronal activity in the globus pallidus of a 1-methyl-4-phenyl-1,2,3,6-tetrahydropyridine-treated primate in response to pallidal microstimulation," *Journal of Neuroscience*, Vol. 24, no. 33, pp. 7410–7419, 2004. PMID: 15317866.

143. Montgomery, E. B., J. T. Gale, and H. Huang, "Methods for isolating extracellular action potentials and removing stimulus artifacts from microelectrode recordings of neurons requiring minimal operator intervention," *Journal of Neuroscience Methods*, Vol. 144, pp. 107–125, may 15 2005.

144. Erez, Y., H. Tischler, A. Moran, and I. Bar-Gad, "Generalized framework for stimulus artifact removal," *Journal of Neuroscience Methods*, Vol. 191, pp. 45–59, aug 15 2010.

145. Drebitz, E., L.-P. Rausch, and A. K. Kreiter, "A novel approach for removing microstimulation artifacts and reconstruction of broad-band neuronal signals," *Journal of Neuroscience Methods*, Vol. 332, p. 108549, 2 2020.

146. Earley, E. J., A. Berneving, J. Zbinden, and M. Ortiz-Catalan, "Neurostimulation artifact removal for implantable sensors improves signal clarity and decoding of motor volition," *Frontiers in Human Neuroscience*, Vol. 16, pp. 1–12, 2022.

147. Maggi, C. A., and A. Meli, "Suitability of urethane anesthesia for physiopharmacological investigations in various systems Part 1: General considerations," *Experientia*, Vol. 42, pp. 109–114, Feb. 1986.

148. Maier, A., "Proportions of slow myosin heavy chain-positive fibers in muscle spindles and adjoining extrafusal fascicles, and the positioning of spindles relative to these fascicles," *Journal of Morphology*, Vol. 242, pp. 157–165, Nov. 1999.

149. Sherrington, C. S., "On the Anatomical Constitution of Nerves of Skeletal Muscles; with Remarks on Recurrent Fibres in the Ventral Spinal Nerve-root," *The Journal of Physiology*, Vol. 17, pp. 210.2–258, Oct. 1894.

150. Yucesoy, C. A., H. Maas, B. H. Koopman, H. J. Grootenboer, and et al., "Mechanisms causing effects of muscle position on proximo-distal muscle force differences in extramuscular myofascial force transmission," *Medical Engineering and Physics*, Vol. 28, no. 3, pp. 214–226, 2006.

151. Taylor, A., K. Appenteng, and T. Morimoto, "Proprioceptive input from the jaw muscles and its influence on lapping, chewing, and posture," *Canadian Journal of Physiology and Pharmacology*, Vol. 59, pp. 636–644, July 1981.

152. Bernabei, M., J. H. van Dieën, and H. Maas, "Enhanced muscle connectivity changes neural control of synergistic muscles during locomotion," *Society for Neuroscience 2015, online*, p. 2012, 2015.

153. Kröger, S., and B. Watkins, "Muscle spindle function in healthy and diseased muscle," *Skeletal Muscle*, Vol. 11, no. 1, pp. 1–13, 2021.

154. Giladi, N., "The mechanism of action of Botulinum toxin type a in focal dystonia is most probably through its dual effect on efferent (motor) and afferent pathways at the injected site," *Journal of the Neurological Sciences*, Vol. 152, no. 2, pp. 132–135, 1997.

155. Keles, C. S. K., and C. A. Yucesoy, "A novel botulinum toxin formula, which diminishes the adverse effects of BTX-A on muscular mechanics," *Gait & Posture*, Vol. 113, pp. 111–112, Sept. 2024.